Doctoral theses at NTNU, 2022:106

Naghme Dorraki

Investigation on Fault Current Making in Medium Voltage Switchgear in Air

Doctoral thesis

NTNU
Norwegian University of Science and Technology
Thesis for the Degree of
Philosophiae Doctor
Faculty of Information Technology and Electrical Engineering
Department of Electric Power Engineering

NTNU
Norwegian University of
Science and Technology

Naghme Dorraki

Investigation on Fault Current Making in Medium Voltage Switchgear in Air

Thesis for the Degree of Philosophiae Doctor

Trondheim, June 2022

Norwegian University of Science and Technology
Faculty of Information Technology and Electrical Engineering
Department of Electric Power Engineering

NTNU
Norwegian University of
Science and Technology

NTNU
Norwegian University of Science and Technology

Thesis for the Degree of Philosophiae Doctor

Faculty of Information Technology and Electrical Engineering
Department of Electric Power Engineering

ISBN 978-82-326-6901-1 (printed ver.)
ISBN 978-82-326-5645-5 (electronic ver.)
ISSN 1503-8181 (printed ver.)
ISSN 2703-8084 (online ver.)

Doctoral theses at NTNU, 2022:106

Printed by NTNU Grafisk senter

§

Preface

This thesis is submitted as a paper collection, partially fulfilling the requirements for the degree of philosophiae doctor (PhD) at the Norwegian University of Science and Technology (NTNU) in Trondheim.

The PhD work has been carried out at the Department of Electric Power Engineering, between February 2019 and March 2022, with Professor Kaveh Niayesh as main supervisor and chief scientist Dr. Magne Runde and Dr. Nina Støa-Aanensen as co-supervisors. The research has been supported by the Norwegian Research Council and is a part of the project in collaboration with SINTEF Energy and ABB.

I would like to express my special gratitude to my supervisor, Professor Kaveh Niayesh, for giving me your trust and helping build my scientific maturity and confidence through the PhD project. I acknowledge all the invested time and the interesting scientific discussions during the program.

I would like to thank my colleagues and friends at the High Voltage Technology group at NTNU and SINTEF Energy for their scientific discussions, and laboratory work supports.

My special thanks to administrative and technical staff at the Department of Electric Power Engineering at NTNU for always being ready to help. This work could not have been done without your support.

Finally, I want to thank my family for their unconditional love and support and my friends, Nasrin and Sanaz, for making the tough days easy-going. Thanks for standing by me!

Naghme Dorraki
Trondheim
March 2022

در کیش ما تجرد عنقا تمام نیست
در قید نام ماند اگر از نشان گذشت

[کلیم کاشانی]

Abstract

Closing a switch under a fault condition could result in extensive electrical contact wear and a possible switch failure. A load break switch (LBS), as one of the critical components in medium voltage (MV) power grids, should be able to be closed under short circuit currents of thousands of amperes. The dielectric breakdown between closing contacts creates a pre-strike arc before the contacts touch. Part of the short circuit current flows through the pre-strike arc, and the rest passes through the contacts when sliding through each other. The dissipated energy in the switching arc is partly absorbed by the electrical contact surfaces, increasing their temperature to melting and evaporation points. This increase may result in switch failure because of contacts welding when molten contact surfaces are closed. Depending on the dielectric strength of the insulation gas, the pre-strike arcing time could be different. SF_6 has been the most efficient insulation gas because of its high dielectric strength and thermal properties. However, it should be replaced because it is one of the most potent greenhouse gases.

This PhD thesis focuses on making operations in air MV-LBS. A synthetic test circuit for making short-circuit current and a model switch are designed based on standards. Different measurement methods are employed to investigate the switch degradation and failure in short-circuit making operations. Arc emission spectroscopy is performed to characterize the pre-strike arc properties at different closing speeds. The arc dynamic motion concluded from the spatially resolved temperature profiles at different times shows that the arc gets stabilized after a few hundred microseconds in the middle of the switch between contacts. Based on the derived temperature profiles, an indirect way of estimating the arc voltage has been proposed, which was in agreement with the corrected direct measurements.

Furthermore, electrical characterization of the making is performed at different stages of the operation. For the model switch, higher dissipated arc energies at the same current level result in higher contact mass loss, while an increase in the closing speed over proportionally reduces the contact degradation. The destructive energy of the pre-strike arc causing contacts degradation is measured to be at least one order of magnitude higher than the energy dissipation by ohmic loss when the current flows between sliding contacts in the closed position. Therefore, it can be concluded that the most destructive impact of making operation occurs at the first half-cycle of the short circuit current where the pre-strike arc exists. The results of short circuit current making tests with one half-cycle could be extended to the test conditions according to IEC 62271-103 standard, where the minimum duration of short circuit current flow should be 0.2 s.

Contents

Chapter 1
Introduction

The development of switching devices is closely linked to the growth of power transmission and distribution networks because they are essential to control the power flow through subsystems or components. High reliability and availability of electric power supplies lead to more interconnections in different parts of the power grid. Increasing the number of switchgears makes it possible to selectively isolate different grid parts without disturbing the customers' energy supply [1].

The demand for higher voltage and larger short-circuit capacity for transmission systems is an important driving force for improving the switching equipment design to meet the requirements concerning their tasks and duties in the power grid, classified into two main categories; load current and fault current switching. Load switching is planned by closing the switch to energize different grid parts. In this case, the energy exchange between different storing elements could result in transient overvoltages and overcurrents. The transients may stress other elements in the grid. However, closing the switch under load current generates little stress on the switch itself. Switching a fault current is a rare action with high demand due to its impact on different components in the network. The fault may occur because the power systems and components could be vulnerable from a technical-commercial point of view. For example, it could result from a short circuit between two conductive points of the network with a potential difference, e.g., an insulation failure under a lightning strike. The power flows are getting more unstable and bidirectional because of radical changes in distribution grids to access various power sources. Connecting new power generations and complicated network structures increases the local fault current level.

Consequently, a high level of currents flows through the fault location, which could cause damages to different network components. The fault should be cleared

to limit the destructive effects of short circuits. It could be possible by punctual detection of the fault to open the switch appropriately on time to interrupt the current and clear the fault. Therefore, the power switching devices should be able to withstand fault conditions. There are some requirements that each switch must fulfill to be considered reliable in the power grid. The switch must be a perfect conductor in the closed position to transfer short circuit current and continuous load currents. Therefore, low resistance between closed contacts is crucial to avoid ohmic losses and probable welding. Furthermore, it must be able to interrupt rated currents at any time, e.g., short-circuit currents for circuit breakers and nominally rated load currents for load break switches. Depending on the switch application, it must be capable of being closed at any time against any current, including short-circuit current without welding the contacts to be able to reopen for the next operation [2, 3].

Generation of switching arc is inevitable by interruption/making operations in power switching devices. While opening a current-carrying switch, an arc starts burning from the moment of contacts separation. The current flowing through the arc column causes arc temperature to increase—subsequently, conductivity increases. The arc needs to be cooled to successfully interrupt the current to decrease its conductivity at current zero-crossing, which needs particular attention to the switch design parameters. Apart from opening the switch on time for a successful interruption, contacts wear due to the interaction between the metal surfaces, and the arc should also be considered. When closing the switch on a short circuit, there could be a potential difference across the switch terminals of thousands of volts. As a result, a pre-strike arc ignites between the contacts due to the dielectric breakdown and continuous burning until contacts touch. The dissipated arc energy could be partly absorbed by the contacts surfaces and results in contact wear. The deteriorating impact of arc energy in a load break switch is significantly higher during making operation when a short circuit current of tens of kiloamperes flows through the switch than by interruption of a load current up to 1250 A. Therefore, all load break switches should be designed to make the rated short circuit currents and break any current up to and including their rated breaking currents at assigned recovery voltage [3, 4].

The gas type in gas-insulated switchgears (GIS) plays a prominent role in controlling of switching arc. SF_6 has been the most efficient insulation gas for arc-based switchgear because of its high dielectric strength and superior thermal properties leading to an outstanding arc quenching performance. However, the use of SF_6 has been or is going to be banned because of its environmental impact. The California Air Resource Board (CARB) has planned to start the SF_6 phase-out in 2025, and European countries have aimed to cut the F-gas emission by two-thirds by 2030 compared to 2014 [1]. Therefore, SF_6 alternatives should be chosen to

make the switch design compact and efficient at an affordable price, requiring new design criteria to control the stresses efficiently.

1.1 SCOPE OF THE WORK

This research aims to understand better the short-circuit making behavior of Medium Voltage (MV) air-based Load Break Switches (LBS) at atmospheric pressure. Making the short-circuit current could be divided into two main stages: the current flowing through the probable pre-strike arcing and the closed sliding contacts. The stresses applied to the switch while making a short-circuit current are closely dependent on the time duration and characteristics of the pre-strike arc and the interaction between this arc and the contact surfaces. Air as a cost-efficient alternative to SF_6 has a dielectric strength of approximately one-third of SF_6 at atmospheric pressure, which causes higher arcing time and consequently more significant energy dissipation between contacts than SF_6. Understanding the switching operation with air as the insulation gas could optimize switching parameters. The critical issues in this regard for short-circuit making operation can be summarized as below:

- Understanding the breakdown behavior and pre-strike arc characteristics in the air between closing contacts.
- Understanding how the energy dissipated by pre-strike arc affects the contacts wear.
- Describing the interaction between the pre-strike arc and the contacts surfaces under different closing velocities.
- Exploring switch degradation and failure under different fault conditions.

A key challenge of studying making operations is being close to real-world applications. Therefore, a synthetic test circuit needs to be established to initiate a pre-strike arc at high voltages followed by the short-circuit current flow. Also, a test object similar to the commercial models should be designed to evaluate the role of different elements of the switch. The experimental investigation mainly conforms with relevant standards (e.g., IEC 62271). The outcome of this PhD research project will form the basis for establishing design criteria to be used in product development and optimization in making operations in air-based MV-LBS.

1.2 OUTLINE OF THE THESIS

This PhD thesis is organized into five chapters:

- *Chapter one* is a brief introduction to the concept and a summary of the scientific contributions.
- *Chapter two* introduces load break switches in medium voltage and the potential challenges for switching operations in the power grid. The chapter is organized according to relevant standards to describe the test conditions and range of operations.
- *Chapter three* includes a description of the experimental setup, the synthetic test circuit for operation, and the test object as the load break switch. The diagnostics methods consist of electrical characterization of the process and an optical setup for arc spectroscopy, which are explained in detail in this chapter.
- *Chapter four* briefly discusses the following results: four journal papers and two conference papers.
- *Chapter five* concludes with remarks on the outcomes of the thesis and suggestions for further work.

1.3 SCIENTIFIC CONTRIBUTION

A test object with a spring-type drive mechanism is designed for all tests to facilitate different closing speeds. According to IEC 62271-101 [5], a synthetic test circuit is established to make operations similar to real-world applications. The test circuit includes a grid-connected high current source and a synthetic high voltage DC one. The main research contributions presented in this dissertation are listed as follows:

[Paper I, II, VI] *Optical diagnostics of the pre-strike arc:* the pre-strike arc dynamic motion is studied by employing arc emission spectroscopy. An optical setup is designed to record the temporal and spatial evolutions of the pre-strike arc when the contacts are approaching. The arc ignition is analyzed using only the high voltage DC part of the synthetic test circuit (Paper I). The temperature profile of the pre-strike arc during the making of a short-circuit current is measured, showing the arc dynamic motion accordingly (Paper II) and the effect of different closing speeds on the pre-strike arc behavior is investigated using optical emission spectroscopy (Paper VI).

[Paper II, III] *Electrical characterization of making operation:* Two different methods are proposed for arc voltage measurement because of distortion in voltage waveform in direct measurement. The first method is indirect voltage waveform measurement based on arc emission

spectroscopy. The arc temperature profile, the thermal air plasma properties, and the Lowke model to simulate arc dimension are employed to reach arc voltage waveform (Paper II). A correction technique is applied to the distorted voltage waveform as the second method for arc voltage measurement. The method is based on deconvolution of the measured voltage in time and frequency domains (Paper III). Although both methods have uncertainties and limitations, the resulting voltage values measured indirectly and corrected directly are in good agreement.

[Paper IV, V] *Investigation on switch failure at different fault conditions*: The main objective of the PhD research project is presented in Paper IV, where the correlation between dissipated arc energy before contacts touch and ohmic losses in the closed position with contacts wear is cleared. At different fault conditions, the closing speed and the main contacts preventing switch failure due to arcing contacts welding are studied. It is concluded that the most destructive impact of making operation on switch function occurs in the first half-cycle of short-circuit current, in which the pre-strike arc forms and the short circuit current flows through the sliding arcing contacts before the main contacts touch. Therefore, extending the obtained results to the test conditions with a longer short-circuit current is valid and could be used to support short-time withstand current and peak withstand current tests for circuit breakers making operation in IEC 62271-103 [6].

1.4 LIST OF PUBLICATIONS

The list of journal papers conducted from the outcomes of the PhD research project is as follows:

[Paper I] Naghme Dorraki, and Kaveh Niayesh, "Spectroscopic Investigation of Metal Content in Pre-strike Arc During Making Operation in a Low-Current Model Switch," *IEEE Transactions on Plasma Science, Vol. 48, No. 10, pp. 3698-3704, October 2020.*

Energy dissipation during prestrike arc is the critical factor for electrical contacts erosion and welding in medium voltage load break switches. Using air-filled devices as an alternative to SF_6 makes the switch environmentally friendly, but leads to a more challenging process due to a higher prestrike arcing time between contacts. Therefore, understanding the erosion process of electrical contacts is crucial to improve the switch lifetime. Determination of contacts surface evaporation by optical emission spectroscopy is one of the most precise methods to investigate the prestrike arc interface with the contacts. In this article, the temporal and spatial profiles of copper and

tungsten emitted species during prestrike arc are presented. For this purpose, a circuit consisting of a synthetic dc high voltage part is used to initiate the arc. The temporal evolution of CuI, CuII, and WI shows evaporation of the cathode and the anode surfaces during the prestrike arc, and the spatial profiles show an inhomogeneous distribution of the vapors alongside the arc root.

[Paper II] Naghme Dorraki, and Kaveh Niayesh, "Optical investigation on pre-strike arc characteristics in medium-voltage load break switches," *Journal of Physics D: Applied Physics, Vol. 54, No. 25, p. 255503, April 2021.*

Medium voltage load break switches (MV-LBS) should pass fault current while closing and be able to re-open for the next operation. Replacing SF_6 as a high impact greenhouse insulating gas with air, makes the switch design more challenging because of the higher pre-strike arcing time and energy dissipation between contacts which leads to more contact surface erosion and an even higher possibility of welding. In this paper, a synthetic test circuit is used to emulate stresses applied to MV-LBS during the making of short-circuit currents. Since there are difficulties in accurate direct measurement of arc voltage because of the inherent response of the measurement system, an alternative method using optical emission spectroscopy (OES) is proposed. OES measures the pre-strike arc temperature distribution profile close to the cathode surface at a test voltage of 18 kV and a making current of 17 kA. The arc electrical characterization is achieved using the obtained spectroscopy results, Lowke's model and thermal air plasma transport properties. A maximum arc temperature of 12 500 K while the arc moves from the lower part of the cathode to the center, arc voltage of 30–58 V, and dissipated energy of 79–87 J are calculated for the pre-strike arc considering the impact of copper evaporated from the contact surfaces. Different arc behavior is observed in closing the contacts compared to free-burning arcs, which indicates gas flow blowing the arc caused by the contact movement. This investigation could be used for a better understanding of switching behavior and efficient control of the operation.

[Paper III] Naghme Dorraki, and Kaveh Niayesh, "Deconvolution based Correction of Pre-strike Arc Voltage Measurement in Medium Voltage," *IEEE Journal of Sensors, Submitted March 2022.*

Switching arc characterization, e.g., measuring the arc voltage, is the key to evaluating the performance of power switchgear under different working conditions. Short circuit current making represents one of the most severe operations for medium voltage load break switches (MV-LBS). When closing the switch, a short circuit current starts flowing through a pre-strike arc caused by the breakdown of the gap between the contacts. Therefore, the voltage waveform across the switch shows an abrupt change from the rated voltage of the power network, i.e., tens of thousands of volts, to the switching arc voltage, i.e., a few tens of volts and ultimately zero when the contacts touch. The inherent response of the measurement system to this

very large step overlaps with the switching arc voltage, what makes correction of the distorted voltage waveform necessary.
In this paper, a deconvolution-based correction technique, i.e. deconvolution of the measured voltage in time and frequency domains, is examined using experimentally determined impulse responses of the measurement system. To demonstrate its effectiveness, this method is applied to three different measurement systems with various step responses. The results show practically identical deconvoluted (corrected) voltage waveforms in all three measurement systems, although the directly measured waveforms have significant differences. The corrected arc voltages are in agreement with the indirect measurements proposed in previous studies.

[Paper IV] Naghme Dorraki, and Kaveh Niayesh, "An Experimental Study of Short-Circuit Current Making Operation of Air Medium-Voltage Load Break Switches," *IEEE Transactions on Power Delivery, accepted for publication, February 2022.*

Replacing SF_6, the most potent greenhouse gas, with an alternative is a challenge faced by medium-voltage load break switches (MV-LBS). Air is a possible alternative, but there are some challenges regarding low dielectric strength leading to high arcing time and dissipated energy. Therefore, understanding the switching processes for both interruption and making operations in air MV-LBS is crucial to designing efficient compact switchgear.
This work focuses on making operations in air MV-LBS. A synthetic test circuit and a model switch are designed based on the standards to simulate making operations under fault conditions similar to a real test. The test condition is set to achieve high pre-strike arcing time and energy. The results show that the most destructive impact of the making short-circuit current occurs in the first half-cycle of the load current when the pre-strike arc is formed. With an average short-circuit current with a peak of 22 kA and a breakdown voltage of 20 kV, the switch failed to re-open due to the arcing contacts welding after four successive making operations without main contacts and seven successive operations with main contacts. It has been shown that the total arcing contact mass loss occurs mainly during the pre-arcing time. Increasing the closing speed could be a possible solution to minimize the impact of arcing.

The following is the presented conference paper during the PhD program:

[Paper V] Naghme Dorraki, Marius Strand, Kaveh Niayesh, "Impact of pre-strike arc on contacts degradation after short circuit current making operation in medium voltage air load break switches," *Proceedings of the 30th International Conference on Electrical Contacts (ICEC), Switzerland (Online), June 2021, PP. 111-115* .

Medium voltage load break switches are required to perform a number of making operation while passing of short circuit current that could be more than tens of kiloamperes. Using air-filled devices as an alternative to SF_6,

which is a high impact greenhouse gas, makes the switch more environmentally friendly but leads to more challenging making operation due to higher arcing times and dissipated energies between the contacts. In this case, the pre-strike arc could lead to contacts welding and degradation, which is highly undesirable. This paper reports on an investigation of the pre-strike arc impact on erosion and welding of copper/tungsten (20/80) arcing contacts during short-circuit making operations. For this purpose, a synthetic test circuit consisting of a high current source in combination with a high voltage one is used. Experiments are conducted for different operation voltages, while the short circuit current is kept constant at 22 kA. Mass loss measurement and visual inspection of eroded/welded contacts are examined with regard to pre-strike arc impact on their degradation. The contacts are welded by three times repeating the test at operation voltage of 20 kV and short-circuit current of 22 kA and failed to re-open. Besides, an increase in the contacts' mass loss with arcing time is observed while the making current is constant. This is an indication that the pre-strike arc energy highly impacts the switch reliability and service life.

[Paper VI] Naghme Dorraki, Kaveh Niayesh, "Spectroscopic Analysis of Pre-strike Arc in Medium Voltage Load Break Switches (MV-LBS) at Different Closing Speeds," *Submitted to the 23rd International Conference on Gas Discharge and their Applications (GD), Greifswald, Germany, August 2022.*

Making (closing) operations of MV-LBS when passing short circuit current could cause a highly destructive impact on the switch because of extensive contacts degradation, which is mainly because of current flow through the pre-strike arc channel before contacts touch. The dissipated energy in the pre-strike arc could be absorbed by contacts surfaces and results in rising of the surfaces temperature to melting and evaporation points. This could lead to contacts welding in the closed position. Regarding the switch insulation gas, replacing SF_6 as the most potent greenhouse gas with air could make the process even more complicated because of the lower dielectric strength of air.
This work focuses on the effect of switch closing speed on the pre-strike arc behavior. Optical emission spectroscopy is used to investigate the pre-strike arc dynamic motion while closing the switch. The arc temperature profile close to the surface of the fixed contact shows a higher rate of increase in arc conductivity and cross-section by faster closing speed. This is in agreement with the direct arc voltage measurement, which shows lower voltage values for faster closing speed at the same instantaneous current.

Chapter 2
Load Break Switches in Medium Voltage

Switching action is crucial for a steady power flow from generation to load. Isolating components in the network because of maintenance or replacement and isolating faulted sections of the network to avoid damages and/or system instability are examples of switching duties in the power grid by making and breaking currents. The most well-known example of switching operation is the interruption of short-circuit currents. Faults cannot be avoided in the network. However, they could be under control by adequate switching components combined with protection systems. The devices that carry out the switching actions in the power grid are circuit breakers, load break switches, disconnecting switches, and earthing switches. Examples of breaking capacity as one of the switching duties are shown in Figure 1, according to IEC62271-103 [6]. In both figures, the switch NO can be closed to avoid loss of service for downstream users. In Figure 1(a), the switch NC located in the same loop can be open, for example, to maintain a branch of the loop. Both switches and transformers may not be located in the same area. In Figure 1(b), the switch NC located in the other branch can be open, for example, for maintenance. In this case, generally, both switches and transformers are in a close location.

2.1 GAS-INSULATED SWITCHGEAR

The development in systems and components increases the demand for more compact switchgears accessible by gas-insulated switchgears (GIS). A high number of successful and reliable operations is required for GIS, while the use of SF_6 is going to be considerably limited due to its environmental impact.

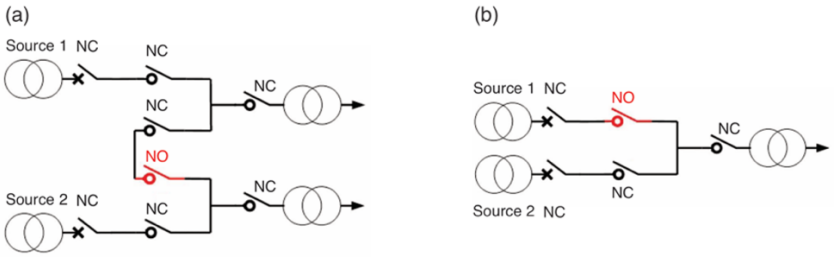

Figure 1. Examples of breaking capacity when opening a closed-loop distribution line circuit. NC: Switch or circuit-breaker normally closed, NO: Switch normally open [6].

SF_6 has been the most efficient insulation gas for arc-based switchgears because of its high dielectric strength, and superior thermal properties leading to an outstanding arc quenching performance. Alternative insulation gases need to operate at higher pressures in larger interrupters to provide operational efficiency similar to SF_6. These gases should be chosen to make the switch design compact and efficient at an affordable price. The properties of the selected alternative gases should be chosen not to be explosive with no ozone depletion potential (OPD) and nontoxic according to safety data sheets available from the chemical manufacturer. CO_2, as one of the interesting gases, has a dielectric strength comparable to air, which is significantly less than SF_6. C5 Perfluoroketone (C5-PFK) and C4 Perfluoronitrile (C4-PFN) have dielectric strength twice that of SF_6. However, the boiling points of C5-PFK and C4-PFN are 26.5 °C and -4.7 °C, respectively, which are significantly higher than SF_6 with a boiling point of -64 °C at atmospheric pressure [7, 8].

Gas mixtures could also provide reasonable interrupting performance. Adding C5-PFK and C4-PFN to the other insulation gases could increase the dielectric strength of the gas mixture. For instance, the dielectric strength of air as the buffer

Table 1. Properties/performances of gases and mixtures in MV switchgear applications [2].

	C_{ad} [1]	**P_{min}/MPa [2]**	**T_{min}/°C [3]**	**GWP**	**Dielectric Strength**	**Toxicity LC50 ppmv**
SF_6	-	0.43 – 0.6	- 41 – -31	23 500	0.86 – 1	-
CO_2	-	0.6 – 1	≤- 48	1	0.4 – 0.7	> $3e^5$
Air/C5-PFK (MV)	≈ 7 – 13	0.13	-25 – -15	0.6	≈0.85[e]	$1e^5$
N_2/C4-PFN (MV)	≈ 20 – 40	0.13	-25 – -20	1300 – 1800	0.9 – 1.2	> $2.5e^4$

[1] concentration of admixture is in mole % referred to the gas mixture

[2] typical lock-out pressure range

[3] minimum operating temperature for P_{min}

gas for MV applications with C5-PFK could be almost approached to SF_6 at a pressure of 0.13 MPa. The properties of gases and mixtures when used in MV switchgears are shown in Table 1. Among non-synthetic alternative gases, CO_2 and air are abundant in nature and are and chemically and thermally stable despite their relatively low dielectric strength compared to SF_6. Air as a cost-efficient alternative to SF_6 has a dielectric strength of approximately one-third of SF_6 at atmospheric pressure, which needs a larger interrupter with a higher gas pressure for a successful interruption performance. Therefore, a total change in the design of SF_6-based switchgears is necessary to make them compatible with air as the insulation gas.

2.2 CURRENT INTERRUPTION IN MV-LBS

The switching operation is mainly focused on interrupting capacity. Load break switches should be capable of breaking 1250 A at rated medium voltage according to IEC 62271-200 [9]. The load break switches have typically two sets of contact pairs, i.e., arcing contacts (which is normally exposed to the switching arc) and main contacts (which carry the current when the switch is in closed position). The design has to be adapted to the insulation gas used. The influence of different design parameters on the interruption capability has to be recognized to achieve an optimized design.

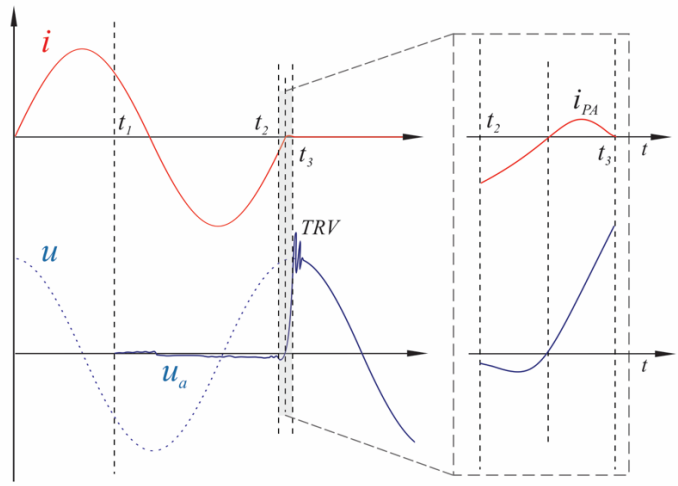

i	breaking current	t_1	instant of contact separation
u	power-frequency voltage	t_2	start of significant change in arc voltage
u_a	arc voltage	t_3	instant of cessation of post-arc current
TRV	transient recovery voltage	t_3-t_2	interaction interval
i_{PA}	post-arc current		

Figure 2. Interrupting process according to IEC 62271-101 [5].

Current interruption in MV-LBs occurs at natural current zero (CZ) crossing. By opening the contacts, an arc forms between the separating contacts. After CZ crossing, if the current is successfully interrupted, the voltage across the contacts rises rapidly toward the grid voltage, called Transient Recovery Voltage (TRV). Due to residual electrical conductivity, a post arc might form between the separated contacts. It is crucial to cool down the gas to reduce its conductivity to avoid reignition of the switching gap caused by excessive heating of the arc channel by post arc current flow. This stage of the interruption process is called the thermal phase. After the post arc is interrupted, the dielectric strength needs to be increased to avoid a breakdown caused by the rapidly rising TRV in the dielectric phase. The principle of the breaking process is summarized in Figure 2. according to IEC 62271-101 [5]. The switch is opened at t_1, and the arc burns between t_1 and t_2. The time interval between t_2 and t_3 is called interaction interval, which starts at the time of significant change in arc voltage prior to current zero and ends when the current, including the post-arc current (if any), ceases.

SF_6 has been an ideal insulation gas as an electronegative gas with high dielectric strength. The design parameters need to be optimized for a successful current interruption in both the thermal and dielectric phases to replace SF_6 with air. It has been shown that the blowing pressure of atmospheric air has a critical role in the interruption capability [10, 11]. Since load current interruption in MV is a predominantly thermal issue rather than a dielectric problem, it is essential to cool down the arc around current zero (CZ). The thermal interruption capability increases linearly with increasing blowing pressure. However, the size and geometry of contacts and nozzles beside the contacts gap length should be considered in the process [12]. Although reducing the size of the contacts and increasing the nozzle throat length could result in better thermal capability and faster dielectric recovery [13], the mechanical stresses and contacts erosion while closing the switch should be considered.

Self-blast current interruption is another solution to improve compactness and cost-effectiveness in MV-LBS in atmospheric air. This result could be achieved by placing polymers adjacent to the arcing contacts—the interface of the polymer surface with the arc results in polymer ablation and injection to the arc. Consequently, it changes the plasma composition and results in arc quenching (Hartgas effect). There are several studies introducing polytetrafluorethylene (PTFE), polypropylene (PP), and polymethylmethacrylate (PMMA) as suitable nozzle materials for arc quenching [14, 15]. However, PP and PMMA evaporate faster than PTFE by exposing them to the same amount of dissipated arc energy.

2.3 MAKING OPERATION IN MV-LBS

A load break switch must be able to interrupt load current and be required to be closed under fault conditions. Although closing against a fault is rare during service, it is one of the most demanding type tests for MV switchgear. The reinforced network structure could increase short-circuit current levels. Furthermore, a reduction in network losses leads to larger DC-time constants of the short-circuit current, leading to larger peak values of the fault current. Therefore, the switch should be able to pass short-circuit currents of tens of kiloamperes while closing and be able to reopen for the next operation.

While the distance between the contacts decreases by closing the switch, a breakdown occurs at a specific distance depending on the potential difference across the switch terminals and the dielectric strength of the insulation gas, which results in the ignition of a pre-strike arc. The short-circuit current flows through the arc column before contacts are fully closed. The contacts could partly absorb the dissipated arc energy, resulting in the contact surfaces melting and evaporating. Subsequently, the contacts with molten surfaces could be welded in the closed position when most fault current passes through them, preventing the switch from reopening [3]. Figure 3 shows principles of making short-circuit current process according to IEC 62271-101 [5]. After the breakdown at t_1, the switch is subjected to making current. The current flows through the arc column between $t_1 - t_2$. During the latching time (from the moment of the first touch to the

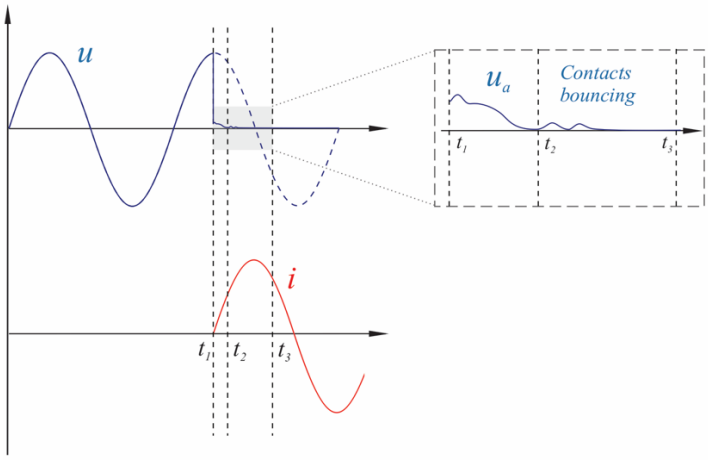

Figure 3. Making operation according to IEC 62271-101 [5].

time when the switch is fully closed; $t_2 - t_3$), the contacts may bounce, and an arc would form between them, which enhances the contacts' erosion. Therefore, special consideration in mechanical design is needed to avoid contacts bouncing while passing short-circuit currents.

Since air as an insulation gas alternative to SF_6 has lower dielectric strength, a higher arcing time and larger dissipated energy in the pre-strike arc are expected. Therefore, the impact analysis of making operation for air-based MV-LBS is crucial for optimizing the switch design and estimation of its service life. Although several studies on electrical contacts erosion as a consequence of arc [16-18], there is still a research gap in understanding the erosion mechanisms of sliding contacts under short-circuit conditions. Pre-strike arcing between the contacts sliding through each other with molten surfaces while passing short-circuit current of kiloamperes represents a complicated case, which has not been investigated thoroughly in the literature. This result is not only the case in MV-LBS but also in earthing switches used in power switchgear. Therefore, understand the switch behavior while operating to avoid switch failure because of contact welding.

2.4 ARC EROSION OF ELECTRICAL CONTACTS

To design an MV-LBS, understanding the arc interaction with the electrical contacts is crucial to avoid/reduce the destructive consequences of arcing on the contact erosion. The erosion occurs because both the cathode and anode can be heated up to the boiling point of the contact material by absorbing the dissipated arc energy. The amount of erosion per operation for the contacts depends upon many parameters like arcing time and energy, the contacts material, structure and geometry, the opening/closing velocity, the design of the arc enclosure (gas flow, insulation medium), etc. [4, 19-21].

Considering all the parameters mentioned above, besides the mechanical stresses the switch faces during operation, makes it challenging to model the erosion mechanism. The measurements are only the electrical characterization and final resulted erosion like mass loss and visual inspection. However, there is the possibility to employ in-direct measurements to investigate the arc behavior like dynamic motion, temperature, and pressure, which paves the way to understand the process [22-24]. Some general principles can be applied to provide guidelines for designing parameters. For example, the contacts' mass lost per operation can be defined as a function of total arc energy input as follows [4]:

$$\text{mass loss} = f(\text{total power input into the contacts}) \quad \text{Eq. 1}$$

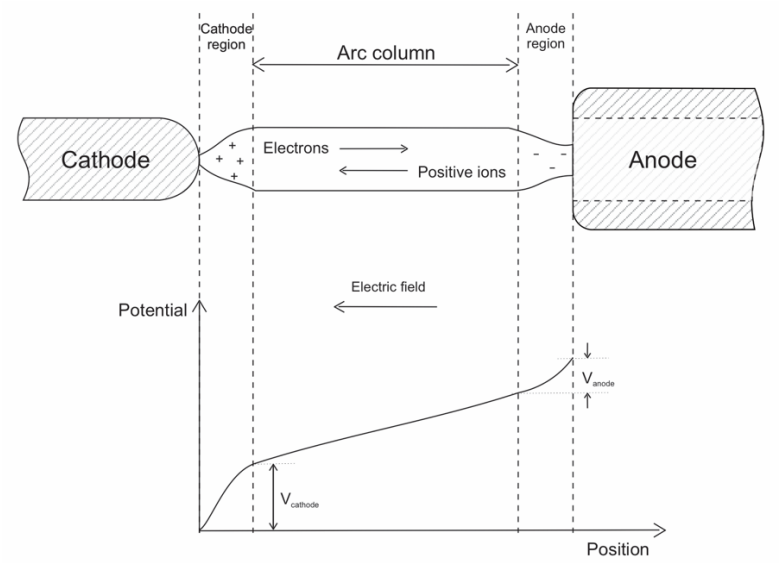

Figure 4. Schematic of electric arc column with potential distribution along the arc axis [3].

Although both sides of Eq. 1 look simple, the meaning of total power input to the contacts has to be clear. The total dissipated arc energy between the contacts could be given by arc voltage and current following Eq. 2.

$$E_{total} = \int_{t_1}^{t_2} i_{arc}(t).\ u_{arc}(t)\ dt \qquad \text{Eq. 2}$$

Where t_1 and t_2 are the start and end of arcing time, the contribution of total dissipated arc energy in contacts mass lost is controversial. Figure 4 shows the voltage changes across the arc column. Electrons and positive ions carry the electric current in the arc column. Most of the current is carried out by the electrons, which are generated partly by gas molecules ionization and partly by emissions from the cathode surface [3]. Therefore, the total power input into the cathode could be divided as power input from the ions [f_1(I × cathode fall voltage)], power input from radiation [f_2 (I × U_{arc})], power input from neutral atoms [f_3 (I × U_{arc})], and joule-heating of contact [f_4 (I^2)] [4].

The only method to directly measure the input power is by experimentally measuring arc voltage and current, which leads to total arc energy, including all types of power input (f_1-f_4). Theoretically and experimentally, distinguishing between different power inputs of the arc power and approximations required to find the effective contribution of each element is complicated. However, some comparative studies assume that contact erosion occurs only due to cathode/anode fall energy [16, 25]. The total arc energy (f_1-f_4) and the cathode/anode fall energy

(f_l) are measured in this study to figure out the correlation between contacts erosion and arc energy. The detailed measurement methods are presented and discussed in Paper IV.

2.5 SUMMARY AND IMPLICATION

An MV-LBS should withstand fault conditions in making short-circuit current and reopen for the next operation, which is the main focus of this research. Understanding the making process is essential to improve the switch design parameters in order to avoid the switch failure while closing against fault conditions.

According to IEC 62271-101, a synthetic making test method which is equivalent to direct test is employed to perform making operation in laboratory. Different diagnostic methods are implemented to study pre-strike arc behaviour and electrical measurements, which are explained in the upcoming chapters. To evaluate the impact of arc erosion on switch failure in making test, the coordination of both total arc energy and the electrodes fall energy in contacts erosion are investigated.

Chapter 3
Research Methodology

This chapter describes the research design for investigation on making operation in air-based MV-LBS to achieve the aims and objectives stated in section 1.1 of Chapter 1.

A detailed description of the structure and performance of the synthetic test circuit for making operation and the test object as the MV-LBS are discussed in section 3.1. The diagnostic methods, including the electrical measurements and optical emission spectroscopy, are discussed in section 3.2.

3.1 EXPERIMENTAL SETUP

The flow of short-circuit current in operation can be divided into two main stages; the current passing through the pre-strike arc and the current passing through the contacts when they touch. The experiments are designed to achieve the highest arcing time and energy level to investigate the effect of the pre-strike arc on the switch failure.

The switch could be subjected to different arcing times, depending on the moment of closing. In real-world applications, the switch could be closed at each phase of the power-frequency voltage. Figure 5 shows current and voltage waveforms in a simple making operation at three different closing moments. If the switch closes when the applied voltage is zero, an asymmetrical network frequency current passes through the switch, shown in Figure 5 (a). In this case, the arc energy is negligible, but the largest current amplitude flows through the switch; this case is called the high current case.

In contrast, if the breakdown occurs at the peak of the applied voltage, a symmetrical network frequency current passes through the switch. In this case, the largest possible arc energy is dissipated between the contacts; this case is called the high-energy case (see Figure 5 (c), where u is the network voltage, and

i is the making current). The pre-strike arc burns the interval between t_0 and t_1; the breakdown occurs at t_0, and the switch is closed at t_1. Figure 5 (b) shows a random moment of closing operation. The current waveshape is between the cases shown in Figure 5 (a) and (c) so that the maximum current is less than case (a), and the maximum energy is less than the case (c).

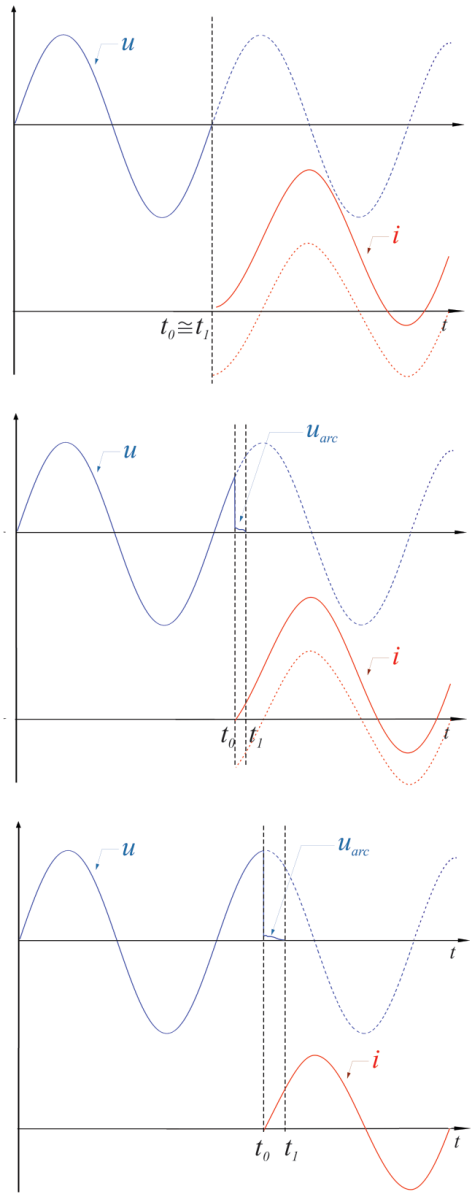

(a)
Asymmetrical making current:
Close at voltage zero
Highest current peak
Negligible arc energy

(b)
Randomly closing moment:

$I_{peak(c)} < I_{peak(b)} < I_{peak(a)}$
$0 < t_{arc(b)} < t_{arc(c)}$
$0 < t_{arc(b)} < t_{arc(c)}$

(c)
Symmetrical making current:
Close at peak voltage
Highest arcing time
Highest arc energy

Figure 5. Three typical cases for the moment of closing the switch in making process, the dashed red lines show the ac component of the current.

3.1.1 Synthetic test circuit

synthetic test circuit for the making operation according to IEC 62271-101 is established [5]. In this case, the high energy test is performed, which corresponds to the largest energy dissipation in the making switching arc. The schematic of the synthetic test circuit is shown in Figure 6.

The circuit consists of two parts: the high current and the high voltage ones. The high current circuit includes a high-power transformer that can supply network frequency short-circuit currents of tens of kiloamperes. The high voltage circuit subjects the test object to the operation voltage by energizing the charged capacitor. The capacitor is charged to the operation voltage by the DC high voltage power supply (S_1 connected, S_2 disconnected). Once charged, switch S_1 is disconnected. By closing the model switch, a pre-strike arc ignites between the contacts at a specific distance due to a dielectric breakdown of the air. Immediately after the breakdown, a signal will be sent to the triggered vacuum switch (TVS). The high current circuit injects one half-cycle of the 50 Hz short circuit current by connecting the transformer output to the test object. The time delay between detecting a current flow caused by the breakdown of the switch and connection of the high current circuit is less than 50 µs. Switch S_2 is open during the making test and is closed when the test is over for the sake of safety.

A 6015A Tektronix voltage probe and TDS2014B Tektronix oscilloscope 8-bit measure the arc voltage. The time resolution of the measurements has been 4 µs, and a Rogowski coil is employed to measure the arc current. An additional voltage measurement is used to measure the charging voltage of the capacitor.

A view of the experimental setup for the synthetic test circuit is shown in Figure 7. The high voltage part includes a 0.1 µF fast discharging capacitor

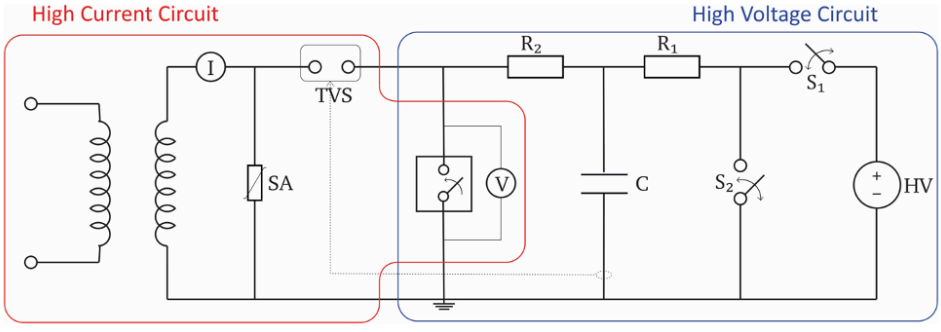

Figure 6. Schematic of the synthetic test circuit for performing the making operation.

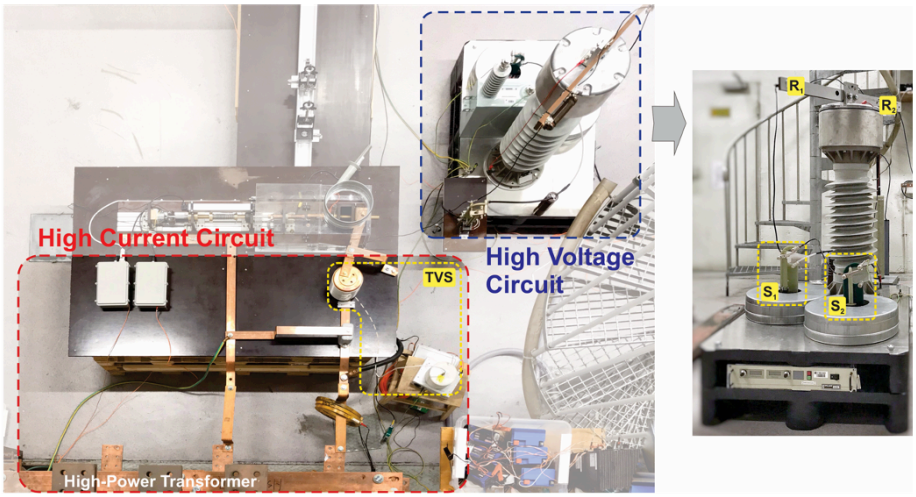

Figure 7. A view of the synthetic test circuit in the experimental set-up for making operation.

controlled by mechanical switches S_1 and S_2. The grid-connected high power transformer is shown in the high current circuit. At a voltage of 700 V, the short circuit current could reach 60 kA. However, due to limitations of the setup, a maximum test short circuit current of 25 kA has been chosen for the tests by adjusting the circuit inductances.

The TVS located in the high current circuit is switching the short circuit current to the test object, shown in Figure 8. A short transient current forms by discharging the high voltage capacitor. After the short transient current is detected, a triggering signal is sent to the trigger unit of the TVS. The unit generates a voltage pulse, which results in a breakdown between the electrodes in the vacuum bottle and forms a conductive plasma channel to pass the short circuit current to the test object. The total delay time between the pre-strike and the short circuit current flow does not exceed 50 µs. A surge arrester is located between the high-power transformer and the vacuum bottle to protect the transformer from the overvoltage transients.

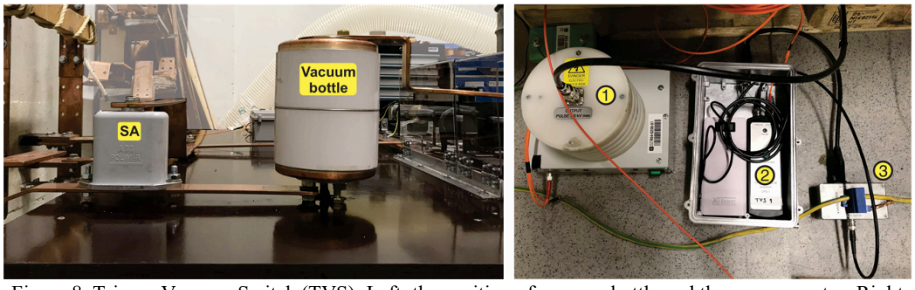

Figure 8. Trigger Vacuum Switch (TVS); Left: the position of vacuum bottle and the surge arrestor, Right: Trigger unit (1), Optical pulse shaper (2), and signal detector (3).

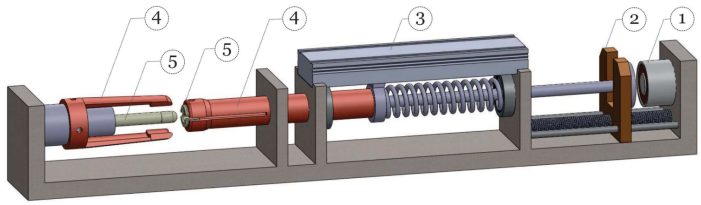

Figure 9. Spring-type test object; (1) Solenoid magnet, (2) Contacts' separator, (3) Position sensor, (4) Main contacts, and (5) Arcing contacts.

3.1.2 Test Object

A spring-type drive mechanism is designed to realize the opening and closing of the test object. A schematic of the test object is shown in Figure 9. The breakdown moment is adjusted by triggering the solenoid magnet (1) to release the dynamic contact. A position sensor (KTF-225 Linear displacement sensor) (3) records the movement of the contacts. The arcing contacts (5) include a pin with a diameter of 10 mm and a split tulip with an outer diameter of 20 mm and an inner diameter slightly less than 10 mm to provide full touch in the closed position. The arcing contacts are made of copper/tungsten (20/80). The main contacts (4) are designed in clamp shape to avoid bouncing in the closed position. The main contacts are made of copper. The focus of the thesis is on the arcing contacts erosion/welding. Thus, the main contacts are the same for all the tests, and four pairs of arcing contacts have been examined for different test conditions. However, the main contacts erosion is inspected during the tests.

The model switch is designed to minimize the mechanical stresses applied to the contacts while closing, so that the bouncing of the contacts is minimized. The contacts' material and the closing speed of 2.9-4.2 m/s are chosen for the model switch not to be too different from the commercial switches. A higher closing speed can shorten the arcing time and reduce the arc energy while keeping the other design parameters constant. Figure 10 shows a view of the test object in the experimental setup, where the length of the spring is adjusted for a closing speed of ~ 4 m/s. The experimental data resulting from higher closing speed could

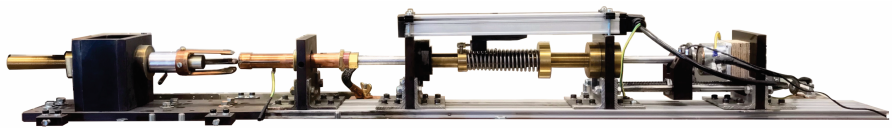

Figure 10. A view of test object as LBS in the experimental set-up for closing the switch.

Table 2. Copper-Tungsten material properties [4].

Material	Melting Temperature (°C)	Resistivity 20 °C (μΩ cm)	Thermal Conductivity 20 °C (W m^{-1} K^{-1})	Hardness (× 10^2 Nmm^{-2})
CuW (50/50)	1083	4.2	200	11-16
CuW (40/60)	1083	4.5	195	14-20
CuW (30/70)	1083	5.0	175	16-22
CuW (25/75)	1083	5.3	160	17-24
CuW (20/80)	1083	5.6	150	20-26

provide information on how an increased closing speed would reduce the destructive effects of the making operation on the switch.

At high switching arc currents, the erosion process involves material evaporation, the molten metal eruption from contacts surfaces, and cracks on the surface of the material composite. The contacts material is chosen to withstand well against the stresses the switch faces during operation. Some comparative studies show the difference in contacts material [26, 27].

The closing of the switch results in mechanical stresses besides thermal ones are due to arc burning and current flow in the closed position. Tungsten is a good choice of material to withstand mechanical stresses and physical deformations due to a high level of hardness. However, it should be considered that high tungsten contents are prone to brittle behavior. The properties of different proportions of copper-tungsten are shown in Table 2, where tungsten can provide a high level of hardness and resistance to mechanical stress and physical deformation. At the same time, the copper portion increases the electrical and thermal conductivities. The melting temperature is the same for all the different proportions of the material. However, increasing the percentage of tungsten in the alloy increases the hardness and reduces the thermal conductivity. Therefore, the choice of copper-tungsten (20/80) as the material of the arcing contacts is for erosion and weld resistance.

3.1.3 Time intervals

During closing the switch to a short circuit current, the switch is subjected to different stresses according to the timing of the process. The operation is divided into time intervals based on the dynamic contact displacement and the short circuit current for a detailed understanding of the process. A typical 50 Hz half-cycle current waveform as the output of the synthetic test circuit and a travel curve of the dynamic contact with an average moving speed of ~ 4 m/s are shown in the first and second column of Figure 11 respectively. A schematic of the arcing and

main contacts displacement according to the time interval is shown in the third column of Figure 11.

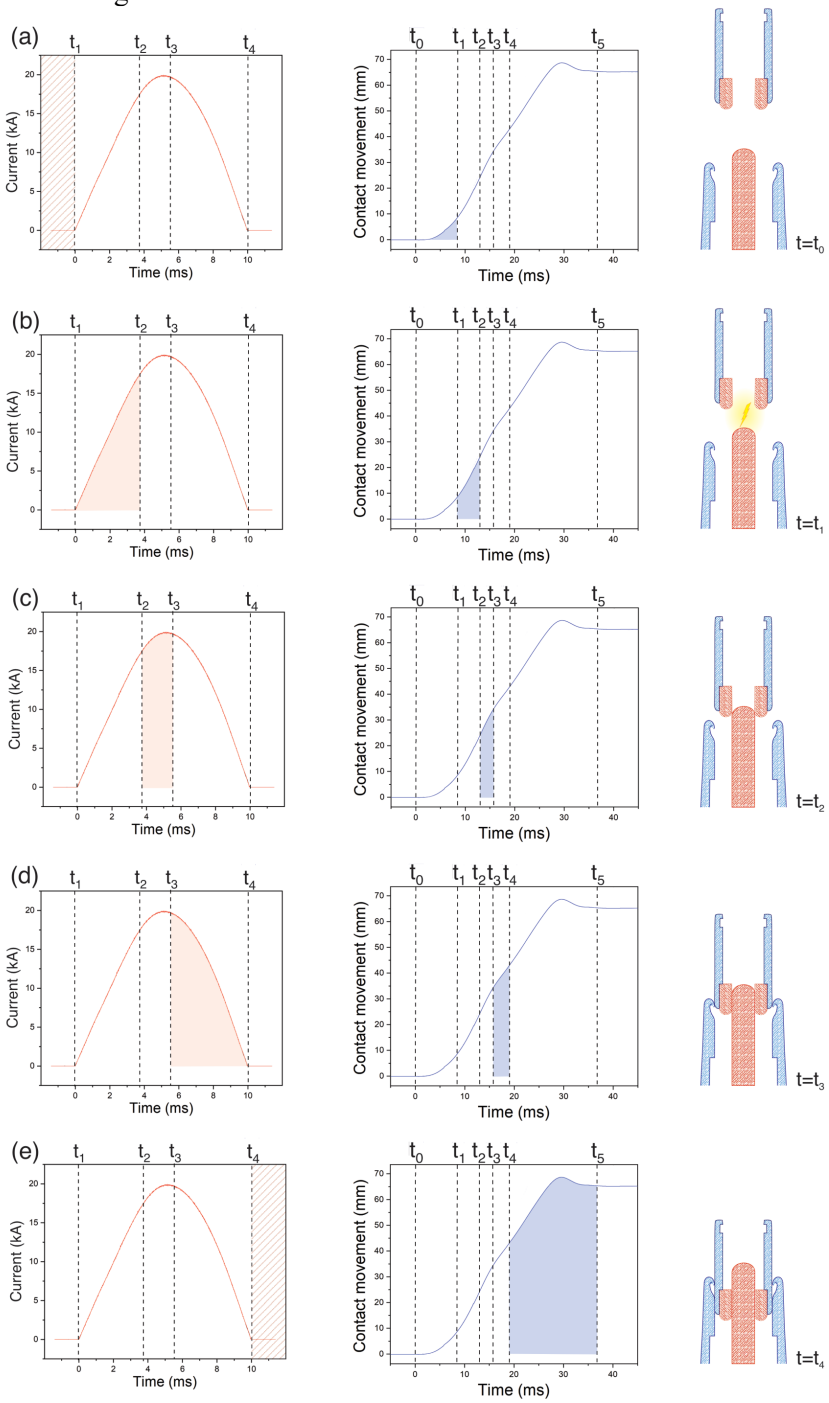

Figure 11. making operation over the process time, (a) high voltage interval, (b) pre-arcing interval, (c-e) latching interval. The first column is the current waveform, the second one is the travel curve, and the third one shows arcing (red) and main (blue) contacts.

The main intervals could be categorized as follows according to IEC 62271-101 [5]:

High-voltage interval (t_0-t_1):
The high-voltage interval is the period from the release of the dynamic contact in the open position to the moment of breakdown across the arcing contact gap. During this interval, the test circuit could stress the switch due to the starting conditions for the arc ignition (Figure 11 (a)). At this stage, there is no current flow through the contacts.

Pre-arcing interval (t_1-t_2):
The pre-arcing interval is the period from the moment of breakdown across the contacts gap to the touching moment of the arcing contacts. During this interval, the switch is subjected to electrodynamic forces due to the flow of high current through the conductive arc column and deteriorating impact of dissipated arc energy in contacts erosion (Figure 11 (b)).

Latching interval (t_2-t_5):
The latching interval is the period from the touching moment of arcing contacts to when the contacts reach the fully closed position- when the dynamic contact stops moving. Considering the presence of main contacts and short circuit current zero after approximately 10 ms, the latching interval is divided into three parts: shown in figure 11 (c-e), where t_2-t_3 is the time duration when the arcing contacts are in touch. t_3 is the moment when the main contacts meet. Thus, after t_3 the short circuit current passes through both arcing contacts and main contacts. t_4 is the zero-crossing of the short-circuit current. The switch is stopped moving at t_5. During these intervals, the switch is stressed by the contact friction forces and the electrodynamic forces due to high current flow, reducing the closing speed by repelling the contacts.

3.2 MEASUREMENT METHODS

Laboratory diagnostic methods for electrical characterization and understanding the pre-strike arc behavior could facilitate the evaluation of the switch operation while closing under fault conditions. Optical emission spectroscopy is employed to study the pre-strike arc behavior, and the electrical characterization is performed for the entire making process.

3.2.1 Optical Emission Spectroscopy

Arc emission spectroscopy is employed to study the pre-strike arc properties in time and space evolution, including arc dynamic motion and temperature. The

optical setup is designed to record temporal and spatial-resolved spectroscopy. Since the formation of the pre-strike arc is approximately independent of the size of the arcing contact, a 6 mm diameter for the stationary contact is chosen to cover the full width of the pin in the observation window. For this purpose, the pin diameter is chosen 6 mm, and the outer diameter of the tulip is 15 mm.

Optical Emission Spectroscopy (OES) records the arc composition changes close to the stationary contact surface (Pin). During the arcing time, the optical emissions from different particles are analyzed to reach the pre-strike arc properties. The spectroscopic setup consists of a spectrograph (Princeton Instrument Acton SP-300i) and a high-speed camera (Photron FASTCAM mini UX50) with a 1280×1024 pixel matrix. Figure 12 shows the schematic of the spectroscopic setup and the position of the observation window. The spectrograph has a focal length of 300 mm, 600 lines/mm grating, and slit width of 10 µm. The cathode's front-face is imaged to the spectrograph entrance slit since most injection of metallic particles to the arc column is expected from the cathode surface (Figure 12 (a)- red dashed line). The recording speed is set to 25000 fps with an exposure time of 30 µs to reach a good side-on view and time evolution of the arc while the contacts are approaching. Different closing speeds are investigated with a recording speed of 10000 fps with an exposure time of 80 µs. Because of the limited bandwidth in video spectroscopy and the high transition probability of copper species compared to tungsten, the emission spectrum bandwidth of 472-537 nm was chosen to include the major atomic and ionic copper emission lines as required for arc temperature calculation. The spectral and spatial resolutions are ~0.15 nm and ~8 pixels/mm, respectively.

Arc emission spectroscopy determines excitation temperature that can be calculated using the Boltzmann plot method under the Local Thermal Equilibrium (LTE) condition. The method is widely used for plasma temperature measurement [23, 28]. The dependency of integrated intensity I_{ul} of the recorded spectral lines

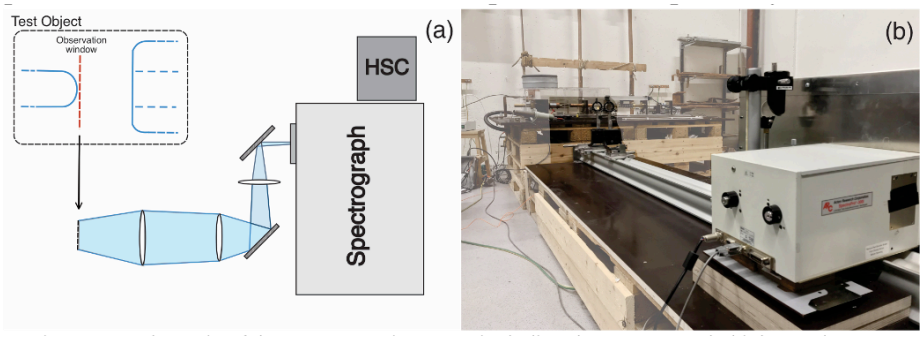

Figure 12. Schematic of the spectroscopic set-up, including the spectrograph, high speed camera (HSC) showing the location of the observation window (a), and a view of the experimental set-up (b).

which transmit from upper energy level E_u to lower energy level E_l to plasma temperature T is given by:

$$I_{ul} = \frac{hc}{4\pi \lambda_{ul}} A_{ul}\, g_u\, \frac{n_u}{P} L \exp\left(\frac{-E_u}{k_B T}\right) \quad \text{Eq. 3}$$

Where h is the Planck constant, c is the speed of light, L is the length of the arc, A_{ul} is the transition probability, λ_{ul} is the transition line wavelength, n_u is the number density, P is a partial function, g_u is the upper-level degeneracy, and k_B is the Boltzmann constant. Normalizing the output spectra with an instrumental profile of the spectroscopic system makes it possible to measure different plasma properties like electron density, pressure, temperature, and different emitted species density [24, 29-31]. However, it is possible to directly reach arc temperature by considering at least two emission lines that are spectrally integrated [28]. The arc temperature can be calculated from the inverse slope of the Boltzmann plot as follows:

$$\frac{1}{T} = \frac{k_B}{(E_{u2} - E_{u1})} \ln\left(\frac{I_1 \lambda_1}{g_{u,1} A_{ul,1}} \times \frac{g_{u,2} A_{ul,2}}{I_2 \lambda_2}\right) \quad \text{Eq. 4}$$

The chosen spectral lines for Eq. 4 should have enough excitation energy gap for temperature measurement. Since the equation is derived for a ratio of spectral lines emission intensities, an absolute calibration of the intensities is not required. The applicability of Eq. 4 is also limited to LTE and optically thin plasma conditions. CuI emission spectral lines at 510.55, 515.32, and 521.82 nm are well suited for Boltzmann Plot method-based arc temperature measurement because of the energy gap of 2.4 eV between excitation energy levels. This approach is followed in this work for measuring the pre-strike arc temperature. The three lines are used to check the validity to apply the Boltzmann plot method, and the spectral lines at 510.55 and 515.32 nm are used to calculate the arc temperature by Eq. 4.

A different spectroscopy setting is adjusted to reach a higher spatial resolution to investigate the switching arc ignition. For this purpose, a low current making operation is performed using a 0.7 µF capacitor in the high voltage circuit without using the high current part. The discharge resistor R2 chooses two different pre-strike arc durations. The spectrograph slit is set alongside the arc root. A recording speed of 80000 fps with a spatial resolution of 26.2 Pixels/mm is chosen to record the emitted species distribution in the arc column. A detailed description of the setup can be found in Paper I.

3.2.2 High-Speed Photography

A limitation in OES is the observation window. High-speed photography could be a complementary method to visualize the arcing evolution at different stages to confirm the results obtained by emission spectroscopy for arc dynamic motion. However, arc emitted light needs to be filtered to avoid image saturation, resulting in losing the whole arc dimension and boundaries.

A monochromatic Photron NOVA S16 camera is chosen for arc photography. A proper set of optical lenses and neutral density filters are chosen to record arc evolution with a speed of 100000 fps and an exposure time of 3.3 µs.

3.2.3 Electrical characterization

Measuring the current and voltage is necessary for calculating the pre-strike arcing energy. The energy corresponds to the ohmic loss when the contacts are in touch at different stages of closing movement. A Rogowski coil measures the making current. Measuring the arc voltage is challenging because of the inherent system response. The response of the measurement system to an abrupt change from many tens (or hundreds) of kilovolts to zero causes of distortion in the measured voltage waveform. Two different voltage measurement methods are proposed as direct and in-direct measurements.

Direct voltage measurement:

The dramatic change of voltage distorts low values as arc voltage which needs to be corrected. Previous studies have proposed a deconvolution-based correction [32, 33]. Various methods based on convolution/deconvolution techniques in frequency and time domains have been introduced to correct the measured voltage waveform in many applications [34-37]. However, to apply these methods, some knowledge about the impulse response of the measurement system is required.

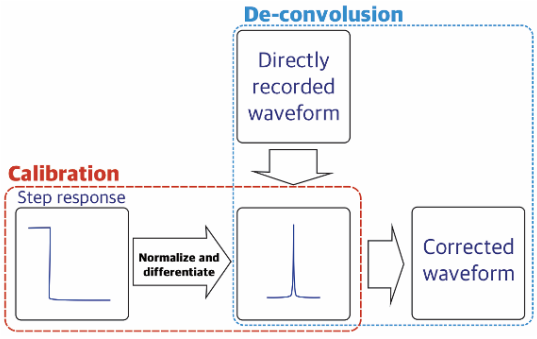

Figure 13. Procedure of directly measured voltage waveform correction using step-response and de-convolution method.

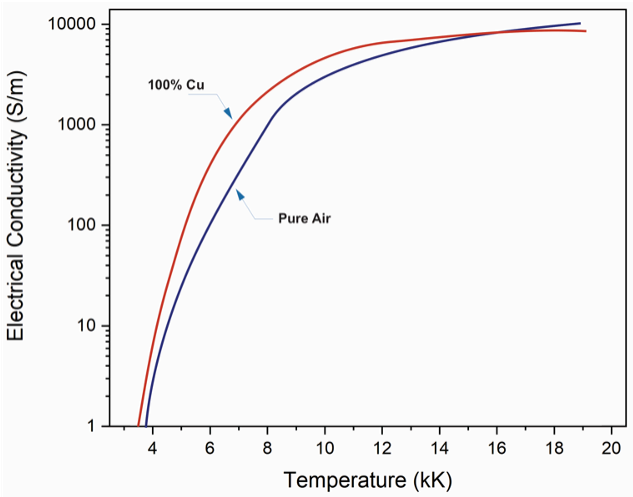

Figure 14. Electrical conductivity as a function of temperature for dry thermal air plasma and 100% saturated with copper vapor adapted from [38]

For correcting the direct measured pre-strike arc voltage, the step response of the measurement system is recorded to identify the system error, and a discrete classical time-domain deconvolution derived by a set of equations is applied for all the measurements. A schematic of the correction process is presented in Figure 13, and a detailed description of the method is presented in [paper IV].

In-direct voltage measurement:

There is a possibility to calculate the arc voltage using arc temperature measured by OES. Referring to thermal air plasma transport properties at atmospheric pressure, the electrical conductivity of the pre-strike arc can be estimated by the dependency on arc temperature (Figure 14).

The arc column dimension needs to be determined to measure the arc resistance and subsequently arc voltage using the directly measured arc current. Assuming that the pre-strike arc is cylindrically shaped, the arc length can be approximately determined by using the travel curve of the dynamic contact (see Figure 11). For the cross-sectional area, Lowke's analytical model of free-burning arcs is employed [19]. The model is based on theoretical prediction and experimental measurements of high current arcs at atmospheric air pressure. The arc radius expression is derived from the conversion equations for energy and momentum as follows:

$$R = 1.11 \left(\frac{z}{h\sigma}\right)^{\frac{1}{4}} I^{\frac{3}{8}} \Big/ (\mu j_o \rho)^{\frac{1}{8}} \qquad \text{Eq. 5}$$

where h is enthalpy and $\mu = 0.126$ dyne/A^2. The agreement of the theory and experiment by Lowke is evidence that j_0 is constant with changes in current. Otherwise, the theoretical predictions differ markedly from experiments. Therefore, an estimated error of 20% is considered because of uncertainty in the value of j_0.

3.2.4 Contacts' Mass Loss

Electrical contacts' mass loss indicates erosion during the making process, as discussed in 2.4. Therefore, the arcing contacts mass loss is measured after each test to find a correlation between the contacts erosion and the different parameters involved in making the operation. The arcing contacts, including the pin as the stationary contact and the tulip as the dynamic one with a total average weight of ~52 g, are shown in Figure 15. The low average weight of arcing contacts makes it possible to measure the contacts' mass loss with a precise scale with an accuracy of ±0.00001 g. Figure 15. shows an example of eroded arcing contacts with a mass loss of 53.302 mg. To avoid the contacts being contaminated during the process, each pair of contacts were kept in a separate enclosure. No specific cleaning procedure was used to be close to the actual operation.

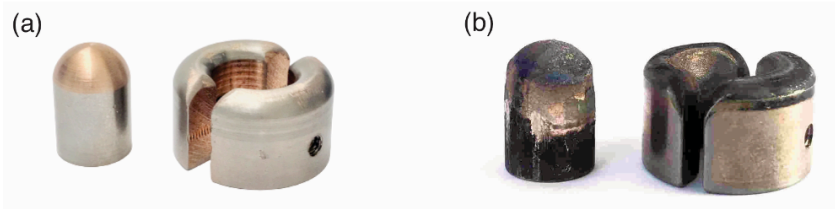

Figure 15. Arcing contacts made of W/Cu (80/20) before (a) and after (b) making tests with total mass loss of 53.302 mg.

Chapter 4
Summary of Results and Discussion

This chapter summarizes results obtained by the diagnostic methods described in Chapter 3.
The results are divided into optical and electrical investigations, referring to the corresponding papers. The chapter is followed by published articles for detailed results and discussions regarding the investigation on making operation in medium voltage load break switches.

4.1 OPTICAL INVESTIGATION

The optical investigation focuses on the pre-strike arc formation and its dynamic behavior while the arcing contacts are approaching. This investigation refers to the "pre-arcing interval (t_1-t_2)" described in section 3.1.3 (Figure 11-b). The arc emission spectroscopy is employed in two settings to investigate arc ignition and the evolution in time and space.

4.1.1 Pre-strike Arc Ignition

A high current arc ignited by an electrical breakdown emits high-intensity light which could saturate the high-speed camera. Therefore, a low current model switch is used to evaluate the pre-strike arc ignition by implementing the high voltage circuit with two different capacitances instead of the entire synthetic test circuit.

The arcing contacts material has a refractory microstructure of 20% copper and 80% tungsten. The first emission spectrum of the arc at 25 µs shows a sharp emission peak of tungsten at 518.4 nm, indicating the ablation of tungsten to reach more conductive regions of copper for carrying the short circuit current. The

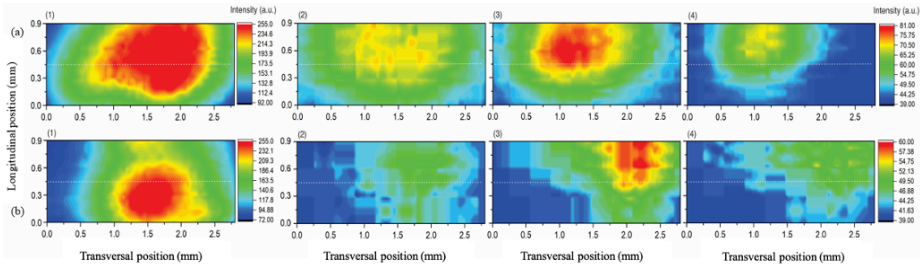

Figure 16. 2-D distribution of copper vapor (521.8 nm) at anode for the arc current profile 1 (a) at 50 µs (1), 112.5 µs (2), 137.5 µs (3), and 412.5 µs (4) and for the arc current profile 2 (b) at 25 µs (1), 162.5 µs (2), 350 µs (3), and 412.5 µs (4).

following recorded arc emission spectra show more intense copper's atomic emission lines, which indicates the evolution of metal vapor in the medium.

Figure 16 shows the time evolution of spatially resolved spectroscopy close to the surface of the anode. Two current profiles are examined; the first current amplitude starts at 200 A and decays to almost zero within 270 µs, and the second begins at 80 A and lasts for 600 µs. The arc is ignited when the contacts are at a distance of 7 mm while are closing with a speed of 3 m/s according to the dynamic contact travel curve. The spatially resolved distribution of metal content makes it possible to trace particles in the arc column. The first 50 µs of arcing time shows the highest concentration of metal content for both current profiles at copper atomic emission lines, which is partly diffused afterward. A fraction of the metallic particles moves across the arc axis, as shown in Figure 16. This observation contrasts some computational studies that showed no displacement of metal vapors when the arc current is lower than one kiloampere [39, 40].

The increase in metal vapor concentration could result from either the cathode surface evaporation or a part of the copper vapor evaporated from the anode surface. However, the clear point is that the distribution of metal vapor is inhomogenous in the axis of the arc column due to the closing operation. The pre-strike arc ignition emission spectroscopy results are presented in [Paper I].

4.1.2 Pre-strike Arc Dynamic Motion

The spectrograph slit width is reduced to 10 µm to minimize the probability of camera saturation due to high intense arc emitted light. By reducing the slit width compared to the setting for low current pre-strike arc spectroscopy, the spatial resolution is reduced from 26.2 Pixels/mm to 8 Pixels/mm. However, the obtained

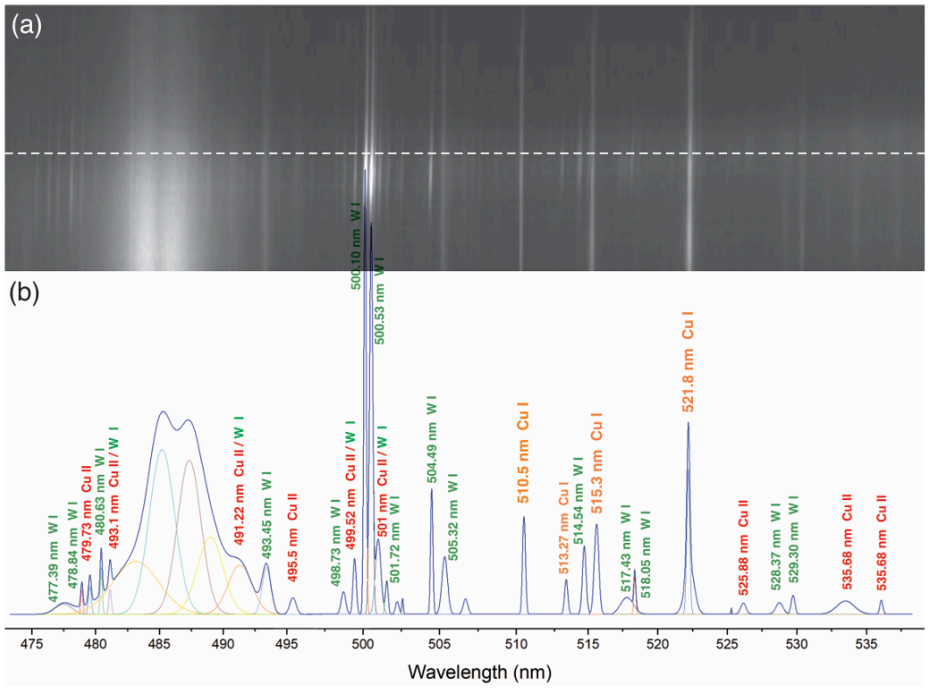

Figure 17. (a)An example of 2D spectrum with exposure time of 30 µs recorded during pre-strike arc, (b) Spectral arc emission wavelengths for the dashed line shown in 2D spectrum.

spectral resolution of ~ 0.15 nm makes it possible to measure distinctive emission wavelengths for calculating different parameters like the arc temperature. On the other hand, there are some limitations regarding the observation window position in arc emission spectroscopy with dynamic contact, making it difficult to scan the whole arcing time evolution because it partly burns inside the dynamic tulip contact before the touch moment. In addition, the spectral bandwidth is limited to 65 nm for this optical setting, which is set to 472-537 nm to include the significant atomic and ionic copper emission lines required for arc temperature calculation.

As discussed in section 3.2.1, the arc temperature is measured by spectrally integrated CuI emission lines at 510.55, 515.32, and 521.82 nm using the Boltzmann-Plot method (Eq. 4). An example of a two-dimensional emitted spectrum at 240 µs of arcing time with 30 µs exposure time is shown in Figure 17 (a). The white dashed line indicates the position of spectral arc emission wavelengths presented in Figure 17 (b).

Figure 18 (a) shows the pre-strike arc temperature profile, and the short circuit current waveform for the making operation is shown in Figure 18 (b). The pre-strike arc burns for 1.2 ms before the contacts touch. The grey shadowed region marked in the current waveform shows part of the arc current scanned by OES. The arc dynamic motion can be inferred from the temperature profile. The arc

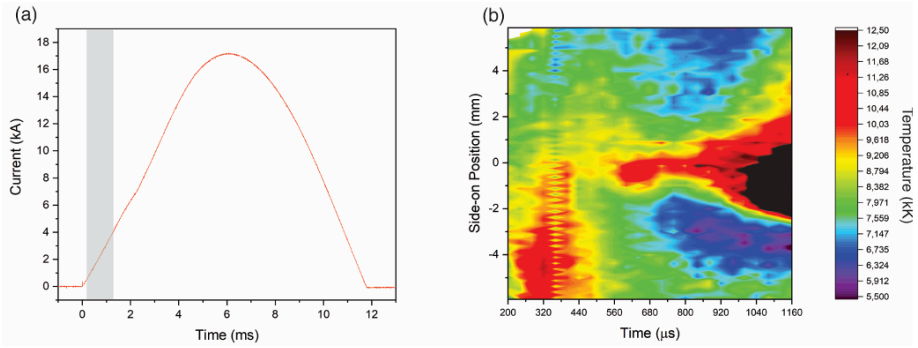

Figure 18. (a) the short circuit current waveform and (b) the arc temperature profile for the shadowed part of the current waveform.

ignites in the lower half of the cathode (stationary contact) and moves to the center while the contacts are closing. A temperature drop is observed in the time interval of 400-560 µs before the arc is stabilized in the center, considering the highest temperature in the center of the arc column. The contact movement could cause the arc to cool during the closing operation by creating a gas flow blowing the arc. A few tests have been conducted under the same test conditions for reproducibility. Similar arc composition and approximately equal species emission intensities have been observed. The difference is in the spatial distribution of emission lines in the side-on position for the first 500 µs because the arc ignites randomly at different spots of the contact surface. The rest of the arc burning time results in similar coherent temperature behavior in all the tests, like the arc temperature shown in Figure 18 (b) between 500 and 1160 µs. A detailed description of the optical setting and the pre-strike arc temperature calculation can be found in [Paper II]. The investigation by OES for different closing speeds shows that the arc cross-section increases by increasing the closing speed. This speed results in higher conductivity and subsequently lower arc voltage by increasing closing speed, which agrees with direct arc voltage measurements. Detailed results can be found in [Paper VI].

High-speed photography could also visualize the dynamic arc motion, as discussed in section 3.2.2. The recording has been done for a breakdown voltage of 20 kV and short circuit current at case 1 shown in Figure 21. The eroded surface of arcing contacts caused an arcing time of 4.7 ms. Using a neutral density filter with a transmittance of 0.09 resulted in the sequence of images of the pre-strike arc evolution shown in Figure 19. The contacts are placed horizontally while the pin is constant and the tulip is moving. Although most arc emission is filtered, the arc root is still visible while contacts are closing. It can be seen that the arc motion is limited to the distance between the contacts. It could result from electromagnetic forces and/or the air flow due to contact movement. The result is

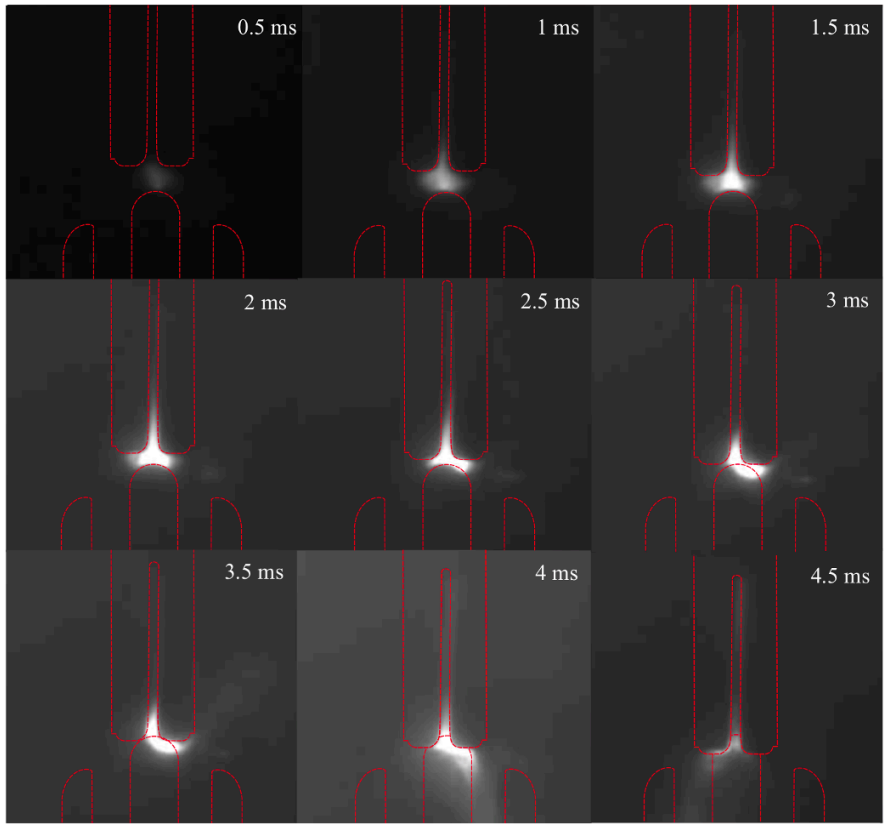

Figure 19. High-speed photography of pre-strike arc evolution for ~4.7 ms arcing time at peak current of ~ 20 kA (closing speed 3 m/s).

in good agreement with the arc dynamic motion inferred from the arc temperature profile obtained by OES close to the surface of stationary contact.

4.2 ARC ELECTRICAL PROPERTIES

The contact surface erosion could be resulted from partly absorbing the dissipated pre-strike arc energy, as discussed in section 2.4. Therefore, finding the correlation between dissipated arc energy and the contacts mass loss could provide quantitative aspects of arc erosion on closing the switch. This result could be possible by measuring the arc voltage and current, as discussed in section 3.2.3.

The pre-strike arc voltage is calculated using the obtained spectroscopy results as indirect measurement methods (section 3.2.3). The arc voltage waveform can be approximately estimated using the temperature profile (Figure 18 (b)), arc dimension by Lowke's model and the travel curve, and the thermal air plasma properties (Figure 14). However, there are still some limitations. Since the density of copper vapor is not clear to achieve the exact arc conductivity, the voltage is

measured for the arc free of copper vapor and 100% saturated with copper vapor. Therefore, the voltage could be limited to the area bounded by two curves shown in Figure 20 (a). In addition, the arcing time is limited to the observation window, where the optical system can detect the emitted light. A comprehensive description of the method can be found in [Paper II].

The deconvolved waveforms as the direct voltage measurement method show approximately similar changes in arc voltage, although there is a clear difference in directly measured waveforms. In all the cases, the corrected arc voltage increases to less than 60 V and gradually increases until the voltage falls from ~17 V to zero. The voltage-drop recorded in all the measurements corresponds to the cathodic plus anodic voltage for tungsten/copper (80/20) as the material of the electrical contacts [4, 41]. Comparison between deconvolved waveforms in time and frequency domains shows a slight difference, stemming from noise interference in the correction process. In addition, the low sampling rate could be another factor in increasing the uncertainties in frequency domain deconvolution. An example of a corrected arc voltage waveform by deconvolution in the time domain is shown in Figure 20 (b). A full description of the deconvolution in time and frequency domains is explained in [Paper III].

The deconvolved waveforms are compared with the in-directly measured voltage waveform (Figure 20) to prove whether the arc voltage range is in the correct order. Despite the mentioned uncertainties and limitations in the measurement methods, the peak voltage value is measured in the range of 30-58 V by the indirect method, which matches the values of the deconvolved voltage waveforms with a maximum voltage of 40-52 V obtained using the deconvolution method.

The time-domain deconvolution is chosen as the correction method to apply to the discrete output voltage values of the measurement system to achieve stable

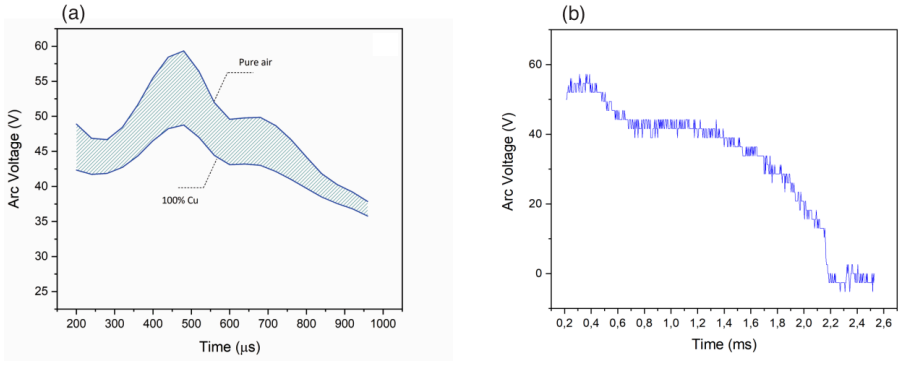

Figure 20. The pre-strike arc voltage calculated by in-direct measurement method based on arc emission spectroscopy (a), and the direct method based on deconvolution in time domain (b).

results. Consequently, the arc energy is measured using the corrected voltage waveform to evaluate the model switch operation in closing against fault current.

4.3 SWITCH FAILURE UNDER FAULT CONDITION

The experiments are designed to achieve the highest level of arc energy (Figure 5 (c)), to testify the test object as the model LBS switch explained in section 3.1.2. Two levels of short circuit current and breakdown voltages of 10 and 20 kV, which are equivalent to rated voltages of 12 and 24 kV, are examined. Figure 21 (a) shows half-cycle 50 Hz current waveforms considered two short circuit current levels used in the experiments. Figure 21 (b) shows arc voltage waveforms for a series of making tests on one pair of arcing contacts under the short circuit current of case 1.

The difference in breakdown voltages is discussed in [Paper V], where the important contact erosion observed for higher arcing times resulted from higher breakdown voltages for constant short circuit current. As a result, the experiments continued with a breakdown voltage of 20 kV for evaluating the switch operation in making a short circuit current.

In the following, the role of main contacts in extending the switch service life is investigated for two closing speeds. The switch operation is evaluated based on the time intervals discussed in section 3.1.3.

4.3.1 Pre-arcing Interval

For the model switch, including the arcing contacts (without the main contacts), the switch failed to reopen after the fourth test in case 1, with a closing speed of 3 m/s. The failure for the switch with arcing and main contacts happened after seven successive operations at short-circuit current in case 1 and a closing speed of 3 m/s. The breakdown voltage for both cases has been 20 kV.

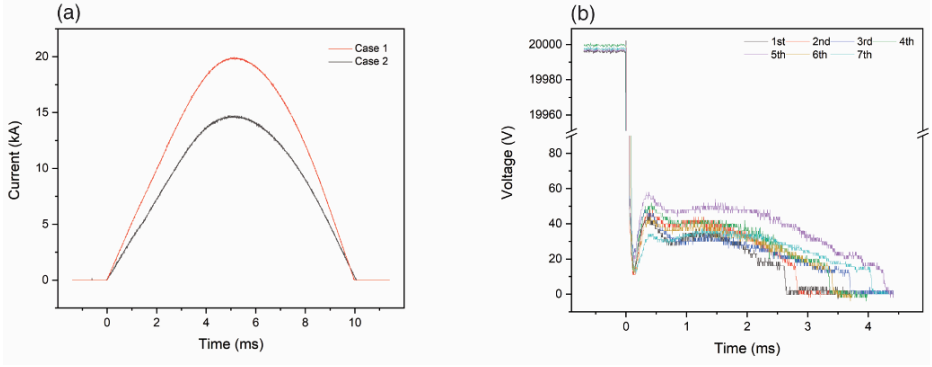

Figure 21. Half-cycle 50 Hz short circuit current with a peak of 14.8 and 20.2 kA (a), Arc voltage measurements for seven successive tests at Case 1 (b).

As discussed in section 2.4, the contribution of arc energy dissipation in contact erosion is still controversial and complicated. After each test, the arcing contact mass loss and arc dissipated energy are measured to find a correlation between the contacts erosion and the arc dissipated energy. The mass loss is a function of total arc energy (Eq. 2) to perform a comparative analysis regarding the arc energy factors affecting the contacts erosion. The energy calculated by cathodic and anodic voltage fall is presented in Figure 22 and Figure 23, respectively. It can be inferred that the variation of total dissipated arc energy is more pronounced than the electrode fall energy with the increase in the electrodes' mass loss. There is a significant difference between them in a high mass-loss rate. The mass loss correlation with arc energy and electrode fall energy is measured with a good coefficient of 0.97 and 0.94, respectively. Since the process of arc interaction with electrical contacts surfaces is not clear, it could be recommended to consider the total arc energy as the main factor in contacts erosion during the pre-arcing interval. Besides, it can be seen that the same amount of total arc energy at different current levels causes approximately the same contacts mass loss (Figure 22). The results obtained for the electrodes' fall energy are shown in Figure

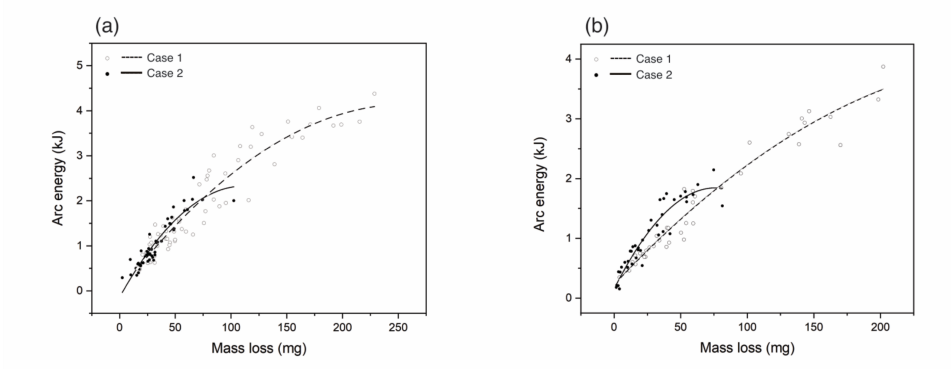

Figure 22. The mass erosion rate as a function of pre-strike arc energy for a series of operations with (a) and without (b) main contacts.

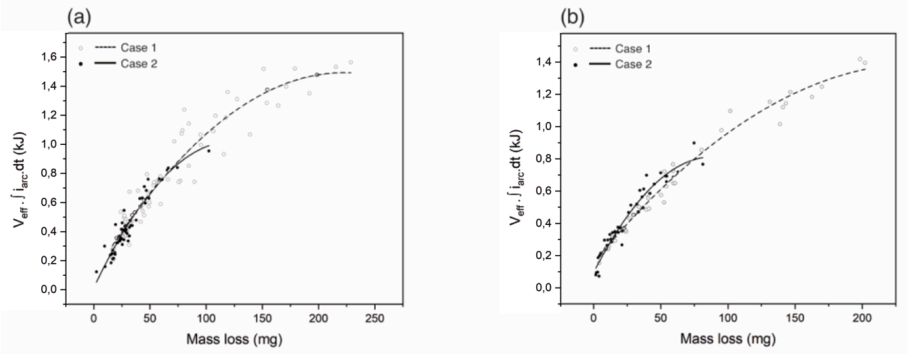

Figure 23. The mass erosion rate as a function of electrodes fall energy for a series of operations with (a) and without (b) main contacts.

23. However higher level of short-circuit current increases the probability of a higher amount of dissipated energy, taking into account that the arcing time could not be longer than the first half-cycle of short-circuit current.

4.3.2 Latching Interval

The latching interval is the time duration from arcing contacts touch moment to the time contacts reach the fully closed position (Figure 11 c-e). The possible destructive force involved in the switch failure due to contacts welding is ohmic loss. After the arcing contacts touch, the fault current flows through the molten contacts, contributing to more energy dissipation. A part of current flows through the molten bridge between sliding contacts, further increasing the dissipated energy and possibly contributing to the contact deterioration. While closing the switch, expansion of the molten zone between two sliding contacts changes the contact resistance during latching time [42]. A separate voltage measurement is performed from arcing contacts touch to the end of short circuit current flow (latching time) to measure the resistance. Subsequently, the destructive energy corresponded to ohmic loss. An example of the voltage across the sliding contacts during latching time is shown in the zoom-in part of Figure 24.

The resistance of sliding contacts during latching interval is calculated for operations with just arcing contacts for four successive testing with a closing speed of 3 m/s which resulted in the contacts welding, and for six successive testing with a closing speed of 4 m/s. To estimate the energy dissipated by the ohmic losses between the arcing contacts, an equivalent circuit at the stage of arcing contacts touching, and the position where the main contacts approach (if any exists) is considered as shown in Figure 25 (a) and, Figure 25 (b) respectively. r_c is the resistance of the contacts' touchpoint where the surface temperature is

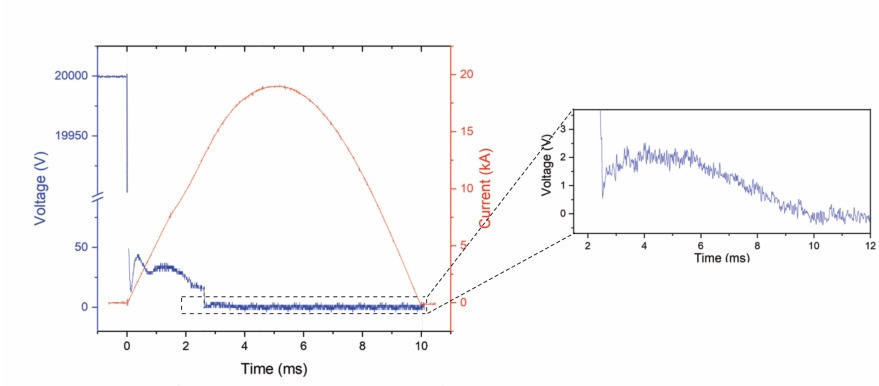

Figure 24. Typical current and voltage waveforms in a full making operation (Zoom-in; latching time).

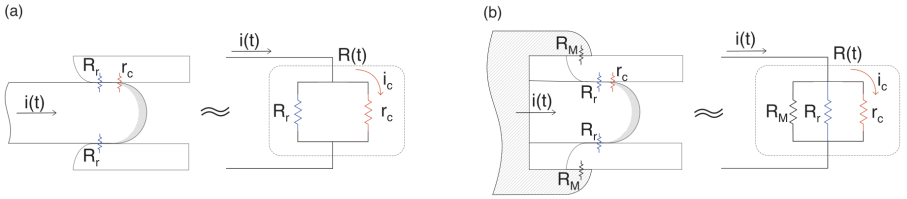

Figure 25. Schematic of the switch in closed position and the equivalent circuit with arcing contacts (a) and arcing and main contacts (b).

highest (and the surface is probably molten) due to exposure to the pre-strike arc. R (t) is the total resistance between the switch contacts. If the main contacts are involved, R_M is the resistance of the main contacts in the closed position, which is considerably smaller than r_c. Therefore, if the main contacts exist in the switch, most of the current passes through them, increasing the switch service life from four series of operations to seven times based on the obtained results. The current flowing through the contacts' touchpoint (i_c) is defined as follows:

$$i_c(t) = i(t) \,.\, \frac{R(t)}{r_c} \qquad \text{Eq. 6}$$

Where i(t) is the total current flowing through the switch, r_c is the resistance of the touchpoint at t_2, according to Figure 11 (c). Consequently, the energy dissipated (Ohmic losses) when the arcing contacts touch is described as follows:

$$E_c = \int_{t_2}^{t_4} r_c \,.\, i_c^2(t) \,.\, dt = \int_{t_2}^{t_3} \frac{R_1^2(t)}{r_c} \,.\, i^2(t) \,.\, dt + \int_{t_3}^{t_4} \frac{R_2^2(t)}{r_c} \,.\, i^2(t) \,.\, dt \qquad \text{Eq. 7}$$

Where $R_1(t)$ and $R_2(t)$ are the total resistance between the switch contacts without (Figure 25 (a)) and with (Figure 25 (b)) main contacts, respectively, the timing t_2-t_4 is defined according to Figure 11. Table 3 shows detailed time intervals during arcing and latching stages for one of the measured series. The ohmic loss is calculated for each case. An increase can be seen in arcing time after each test t_2-t_3 is going to be smaller, which indicates the arcing contacts erosion. The reduction continues until t_2 becomes equal to t_3, which means the arc still burns between arcing contacts when the main contacts touch (if any). This contact causes partial arc formation between the main contacts leading to contact erosion.

4.3.3 Extension of Results to Standard Stress Conditions

Comparing the Ohmic loss energy (E_{OL}) shown in Table 3 with the dissipated arc energy discussed in section 4.3.1 in both forms of total arc energy (Figure 22) and

Table 3. Making operation time intervals and Ohmic losses at two closing speeds (3 and 4 m/s) with arcing contacts at case 1.

Closing speed	Test number	t_{arcing} (ms)	$t_{latching}$ (ms)		E_c (J)	
			t_2-t_3	t_3-t_4	t_2-t_3	t_3-t_4
3 m/s	1	3.4	1.15	4.35	62.9	38.7
	2	5.3	0.73	5.17	46.1	126.2
	3	6.1	-*	4.23	-	90.4
	4	6.4	-*	5.1	-	182.2
4 m/s	1	3.6	0.68	5.82	29.07	131.6
	2	4.2	0.77	5.93	43.98	156.5
	3	4.5	0.32	4.98	17.15	133.7
	4	4.6	0.33	4.87	16.5	121.5
	5	4.8	-*	5.29	-	139.2
	6	4.8	-*	5.06	-	134.4

*. at this timing, t_2 would be equal to t_3

the electrodes fall energy (Figure 23) shows E_{arc} is more than one order of magnitude higher than E_{OL}.

According to IEC 62271-103 [6], the duration of the short circuit current shall be at least 0.2 s. If the switch includes both arcing and main contacts, R_m as the resistance between the main contacts in the closed position is significantly smaller than r_c, which results in the flow of most of the short circuit current through the main contacts after t_3 (Figure 11). Therefore, the destructive joule heating energy that causes switch failure with main and arcing contacts could be defined as follows:

$$E_{destructive} = E_{arc} + E_{OL} \approx \int_{t_1}^{t_2} i_{arc}.V_{arc}.dt + \int_{t_2}^{t_3} i_c^2(t).r_c\,.dt \qquad \text{Eq. 8}$$

Therefore, it can be concluded that the most destructive impact of making operation on switch function occurs in the first half-cycle of short-circuit current, in which the pre-strike arc forms and the short circuit current flows through the sliding arcing contacts before the main contacts touch (t_1-t_3). Therefore, the results obtained for the first half-cycle could be extended for longer short circuit-making currents stated in IEC standards.

The presence of main contacts could prolong the switch's lifetime. However, it is not the final solution since the arcing contacts welding occurred after seven successive making operations (Case 1). Increasing the closing speed is one of the solutions to reduce the impact of pre-strike arc on switch failure in operation. The results show that a slower mass loss and less dissipated arc energy are achieved

by increasing the closing speed. Detailed results regarding these parameters can be found in [Paper IV].

Paper I

Spectroscopic Investigation of Metal Content in Pre-strike Arc During Making Operation in a Low-Current Model Switch.

IEEE Transactions on Plasma Science, Vol. 48, NO. 10, pp. 3698-3704, October 2020.

Spectroscopic investigation of metal content in pre-strike arc during making operation in a low-current model switch

Naghme Dorraki, Kaveh Niayesh, *Senior Member, IEEE*

***Abstract* — Energy dissipation during pre-strike arc is the critical factor for electrical contacts erosion and welding in medium voltage load break switches. Using air-filled devices as an alternative to SF_6, makes the switch environmentally friendly, but leads to a more challenging process due to a higher pre-strike arcing time between contacts. Therefore, understanding the erosion process of electrical contacts is crucial to improve the switch lifetime. Determination of contacts surface evaporation by optical emission spectroscopy is one of the most precise methods to investigate the pre-strike arc interface with the contacts. In this paper, the temporal and spatial profiles of copper and tungsten emitted species during pre-strike arc are presented. For this purpose, a circuit consisting of a synthetic DC high voltage part is used to initiate the arc. The temporal evolution of CuI, CuII, and WI shows evaporation of the cathode and the anode surfaces during the pre-strike arc, and the spatial profiles show an inhomogeneous distribution of the vapors alongside the arc root.**

***Index Terms*—Arcing contacts, arc erosion, contacts evaporation, Load break switch, Medium voltage, Optical emission spectroscopy.**

I. Introduction

WITH power system development, there are more demands to cut costs. Circuit breaker as one of the primary devices in electrical networks to make, carry, and break the current in normal and abnormal operating conditions, have high maintenance costs due to several types of stresses, ageing and reliability requirements [1]. Medium voltage Load break switches (MV-LBS) could be an inexpensive alternative to circuit breakers in distribution networks [2]. There are several studies on current interruption for MV-LBS in order to improve and design environmentally friendly and cost-effective switches like compact air-based LBS [2, 3]. Beside current interruption, which is typically limited to less than 1kA, MV-LBS should be able to withstand a number of making operations under short-circuit currents of several tens of kilo amperes while avoiding severe contact degradation [4, 5]. Under fault conditions, the switch must be able to close the contacts at any time without welding them together and re-open for the next operation. Therefore, practical condition assessment is necessary to improve the stability and lifetime of MV-LBS regarding contacts erosion and degradation [4, 6].

Erosion of electrical contacts in making operation starts before the contacts touch due to a dielectric breakdown. Therefore, the switching is initiated from the pre-strike arc ignition, which can take up to a few milliseconds before contacts touch. The dissipated energy is partly absorbed by contacts surfaces and can heat them up to the melting and evaporation point, eventually leading to their welding. Even if contacts are separable for the next operation, the eroded surfaces could increase ohmic losses in the close position when current flows and rises the temperature while a low resistance is necessary to obtain a high rated load current [4]. Contacts erosion, because of heating up the surfaces, depends on some parameters, including arc energy, arc time, and material properties. Using air-based MV-LBS instead of SF_6 makes the switchgear environmentally friendly. Unfortunately, it also leads to a more challenging making operation due to a higher arcing time in air because of the lower dielectric strength compare to SF_6 [2, 7, 8].

Among several studies that have been done to investigate electrical contacts erosion during switchgear operation [8-14], arc spectroscopy can provide detailed information of contacts erosion as a result of arc interface [15, 16]. The interface of thermal arc plasma and electrical contacts surfaces causes evaporation of the contacts surfaces. Depending on the material of the contacts and the arcing energy, formed metal vapors can have a significant influence on the arc dynamic motion and properties [17, 18]. The relatively low ionization potential of such additives compared to atomic gases like oxygen and nitrogen modifies the arc conductivity and temperature [19, 20]. Temporal evolution and spatial distribution of metal vapors by optical emission spectroscopy (OES) could pave the way for a better understanding of contacts erosion due to arcing in switchgears.

The pre-strike arc with load current could be dominated by metal vapors [21]. The influence of metal vapors on arc

N. Dorraki and K. Niayesh are with the Department of Electric Power Engineering, Norwegian University of Science and Technology, 7491 Trondheim, Norway. (e-mail: naghme.dorraki@ntnu.no)

characteristics have been studied on free burning arc and arc welding by OES [20, 22]. Some unexpected findings have resulted like temperature fall in the center of arc due to the presence of metal vapors. These results emphasize the importance of a systematic investigation on determining the impact of critical parameters like metal vapors on arc dynamic motion and stability in MV-LBS. This study is a part of a systematic investigation of contacts erosion during making operation in MV-LBS.

There are some limitations in OES measurements for high intense light of the arc as optically thick plasma. Besides, the pre-strike arc burns in the first few milliseconds of currents starting from zero, and the majority of the current passes through the contacts in closed position. Therefore, the systematic investigation started with low-current arc to get an insight into the behavior of pre-strike arc with the highest spatial resolution. For this purpose, a test object with a spring-type drive mechanism is employed to simulate making operation, and an optical emission spectroscopy set-up is designed to record the temporal evolution and spatial profile of metal vapors while contacts are approaching.

II. Experimental Set-up and Methods

A schematic of the experimental arrangement consisting of the test circuit and the optical measurement system is shown in Figure 1. This circuit is a part of the full synthetic making circuit based on the IEC 62271-101 standard.

A. Test Circuit

The test circuit includes a 0.7 µF high voltage capacitor (C). The capacitance is selected in such a way that the discharge current doe not decay after few tens of microseconds and an arc still exists, so that the main current can flow through the pre-strike arc. The capacitor can be charged to a predefined charging voltage up to 20 kV through a resistor (R_1). Once the capacitor is fully charged to a selected voltage, switch S_1 is opened to disconnect the charged capacitor from the high voltage power supply. When a breakdown occurs between the closing contacts of the test object, the fully charged capacitor is discharged through resistor R_2 and further through the test object.

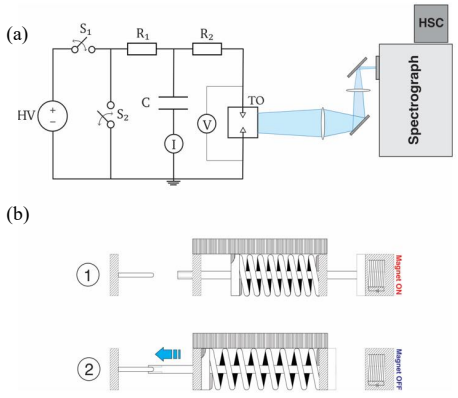

Figure 1. Schematic of the experimental set-up. (a) the test circuit and optical diagnostic set-up, (b) spring-type test object; (1) open and (2) close position

A Pearson current sensor measures the arc current. To avoid the interference of electromagnetic noises, an optical system transmits the measured data to record them [16, 23, 24].

The test object (TO) is a spring-type switch with axisymmetric arcing contacts (Figure 1(b)). The stationary contact (anode) is a pin with a diameter of 6 mm, and the dynamic one (cathode) is a tulip with an outer diameter of 15 mm. The electrical contacts are made of copper-tungsten (20/80), and the closing velocity is 3 m/s. The closing speed and the material type are chosen so that they do not differ too much from the commercial product.

B. Optical measurement

The time evolution of contacts evaporation together with spatial profiles under arc formation are recorded and analyzed employing video spectroscopy. In comparison with other methods for OES, video spectroscopy can provide information on both temporal evolution of different atoms, ions, and neutrals transitions and their spatial profiles simultaneously during a recording.

The spectroscopic set-up (Figure 1(b)) consists of a spectrograph with a 300 mm focal length with a 600 lines/mm grating (Princeton Instrument Acton SP-300i) and a high-speed camera (Photron fastcam mini UX50) with 1280×1024 pixel matrix to record the time evolution of pre-strike arc. The set-up is aligned in 1.2 m from the anode with 26.2 pixel/mm spatial resolution. For all the measurements, the spectrograph slit is set alongside the arc root to obtain quantitative information on metal vapor distribution between the contacts with a focus on the anode.

III. Results

In this section, the interface of arc and anode surface is investigated by electrical measurement and optical emission spectroscopy, which includes both time-resolved and spatial-resolved spectroscopy.

A. Electrical characteristics

To make the pre-strike arc, the capacitor is charged to 18.5 kV and connected to the anode. The arc burns between contacts while the closing operation is performed and the contacts are approaching. Experiments are carried out to study the effect of arcing time on contacts degradation at low currents. Two different pre-strike arc durations are chosen by setting the discharge resistor R2. The current waveforms are shown in Figure 2 (b). The current amplitude starts at 200A for the current profile 1 and decays to almost zero within 270 µs, and the current profile 2 begins at 80A and lasts for 600 µs. Travel-curve of the dynamic contact could reveal the condition of the operating mechanism. Figure 2 (a) shows the travel-curve profile of the moving contact (i.e. cathode). At the time of 31.88 ms, the arc is ignited, and the cathode has reached the anode at 33.84 ms.

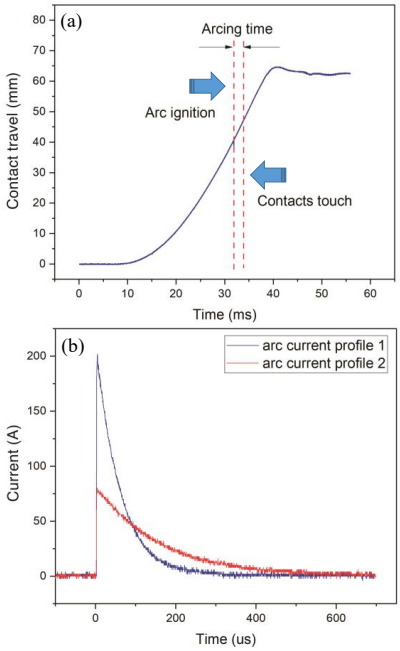

Figure 2. (a) Travel-curve profile of the dynamic contacts, (b) arc current waveforms

B. OES

1) Spectral Bandwidth

To get information on which species are emitted during the pre-strike arc, a series of two-dimensional spectra is recorded with a spectral resolution of ~0.4 nm, recording speed of 40000 fps and an exposure time of 20 µs. The arc current profile 1 is applied for this series of recording. Since the probability of copper emissions is higher than tungsten due to their physicochemical characteristics, the spectral range of 473-538 nm is chosen, which is dominated by atomic and ionic spectral emission lines of copper. Figure 3 shows the observation window of the spectrometer and an example of the recorded 2-D spectral emission lines at 0.4 nm spectral resolution. For temporal evolution analysis, 1-D spectrum is chosen at the

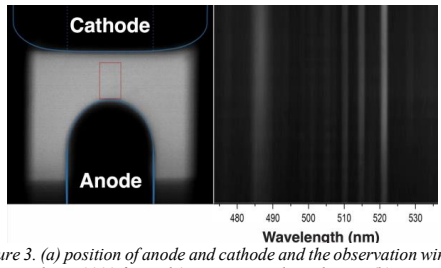

Figure 3. (a) position of anode and cathode and the observation window for recording 40000 fps and 0.4 nm spectral resolution. (b) an example of the spectral lines.

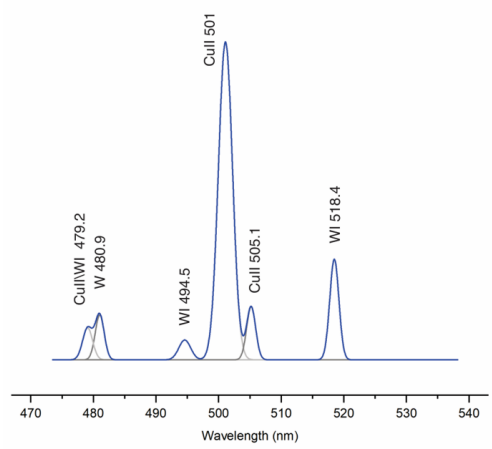

Figure 4. Spectral profile from 2 mm above anode at 25 µs.

position of ~2 mm above the pin (anode) where the maximum intensity of emission lines is reached. The wavelength bandwidth is chosen around 505 nm, where copper spectral lines dominate the emissions. However, some emission lines of tungsten and hydrogen beta Balmer line (Hβ) are also detected.

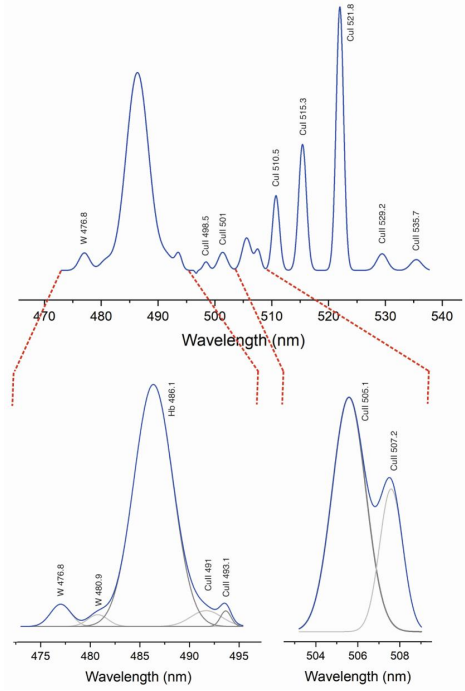

Figure 5. Spectral profile at 100 µs with peak fitting for two overlapped sections.

TABLE 1
WAVELENGTH OF ATOMIC AND IONIC EMISSION LINES USED IN THIS WORK

Species	Wavelength (nm)
CuI	510.5, 515.3, 521.8
CuII	491, 493.1, 501, 505.1, 507.2, 535.7, 529.2
WI	494.5, 518.4
Hβ	486.1
*Undefined**	479.2, 480.9, 476.8

*Close transition levels made it impossible to distinguish some species between WI/II and CuII

Recorded spectral lines in the first 25 µs of the arcing show a different type of species emission lines compared to the rest of arcing time. Figure 4 shows well-resolved spectral lines for this moment. The spectrum is achieved by Gaussian peak fitting with Chi-Square tolerance value of 10^{-9} after baseline correction. For comparison, the same correction applied to all the spectra. The wavelengths related to the recorded emission lines are chosen based on NIST Atomic Spectra Database and earlier studies [25, 26]. The most intense ionic copper lines (CuII) are observed at 501, 505.1, and 529.2 nm. Three atomic spectral lines of WI are recorded at 518.4, 494.5, and 480.9 nm. Another spectral emission line is observed at 479.2 nm, which could be CuII or WI. Due to the close transition of copper and tungsten at this wavelength and the spectral resolution, it is not possible to distinguish between them.

In the recorded spectra after 25 µs of the arcing, there is no sign of tungsten emission lines at 476.8, 480.9, 494.2, and 518.4 nm. Figure 5 shows the spectrum at 75 µs after the arc starts. The same correction method used in Figure 4 is applied here. There are sharp copper atomic lines at 510.5, 515.3, and 521.8 nm that are known to have very high transition probabilities and are often used for temperature analysis [24, 27]. Some of the ionic transition lines of copper are detected at 535.7, 507.2, 505.1, 501, 498.5, and 529.2 nm which are weaker than atomic ones. The hydrogen beta Balmer line Hβ is appeared at 486.1 nm, and because of its strong intensity has an overlap with two ionic emission lines of copper (491 and 493.1 nm) and the emission line of tungsten (480.9 nm). Figure 5 shows the peak fitting around 486 and 506 nm to distinguish peaks from the overlaps. The emission of atomic and ionic metal species are due to electrical contacts ablation and erosion since there is no other metallic source in the test object and the Hβ spectral line emission is observed because of the breakdown in the air as the dielectric medium of the switch. A summary of detected wavelengths is presented in Table 1.

Based on the obtained results and bandwidth limitation for video spectroscopy, distinctive copper atomic lines at 510.5 and 521.8 nm are chosen for this study due to their high intensity and the low probability to overlap with other lines. For this purpose, the center wavelength is set to 515.3 nm. Recording speed of 80000 fps with an exposure time of 10 µs and spectral resolution of ~0.65 nm are chosen.

2) Time evolution:

For the sake of reproducibility of the experiments, several tests have been done. The spectrum showed in Figure 4 is not observed on all the tests. Since the exposure time to record this spectrum is less than 20 µs, the reason for not finding the same first spectrum for all the tests could be a time-mismatch between the high-speed camera triggering and the arc ignition. Therefore, the first spectrum with emission lines at 510.5 and 521.8 nm is considered as the start of the temporal evolution of metals emission in the pre-strike arc which could have a delay

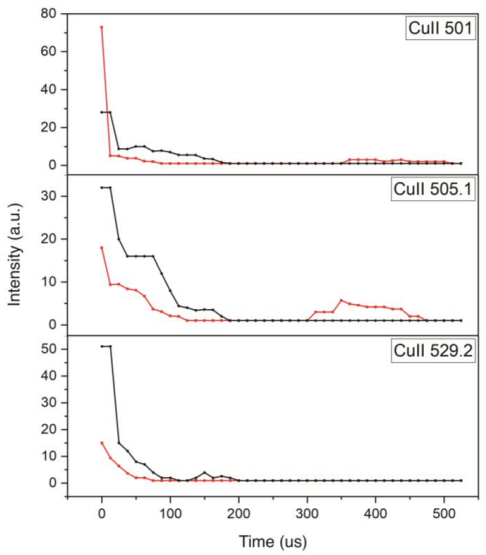

Figure 6. Temporal distribution copper ionic emissions. Black and red lines represent arc current profiles 1 and 2, respectively.

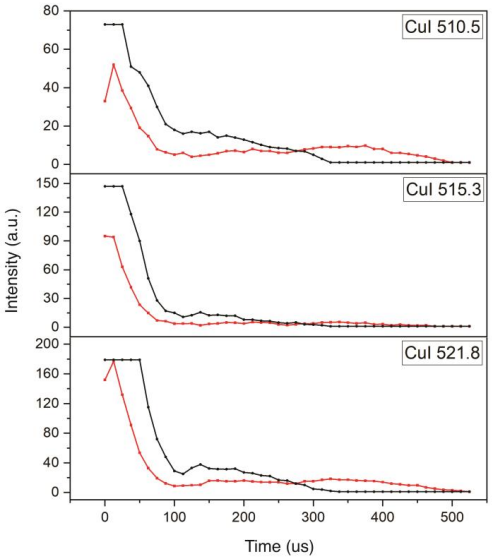

Figure 7. Temporal distribution of copper atomic emissions. Black and red lines represent arc current profile 1 and 2, respectively.

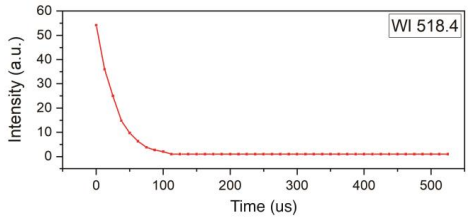

Figure 8. Temporal distribution of tungsten atomic emission at 518.4 nm for the arc current profile 2

less than 12.5 µs to the arc ignition.

Temporal distribution of copper atomic and ionic lines are shown in Figure 6 and Figure 7, respectively, for two different arc current profiles at 2 mm above the anode. Similar copper emission lines are observed in all performed experiments with approximately the same intensity ratio. It has to be mentioned that for the current profile 1, the emission lines intensities are saturated in the first ~12.5 µs for all the species, ~40 µs for 510.5 and 515.3 nm, and ~60 µs for 521.8 nm. The values in the curves at these moments are undefined and reported based on the next unsaturated measurable emission line.

The results indicate that the emission of copper atomic lines are dominating in the contacts gap. They show longer lifetimes and higher intensities compared to ionic ones. During the pre-strike arc, all the lines intensities decrease considerably. Still, there is a slight increase in copper atomic lines intensities for the arc current profile 1 after 130 µs and both atomic and ionic lines intensities for the arc current profile 2 after 350 µs.

Regarding tungsten atomic emissions, the emission lines are not intense enough to be visible during arcing except the emission at 518.4 nm. This spectral line is observed in case of the arc current profile 2. The temporal distribution is shown in Figure 8.

3) Spatial profile:

For a better understanding of metal vapor distribution in the gap, the spatial profile of copper atomic emission at 521.8 nm is investigated. Figure 9 shows recorded images at 1.5 mm above the anode surface at different arcing times for both arc current profiles. The horizontal white dashed line in the middle of images shows the position that is chosen for the temporal investigation of metal vapors in the previous section. As shown in temporal evolution, there is an increase in emission intensities of the species. Images 2-4 in Figure 9 give a better view of copper vapor intensity increase in the 2-D distribution profile. Image 3 shows the maxima at 112.5 µs and 350 µs for the arc current profiles 1 and 2, respectively.

IV. Discussion

Tungsten copper alloy as the material of the electrical contacts in this study has an amorphous refractory microstructure, which consists of 80% tungsten and 20% copper. The contacts have both high conduction of Cu and high erosion resistance of W. Due to the higher conductivity of copper, pre-strike arc usually hits the copper regions to initiate, otherwise the arc formation causes tungsten ablation to pass current. This erosion effect can be seen on the recorded spectrum at the first 25 μs of the arcing time, as shown in Figure 4. As mentioned before, a number of tests have been done to confirm the reproducibility of the emitted pieces. In some of the tests, the first recorded spectrum is different from the rest of the spectra. The presence of a sharp emission peak of atomic tungsten at 518.4 nm and two other emission lines in the first 25 μs and the difference in plasma composition at this time to the rest of the arcing time confirm ablation of tungsten. Also, the emission at 518.4 nm continues during arc burning in just a few of the recordings, which could be the same reason explained and randomly chosen region on the surface of the contact to initiate arc burning, which also depends on the grain size of copper and tungsten.

The time evolution of metal vapor intensities recorded in the selected observation window close to the anode surface shows the highest relative concentrations (Figure 9-1) at the peak of arc currents. For the first 60 µs at the wavelength of 521.8 nm, the emitted light was highly intense and saturated for spectral lines in current profile 1. At the same time, for current profile 2 the emission intensities are measurable. The metal vapor intensities decrease exponentially until a specific time that a slight increase observed. At this moment, the current is about few amperes while the metal vapor emissions increase. The analysis of this increase has to be done taking into account the thermal inertia of metallic contacts and the travel curve of the dynamic contact (the cathode), which is shown in Figure 2 (a).

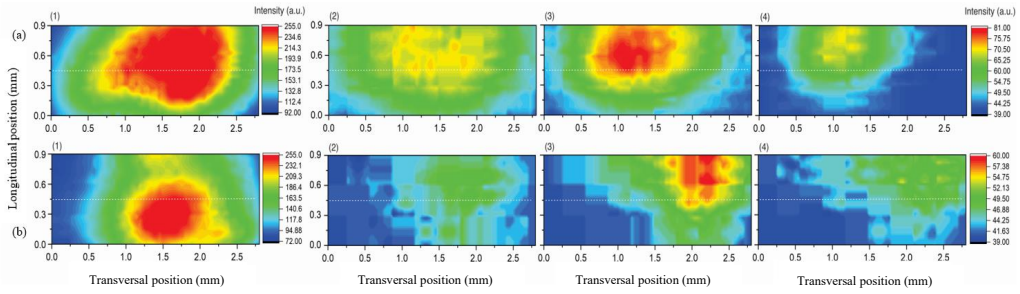

Figure 9. 2-D distribution of copper vapor (521.8 nm) at anode for the arc current profile 1 (a) at 50 µs (1), 112.5 µs (2), 137.5 µs (3), and 412.5 µs (4) and for the arc current profile 2 (b) at 25 µs (1), 162.5 µs (2), 350 µs (3), and 412.5 µs (4).

There is a time delay in temperature rise of metallic surfaces to evaporation point when they are exposed to heat caused by arcing. Since the intensity increase is observed on top-half of the observation window, the thermal inertia could not be the only reason for the intensities increase; otherwise, the growth has to be seen from the closest position to the contact surface.

In closing the switch with the speed of 3 m/s, the arc is ignited when the contacts are at a distance of 7 mm, and the spatial distribution of copper vapor (Figure 9) shows high vapor concentration close to the arc axis. Therefore, the increase could be as a result of either the cathode surface evaporation, which is transferred to the observation window due to contacts approaching or a part of the copper vapor evaporated from the anode surface that is returned to the observation window. It can be seen that the metal species last for a longer time in current profile 2, considering the increase in relative emission intensity compared to current profile 1, which shows the effect of longer arcing time in species distribution.

The presence of metal vapors could affect arc transport properties, particularly conductivity due to the low value of the ionization potential of the metal atoms and arc temperature fall due to radiative emissions[19, 22, 28]. The spatially resolved distribution of metal content makes it possible to trace particles in the arc column. The first 50 µs of arcing time shows the highest concentration of metal content for both current profiles at copper atomic emission lines, which is diffused afterward, and a fraction of metallic particles move across arc axis, as shown in Figure 9. This observation contrasts some computational studies that showed no displacement of metal vapors when the arc current is lower than one kA [29, 30].

In the case of higher current, the distribution of metal vapors could significantly change the pre-strike arc parameters during making operation, which may cause problems with maintenance and reliability of the switching device. The obtained results in this study on the distribution of metal vapors could facilitate a detailed understanding of the pre-strike arc behavior in making operation to improve the lifetime of such devices.

V. Conclusion

The presence and transport of metallic particles as a result of arc-electrical contacts interface have been investigated by optical emission spectroscopy for two different currents with different arcing time. The analysis of the time evolution of metal content during the pre-strike arc shows tungsten ablation and inhomogeneous distribution of copper vapors in the axis of the pre-strike arc without observing any changes in decaying arc current profiles. In addition, spatially resolved distribution of copper vapors shows high diffusion of particles during the first 50 µs of the arcing time and transport a fraction of metal particles in the arc column.

The results of this study provide support for computational studies on low-current arc. Furthermore, the investigation on low current pre-strike arc could be used to clarify metal vapor distribution at higher currents in MV-LBS due to limitations for OES measurements for thick plasma. This study must be continued by applying a higher current to investigate pre-strike arc characteristics (thermal and electrical behavior) and estimate the electrical contacts erosion process.

Acknowledgment

The work was financially supported by the Norwegian Research Council, grant # 269361. The authors would like to thank Erik Jonsson from SINTEF energy research and Bård Ålmos and Morten Flå from NTNU for technical supports.

References

[1] Z. Zhang, J. Zhang, E. Gockenbach, and H. Borsi, "Life management of SF 6 circuit breakers based on monitoring and diagnosis," *IEEE Electrical Insulation Magazine,* vol. 25, no. 3, pp. 21-29, 2009.

[2] N. S. Støa-Aanensen, M. Runde, E. Jonsson, and P. D. Teigset, "Empirical relationships between air-load break switch parameters and interrupting performance," vol. 31, no. 1, pp. 278-285, 2016.

[3] H. Taxt, K. Niayesh, and M. Runde, "Self-Blast Current Interruption and Adaption to Medium-Voltage Load Current Switching," *IEEE Transactions on Power Delivery,* vol. 34, no. 6, pp. 2204-2210, 2019.

[4] K. Niayesh and M. Runde, *Power Switching Components*. Springer, 2017.

[5] M. Seeger, "Perspectives on research on high voltage gas circuit breakers," *Plasma Chemistry and Plasma Processing,* vol. 35, no. 3, pp. 527-541, 2015.

[6] M. Mohammadhosein, K. Niayesh, A. A. Shayegani-Akmal, and H. Mohseni, "Online assessment of contact erosion in high voltage gas circuit breakers based on different physical quantities," *IEEE Transactions on Power Delivery,* vol. 34, no. 2, pp. 580-587, 2018.

[7] E. Jonsson and M. Runde, "Interruption in air for different medium-voltage switching duties," *IEEE Transactions on Power Delivery,* vol. 30, no. 1, pp. 161-166, 2014.

[8] J. Tepper, M. Seeger, T. Votteler, V. Behrens, and T. Honig, "Investigation on erosion of Cu/W contacts in high-voltage circuit breakers," *IEEE transactions on components and packaging technologies,* vol. 29, no. 3, pp. 658-665, 2006.

[9] P. G. Slade, *Electrical contacts: principles and applications*. CRC press, 2017.

[10] F. Pons and M. Cherkaoui, "An electrical arc erosion model valid for high current: Vaporization and Splash Erosion," in *2008 Proceedings of the 54th IEEE Holm Conference on Electrical Contacts*, 2008: IEEE, pp. 9-14.

[11] S. Zhu, Y. Liu, B. Tian, Y. Zhang, and K. Song, "Arc erosion behavior and mechanism of Cu/Cr20 electrical contact material," *Vacuum,* vol. 143, pp. 129-137, 2017.

[12] F. Pons, M. Cherkaoui, I. Ilali, and S. Dominiak, "Evolution of the AgCdO contact material surface microstructure with the number of arcs," *Journal of electronic materials,* vol. 39, no. 4, pp. 456-463, 2010.

[13] S. B. Wang *et al.*, "Electrical Erosion Characteristics of Pt-Ir-Zr Alloy Contact under DC Load," in *Applied Mechanics and Materials*, 2013, vol. 395: Trans Tech Publ, pp. 191-195.

[14] Y. Wu *et al.*, "Visualization and mechanisms of splashing erosion of electrodes in a DC air arc," *Journal of Physics D: Applied Physics,* vol. 50, no. 47, p. 47LT01, 2017.

[15] K. Hartinger, L. Pierre, and C. Cahen, "Combination of emission spectroscopy and fast imagery to characterize high-voltage circuit breakers," vol. 31, no. 19, p. 2566, 1998.

[16] A. Khakpour *et al.*, "Video spectroscopy of vacuum arcs during transition between different high-current anode modes," *IEEE Transactions on Plasma Science,* vol. 44, no. 10, pp. 2462-2469, 2016.

[17] A. Belinger, N. Naudé, J. Cambronne, and D. Caruana, "Plasma synthetic jet actuator: electrical and optical analysis of the discharge," *Journal of Physics D: Applied Physics,* vol. 47, no. 34, p. 345202, 2014.

[18] F. Valensi *et al.*, "Plasma diagnostics in gas metal arc welding by optical emission spectroscopy," *Journal of Physics D: Applied Physics,* vol. 43, no. 43, p. 434002, 2010.

[19] X. Li, H. Zhao, and A. B. Murphy, "SF6-alternative gases for application in gas-insulated switchgear," *Journal of Physics D: Applied Physics,* vol. 51, no. 15, p. 153001, 2018.

[20] A. B. Murphy, "Influence of metal vapour on arc temperatures in gas–metal arc welding: convection versus radiation," *Journal of Physics D: Applied Physics,* vol. 46, no. 22, p. 224004, 2013.
[21] S. Franke, R. Methling, D. Uhrlandt, R. Bianchetti, R. Gati, and M. Schwinne, "Temperature determination in copper-dominated free-burning arcs," *Journal of Physics D: Applied Physics,* vol. 47, no. 1, p. 015202, 2013.
[22] A. B. Murphy, "The effects of metal vapour in arc welding," *Journal of Physics D: Applied Physics,* vol. 43, no. 43, p. 434001, 2010.
[23] A. Khakpour *et al.*, "Investigation of anode plume in vacuum arcs using different optical diagnostic methods," *IEEE Transactions on Plasma Science,* vol. 47, no. 8, pp. 3488-3495, 2019.
[24] A. Khakpour *et al.*, "Time and space resolved spectroscopic investigation during anode plume formation in a high-current vacuum arc," *Journal of Physics D: Applied Physics,* vol. 50, no. 18, p. 185203, 2017.
[25] https://physics.nist.gov/PhysRefData/ASD/lines_form.html.
[26] J. Pettersson, M. Becerra, S. Franke, and S. Gortschakow, "Spectroscopic and Photographic Evaluation of the Near-Surface Layer Produced by Arc-Induced Polymer Ablation," *IEEE Transactions on Plasma Science,* vol. 47, no. 4, pp. 1851-1858, 2019.
[27] A. Khakpour, R. Methling, S. Franke, S. Gortschakow, and D. Uhrlandt, "Vapor density and electron density determination during high-current anode phenomena in vacuum arcs," *Journal of Applied Physics,* vol. 124, no. 24, p. 243301, 2018.
[28] M. Schnick, U. Füssel, M. Hertel, A. Spille-Kohoff, and A. Murphy, "Metal vapour causes a central minimum in arc temperature in gas–metal arc welding through increased radiative emission," *Journal of Physics D: Applied Physics,* vol. 43, no. 2, p. 022001, 2009.
[29] J. L. Zhang, J. D. Yan, and M. T. Fang, "Electrode evaporation and its effects on thermal arc behavior," *IEEE Transactions on Plasma Science,* vol. 32, no. 3, pp. 1352-1361, 2004.
[30] A. Kadivar and K. Niayesh, "Two-way interaction between switching arc and solid surfaces: distribution of ablated contact and nozzle materials," *Journal of Physics D: Applied Physics,* vol. 52, no. 40, p. 404003, 2019.

Naghme Dorraki received the B.Sc. degree in optics and laser engineering from University of Tabriz, Iran, in 2011, and the M.Sc. degree in photonics from Laser and Plasma research institute, Shahid Beheshti University, Tehran, Iran, in 2015. She is currently pursuing a Ph.D. degree in with the Department of Electric Power Engineering Norwegian University of Science and Technology (NTNU), Trondheim, Norway.

Kaveh Niayesh completed the B.Sc. and M.Sc. degree in Electrical Engineering from the University of Tehran, Iran, in 1993 and 1996 respectively. In 2001, he completed the Ph.D. degree from the RWTH-Aachen University of Technology in Electrical Engineering. In the last 19 years, he held different academic and industrial positions including Principal Scientist with the ABB Corporate Research Center, Baden-Dättwil, Switzerland; Associate Professor with the University of Tehran; and Manager, Basic Research, with AREVA T&D, Regensburg, Germany. Currently, he is a Professor in the Department of Electric Power Engineering at Norwegian University of Science and Technology (NTNU), Norway. His research interests are mainly in the broad field of high voltage and switchgear technology; specifically on current interruption in power switching devices in AC and DC power networks, breakdown and aging behavior of insulation materials exposed to HVDC and repetitive fast impulses, as well as diagnostic and condition assessment of power switchgear.

Paper II

Optical investigation on pre-strike arc characteristics in medium-voltage load break switches.

Journal of Physics D: Applied Physics, Vol. 54, NO. 25, p. 255503, April 2021.

Optical investigation on pre-strike arc characteristics in medium-voltage load break switches

Naghme Dorraki, and Kaveh Niayesh

Department of Electric Power Engineering, NTNU, Trondheim, Norway

Email: naghme.dorraki@ntnu.no

Received xxxxxx
Accepted for publication xxxxxx
Published xxxxxx

Abstract

Medium Voltage Load Break Switches (MV-LBS) should pass fault current while closing and be able to re-open for the next operation. Replacing SF_6 as a high impact greenhouse insulating gas with air, makes the switch design more challenging because of the higher pre-strike arcing time and energy dissipation between contacts which leads to more contact surfaces' erosion and even higher possibility of welding. In this paper, a synthetic test circuit is used to emulate stresses applied to MV-LBS during the making of short-circuit currents. Since there are difficulties in accurate direct measurement of arc voltage because of the inherent response of the measurement system, an alternative method using Optical Emission Spectroscopy (OES) is proposed. OES measures the pre-strike arc temperature distribution profile close to the cathode surface at a test voltage of 18 kV and a making current of 17 kA. The arc electrical characterization is achieved using obtained spectroscopy results, Lowke's model, and thermal air plasma transport properties. A maximum arc temperature of 12500 K while the arc moves from the lower part of the cathode to the center, arc voltage of 30-58 V, and dissipated energy of 79-87 J are calculated for the pre-strike arc considering the impact of copper evaporated from the contact surfaces. Different arc behavior is observed in closing the contacts compared to free-burning arcs, which indicates gas flow blowing the arc caused by the contact movement. This investigation could be used for a better understanding of switching behavior and efficient control of the operation.

Keywords: load break switch, medium voltage, arc erosion, electrical contacts, arc-material interaction, optical emission spectroscopy, arc diagnostics

1. Introduction

Arc burning in Medium Voltage Load Break Switches (MV-LBS) directly affects the melting and erosion of electrical contacts, either in current interruption with a limited current range of few hundreds of amperes or in making operation under fault condition. For gas-insulated MV-LBS as one of the critical devices in distribution networks, prediction of switch performance at different operational conditions could prolong its lifetime and reliability. The pre-strike arcing time and energy dissipation between the contacts while closing under short-circuit condition could lead to failure in switch operation caused by significant contacts deterioration or even welding [1]. Several studies have been done to optimize MV-LBS with an alternative gas to reduce the use of

SF_6 as an extremely strong greenhouse gas in encapsulated switchgears [2, 3]. A compact air-based MV-LBS is a possible solution for SF6 replacement. However, air is inferior to SF_6 due to a lower dielectric strength, which results in higher pre-strike arcing time and energy dissipation.

Several tens of kiloamperes of short-circuit currents pass through the contacts during making operation in LBS switchgear [1, 4]. The flow of fault current through the switch causes significant contact erosion by raising the temperature, leading to the melting of the contact surfaces, in the worst case, even welding the contacts and failure to re-open [5, 6]. The contacts' surface erosion and melting partly result from absorbing arc energy dissipated while closing the switch [6-8]. Therefore, it is crucial to measure the dissipated arc energy between the contacts while closing under different fault conditions to understand the phenomenon and to avoid switch failure. To reach dissipated arc energy, precise measurement of arc voltage, current, and time are required. The most challenging part of this measurement is direct measurement of arc voltage because of the inherent system response.

In this study, the synthetic circuit is designed to investigate making operation in MV-LBS, which applies a voltage in the order of thousands of volts to make a dielectric breakdown followed by a sharp drop to arc voltage in the order of a few tens of volts. The inherent response of the measurement system, which is normally calibrated using step voltages of hundreds of volts, to this very large step voltage overrides the actual arc voltage. Therefore, an alternative method is required for arc voltage measurement.

As an in-direct measurement method, analysis of arc emission spectroscopy could determine the arc voltage and the dissipated arc energy between the contacts by considering transport properties of arc as air thermal plasma. Besides, Optical Emission Spectroscopy (OES) could provide detailed information on the arc composition by the emitted spectra of excited particles injected into the arc column [9-11]. Metal vapors in the arc could significantly change the arc properties like temperature and conductivity. The information gained from the arc emission spectroscopy is applicable for understanding the metal-arc interface concerning the contact erosion. It provides experimentally measured thermal and electrical properties of the pre-strike arc.

This work characterizes pre-strike arcs by using emission spectroscopy of the arc-contact interface. For this purpose, a test object with a spring-type drive mechanism and a synthetic test circuit are employed. An optical emission spectroscopy set-up is designed to record the temporal evolution of metal vapors close to the contact surface while approaching.

2. Experimental set-up

A test object with a spring-type drive mechanism and a synthetic test circuit is employed. An optical emission spectroscopy set-up is designed to record the temporal evolution of metal vapors close to the contact surface while approaching. The test object is a spring-type switch with axisymmetric arcing contacts made of copper-tungsten (20/80). The stationary contact (cathode) is a 6 mm diameter pin, and the dynamic one (anode) is a tulip with an outer diameter of 15 mm that closes at a speed of 3 m/s. The closing speed and the material type are chosen not to differ significantly from the commercial product. A sensor records the displacement of the dynamic contact over time, making it possible to measure arc length while closing the switch.

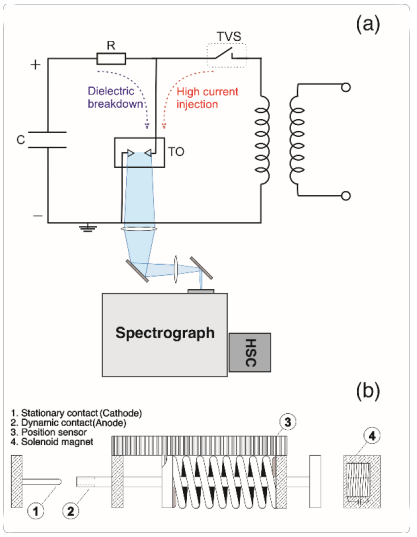

Figure 1. Schematic of the test circuit and spectroscopic set-up (a), and the test-object (b)

Video spectroscopy records the arc composition changes close to the stationary contact surface (cathode). The particle emissions over time are analyzed to investigate pre-strike arc properties. The spectroscopic set-up consists of a spectrograph (Princeton Instrument Acton SP-300i) and a high-speed camera (Photron FASTCAM mini UX50) with 1280×1024 pixels matrix. Figure 1 shows the schematic of the spring type test-object, spectroscopic set-up, and test circuit. The spectrograph has a focal length of 300 mm, 600 lines/mm grating, and slit width of 10 µm. The cathode's front-face is

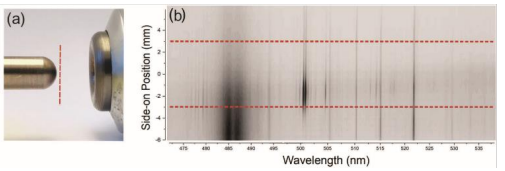

Figure 2. (a) the observation position for arc emission spectroscopy, (b) an example of 2-D spectrum with exposure time of 30 µs recorded during the pre-strike arc.

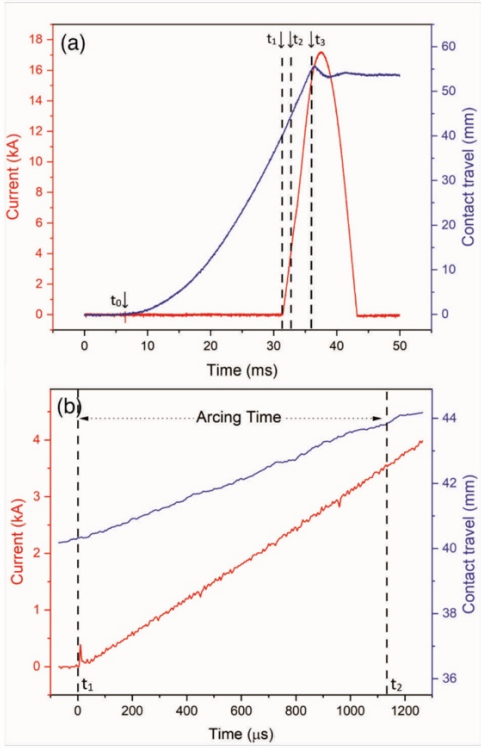

Figure 3. Current waveform and contact travel curve during full making operation (a), and pre-strike arc (b).

imaged to the spectrograph entrance slit (see Figure 2 (a)-dashed line). The recording speed is chosen 25000 fps with an exposure time of 30 μs to reach a proper side-on view and time evolution of the arc while the contacts are approaching. Because of the limited bandwidth in video spectroscopy and the high transition probability of copper species compared to tungsten, the emission spectrum bandwidth of 472-537 nm was chosen to include the major atomic and ionic copper emission lines as required for arc temperature calculation. The spectral and spatial resolutions are ~0.15 nm and ~8 pixels/mm, respectively. Figure 2 (b) shows an example of a two-dimensional image of spectral emission lines.

The test circuit is a synthetic making circuit based on the IEC 62271 standard [12]. The circuit is a combination of synchronized high current and high voltage sub-circuits. The high voltage part makes the dielectric breakdown while contacts are closing. A high-frequency breakdown current is used to trigger the high current circuit to inject the short-circuit current to the test object. A Pearson current sensor measures the arc current. For this study, the test voltage is 18 kV, and the making current is a half-cycle of a 50 Hz sinusoidal current

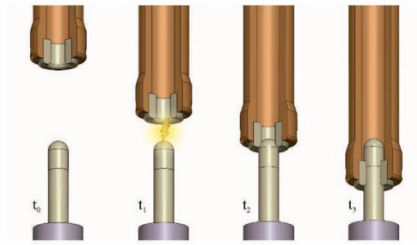

Figure 4. Different stages during making operation-timing is based on the dynamic contact's travel cure

with an amplitude of 17 kA. Figure 3 (a) shows the current waveform and travel curve of the dynamic contacts. The dashed lines show the start and endpoint of the pre-strike arc (t_1-t_2). The arc ignites when contacts are approaching at a distance of ~4 mm and burns for less than 1.2 ms. The fault current in its starting phase, i.e. when the current is between zero and 3.5 kA , flows through the pre-strike arc (t_1-t_2), while the rest of the half-cycle short-circuit current passes through the contacts in closed position where the contacts move through each other between t_2 and t_3, and stop at t_3. Figure 4 shows different stage of contacts position during making operation. The timing corresponds to the travel curve of the dynamic contact shown in Figure 3 (a). Figure 3(b) shows a closer view of the pre-strike arcing time, current, and length. The arc current increases from zero to 3.5 kA during the pre-strike arc. The rest of the short-circuit current flows through the contacts when they are in touch.

3. Results

In this section, the pre-strike arc temperature is measured by the use of OES. Arc dimension is modeled, which follows by calculation of arc voltage and energy.

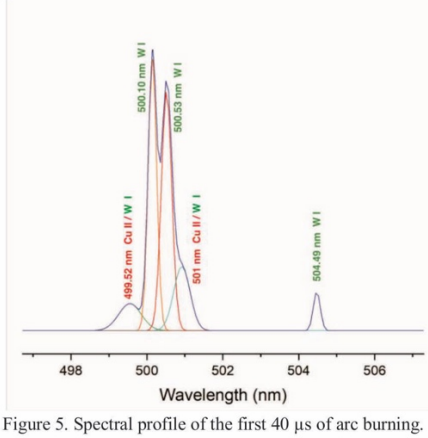

Figure 5. Spectral profile of the first 40 μs of arc burning.

3.1 Optical emission spectroscopy

For emission spectroscopy of the pre-strike arc, the spectrograph slit is aligned perpendicular to the cathode surface (stationary contact) where most injection of metalic particles to the arc column is expected. In Figure 2 (a), the observation window is shown by a red dashed line with a width of twice the pin diameter. A series of two-dimensional spectra is recorded with an exposure time of 30 µs. An example of a recorded 2D image of spectral emission lines is shown in Figure 2 (b). The area limited between red dashed lines shows the pin width (cathode-stationary contact). To get an approach to the arc composition, the spectral lines are determined based on their emission wavelengths. Due to the limited bandwidth of video spectroscopy and high transition probability of copper species compared to tungsten, the emission spectrum center is adjusted to 505 nm with a bandwidth of 65 nm. The chosen wavelength range includes the major atomic and ionic copper emission lines that are required for arc temperature calculation.

The first recorded frame is different from the rest similar to the previous study on the impact of dielectric breakdown low current making operation [13]. The first 40 µs of the arcing time show strong tungsten emission lines at 500.1 and 500.53 nm, indicating air breakdown to initiate the pre-strike arc (see Figure 5). In contrast to the low current making test, an increase in the intensity of the atomic tungsten emissions is observed in the recorded sequence of the pre-strike arc emission spectra in making the short-circuit current. The spectral profile of the pre-strike arc at 240 µs is shown in Figure 6. Besides intense tungsten emission lines at 500.1 and 500.53 nm, more atomic tungsten spectral lines and several atomic and ionic copper spectral lines are recorded, which present the arc composition in the limited chosen bandwidth.

3.2 Boltzmann Plot method

Arc emission spectroscopy determines excitation temperature that can be calculated using Boltzmann plot method if Local Thermal Equilibrium (LTE) condition is given. The method is widely used for plasma temperature measurement [10, 14]. The dependency of integrated intensity I_{ul} of the recorded spectral lines which transmit from upper energy level E_u to lower energy level E_l to plasma temperature T is given by:

$$I_{ul} = \frac{hc}{4\pi\,\lambda_{ul}} A_{ul}\, g_u \frac{n_u}{P} L\, exp\left(\frac{-E_u}{k_B T}\right) \qquad (1)$$

where h is the Planck constant, c is the speed of light, L is the length of the arc, A_{ul} is the transition probability, λ_{ul} is the transition line wavelength, n_u is the number density, P is a partial function, and k_B is the Boltzmann constant. By considering at least two emission lines which are spectrally integrated, the arc temperature can be calculated from inverse slope of Boltzmann Plot. The equation is reduced to:

$$\frac{1}{T} = \frac{k_B}{(E_{u2} - E_{u1})}\, ln\left(\frac{I_1\lambda_1}{g_{u,1}A_{ul,1}} \times \frac{g_{u,2}A_{ul,2}}{I_2\lambda_2}\right) \qquad (2)$$

The chosen spectral lines for equation (2) should have enough excitation energy gap to be used for temperature measurement. Since the equation is derived for a ratio of spectral lines emission intensities, an absolute calibration of the intensities is not required. The applicability of the equation

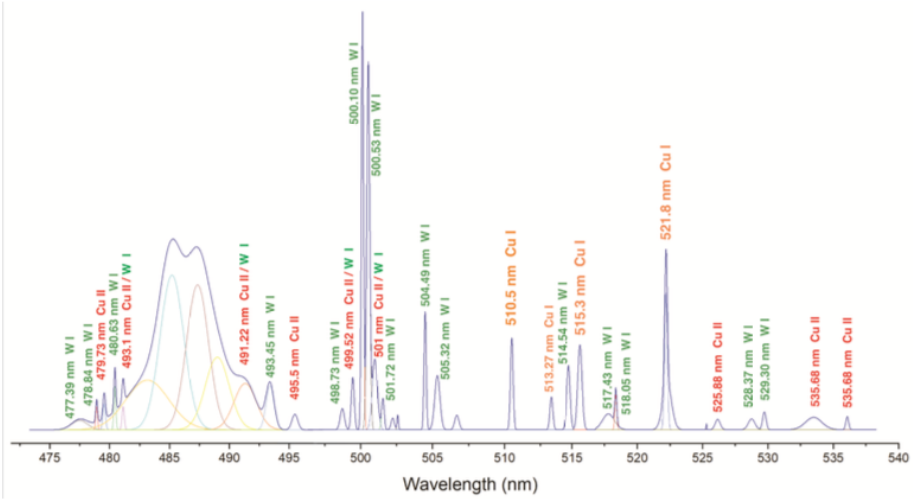

Figure 6. Spectral profile of arc emission at 240 μs with spectral lines corresponds to atomic and ionic copper and atomic tungsten

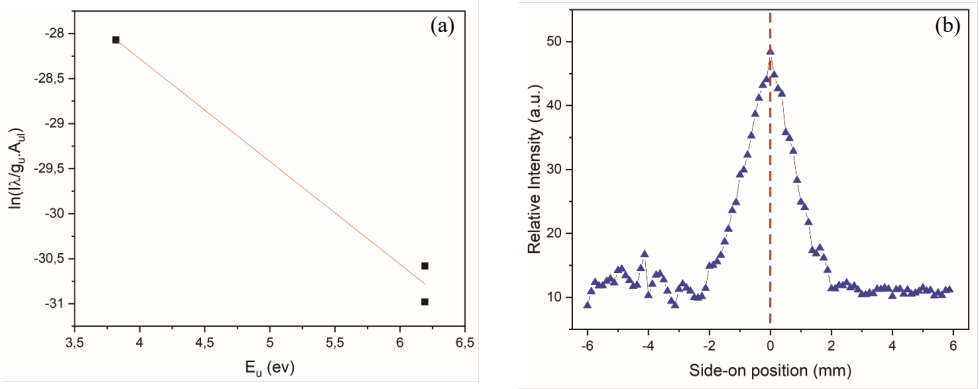

Figure 7. (a) Boltzmann Plot deduced from CuI lines (510.55, 515.32, and 521.82 nm) at 600 μs in the middle of side-on position shows arc temperature of 10168 K, (b) Spectrally integrated relative intensity of CuI emission at 521.82 nm.

is also limited to LTE and optically thin plasma conditions. From visual inspection of the spectra, copper atomic emission lines at 510.55, 515.32, and 521.82 nm are not affected by self-absorption in the most recorded frames. Besides, the energy gap of 2.4 eV between excitation energy levels makes the CuI spectral lines well suited for Boltzmann Plot method-based arc temperature measurement. The spectroscopic parameters for the copper atomic lines are shown in Table 1 taken from NIST atomic database [15]. The arc temperature is obtained by three CuI emission lines using equation (2) at each 40 µs from arc ignition to the contacts touch. Figure 7 (a) shows an example of the Boltzmann Plot from spectrally integrated CuI lines at 600 µs. The plot is made for the middle of side-on position, which is shown in Figure 7 (b) by dashed line. The figure shows the spectrally integrated relative emission of CuI at 521.82 nm. The arc temperature at this point is 10168 K which is calculated as the reverse slope of the line in Figure 7 (a) divided by the Boltzmann constant. The temperature calculation is started at 200 µs because of unacceptable data dispersion for the plot based on the spectrally integrated CuI emission lines for the first 200 µs of the arc burning. From 800 µs, some signs of saturation appeared in the middle of the side-on position at 515.32 and 521.82 nm, which expanded with increasing arcing time until contacts touch moment. The temperature calculation is neglected at these specific positions and is colored black in the temperature profile (Figure 8). The maximum calculated arc temperature is 12500 K, while it could be higher in the black regions. The pre-strike arc temperature distribution shows the arc dynamic motion in time and space. As shown in the temperature profile, the arc ignites in the lower half of the cathode (stationary contact) and moves to the center while the contacts are closing. A temperature drop is observed in the time interval of 400-560 µs before the arc is stabilized in the center, considering the highest temperature in the center of the arc column. The contact movement could cause the arc to cool during the closing operation by creating a gas flow blowing the arc. It has to be mentioned that the periodic discontinues pattern observed at 360 µs of the temperature profile is because of electromagnetic noises interfere with the recording system.

For reproducibility, a few tests have been conducted under the same test conditions. Similar arc composition and approximately equal species emission line intensities have been observed. The difference is in the spatial distribution of

Table 1. Spectroscopic data for atomic copper emission lines used for temperature measurement

Wavelength (nm)	Upper-level E (eV)	Lower-level E (eV)	Upper-level degeneracy	Transition probability (s^{-1})
510.55	3.817	1.389	4	2.0×10^{6}
515.32	6.191	3.786	4	6.0×10^{7}
521.82	6.192	3.817	6	7.5×10^{7}

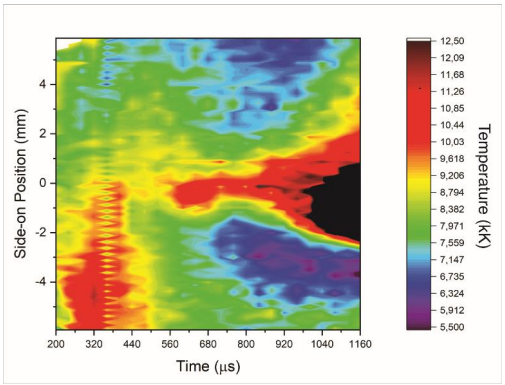

Figure 8. Temperature profile of pre-strike arc for 18 kV breakdown voltage and 17 kA fault current (50 Hz)

emission lines in the side-on position for the first 500 µs because the arc ignites randomly at different spots of the contact surface. The rest of the arc burning time ends up with similar coherent temperature behavior in all the tests like the arc temperature shown in Figure 8 between 500 and 1160 µs.

3.3 Electrical characteristics of pre-strike arc

The dissipated arc energy between the contacts is partly absorbed by the contacts surfaces, which could heat them up to the melting and evaporation points. Therefore, measuring the dissipated energy could provide an appropriate measure of the contacts erosion and welding. The energy could be obtained by arc voltage and current measurement. The arc current is measured experimentally. Challenges exist regarding arc voltage measurement. A distortion in voltage waveform is observed in the direct measurement of the pre-strike arc voltage because of the inherent response of the measurement system to the large step voltage caused by a breakdown in the switch (in this case, a step voltage of 18 kV). An alternative method obtains the pre-strike arc voltage using arc temperature and applying thermal air plasma transport properties in atmospheric pressure. Numerical simulation studies exist on temperature dependency of electrical conductivity for dry air plasma at atmospheric pressure [16-18]. The electrical conductivity is obtained by tracing electrical conductivity as a function of temperature at LTE condition (Figure 9). By assuming the pre-strike arc as dry thermal air plasma, electrical conductivity is calculated as shown in Figure 10. The maximum calculated conductivity is 5300 S/m. The conductivity is not determined for black regions due to the lack of data for arc temperature. Since the electrical conductivity in dry air thermal plasma at atmospheric pressure increases approximately linearly with temperature (for temperatures less than 25000 K) and the arc temperature is expected to be higher than 12500 K in black regions, the electrical conductivity should be higher than 5300 S/m in these areas.

There is no clear information on the percentage of metal vapor in the arc column because of the spectrograph's limited bandwidth. Therefore, the electrical conductivity is also carried out for 100% saturated thermal air plasma with copper in addition to pure thermal air plasma, which makes it possible to discuss the pre-strike arc electrical characteristics in a range of copper perecentage impurity.

To calculate the electrical characteristics of pre-strike arc, it is necessary to estimate the arc dimension. Assuming that the pre-strike arc is cylindrically shaped, the arc length can be approximately determined by using the travel curve of the dynamic contact (see Figure 3). For the cross-sectional area, Lowke's analytical model of free-burning arcs is employed [19]. The model is based on theoretical prediction and experimental measurements of high current arcs at atmospheric air pressure. The arc radius expression is derived

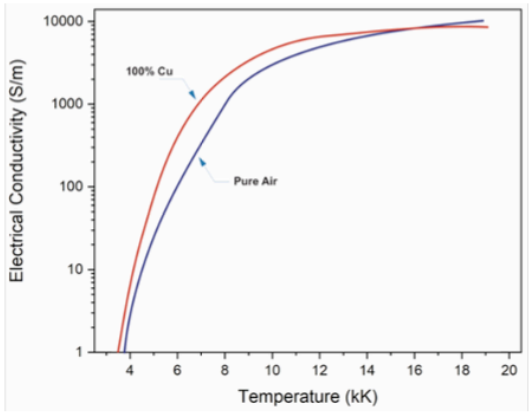

Figure 9. Electrical conductivity as a function of temperature for dry thermal air plasma and 100% saturated with copper vapor adapted from [16].

from the conversion equations for energy (3) and momentum (4):

$$I^2/\sigma A^2 = 4\pi kT/A + U \quad (3)$$

$$\rho v dv/dz = -\rho g - (dp/dz) \quad (4)$$

wherein equation (1) I is the arc current, σ is the electrical conductivity, k the thermal conductivity, and U the net radiation emission coefficient. In equation (2), ρ is the density of the plasma, p the pressure, υ the plasma axial velocity, z axial position, and g the gravity. However, in high current arc density, the radiation loss term (U) is dominant over the conduction term (4πkT/A) because of the high magnetic conduction. The term dp/dz arises due to the magnetic constriction effect on P. Therefore, the term ρg is omitted, which is smaller than dp/dz.

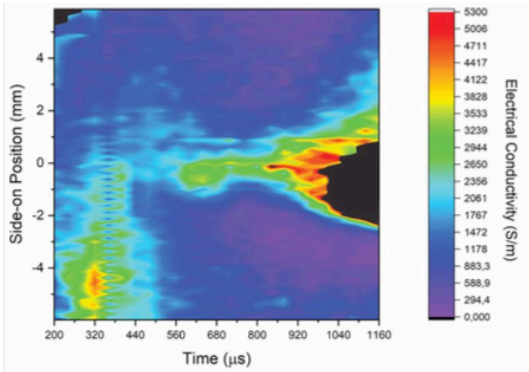

Figure 10. Pre-strike arc electrical conductivity as dry air thermal plasma

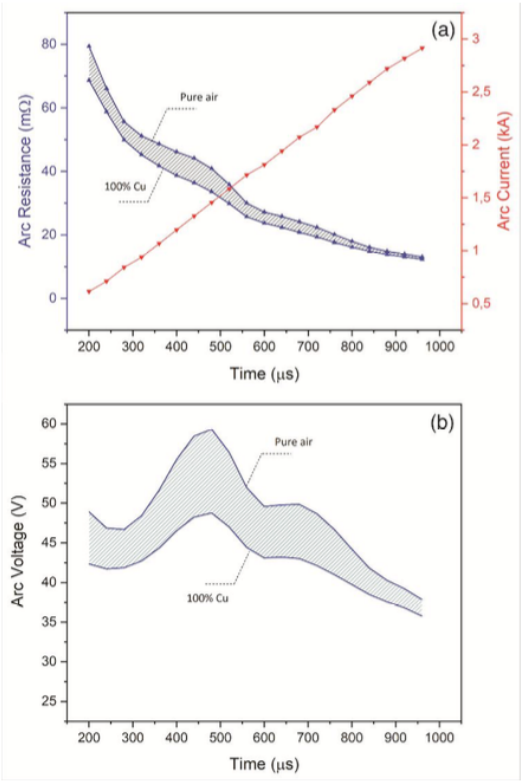

Figure 11. Electrical characteristics of the pre-strike arc influenced by metal vapors when the arc is free of vapor and 100% saturated with copper vapor. (a) arc resistance and current, (b) arc voltage

Considering more approximations regarding radial pressure, radiation, viscous and turbulence losses, the arc radius is obtained by Lowke as:

$$R = 1.11 \left(\frac{Z}{h\sigma}\right)^{\frac{1}{4}} I^{\frac{3}{8}} \Big/ (\mu j_0 \rho)^{\frac{1}{8}} \qquad (5)$$

where h is enthalpy and μ=0.126 dyne/A^2. The agreement of the theory and experiment by Lowke is an evidence that j_0 is constant with current, otherwise the theoretical predictions differ markedly from experiments. Therefore, an estimated error of 20% is considered because of uncertainty in the value of j_0.

Considering the experimentally measured electrical conductivity, the values of enthalpy and density are taken from Capitelli et al. database on thermal air plasma transport properties at atmospheric pressure in the temperature range 50-30000 K [18]. For the sake of accuracy, the electrical characterization is carried out for the arcing time of 200 to 920 μs when OES measures a decent pre-strike arc temperature, and the calculation is neglected for the regions whereby saturation in the CuI emission lines is observed (black regions). In this case, the arc radius is changing in the range of 2.3-3.3 mm.

The arc resistance is calculated by the electrical conductivity concluded from arc temperature and the arc dimension with respect to the anode travel curve and the Lowke model. The arc voltage is obtained using arc resistance and experimentally measured arc current. We should notice the calculated arc voltage does not include a voltage drop across the plasma sheath in front of the contacts. The minimum arc voltage for tungsten and copper as the electrical contact material is measured 13.5 and 13 V, respectively [20]. Since the majority of the contacts material is tungsten (80% tungsten, 20% copper), the minimum arc voltage is considered 13.5 V. The arc resistance and voltage including cathodic voltage drop as a function of time are shown in Figure 11 (a) and (b), respectively. By considering the impact of copper vapor density in arc conductivity [18], the resistance, and the voltage could be limited to the area bounded by two curves shown Figure 11 where the arc is free of copper vapor or 100% saturated with copper vapor.

A comparison between the calculated pre-strike arc voltage and free-burning arc voltage at different distances shows that reasonable voltage values are obtained.

Although we expect the arc voltage to decrease with increasing arc burning time, based on the earlier studies [21, 22], there is an increase in arc voltage while the arc current is linearly increasing. At the same moment of voltage increasing, the arc resistance curve shows almost constant values in Figure 11, and the temperature profile shows the arc moving from the lower part of the stationary contact to the center where the arc evolution looks stable until contacts touch moment.

4. Discussion

Understanding the pre-strike arc behavior during making operation under a fault condition is crucial for improving load break switches concerning contacts erosion. The same approach is necessary for earthing switches in short-circuit fault levels, which shows this investigation's necessity. The dissipated energy due to arc burning between the contacts while closing could be proportional to the degree of contact erosion and welding. The arc energy can be determined by the arc voltage and current over arcing time. There are some challenges regarding this measurement. In the direct measurement of the pre-strike arc voltage, a distortion in voltage waveform is observed due to the measurement system's inherent response to the large step caused by a breakdown in the switch (in this case, a step voltage of 18 kV). Therefore, the pre-strike arc voltage is calculated indirectly using arc temperature measured by OES and the arc

parameters database for atmospheric pressure air thermal plasma. There are some limitations regarding the observation window position in arc spectroscopy when there is a moving contact, which makes it difficult to scan the whole arcing time evolution because it partly burns inside the dynamic tulip contact before touch moment. Therefore, the arc voltage is approximately estimated at these moments based on the adjacent electric field and the arc length. A comparison of the indirectly calculated pre-strike arc voltage with free-burning arc voltage at different distances shows that the obtained voltage values are reasonable. The dissipated energy between the contacts during 1.2 ms pre-strike arc burning could range from 79 to 87 joules.

From the temperature profile of the pre-strike arc, information on arc dynamic motion is concluded. It can be seen that the arc evolution is different from the free-burning arc [21, 22]. The arc is unstable for the first 500 μs of burning. Afterward, it gradually gets stable and expands in the center of the arc column. A temperature fall happens before the arc starts expanding in the center, caused by arc cooling because of gas flow through the contact movement. The enhanced cooling at this time can be observed as an increase in the arc voltage. Reducing the arcing time by closing the contacts faster could be an idea to reduce the impact of prestrike arc on contacts erosion.

Another factor that has a direct impact on dissipated energy between contact is insulation gas. This study is done in air as an alternative to SF_6. Some additives could be mixed with air to increase its dielectric strength and reduce the arcing time under making operation to reduce the pre-strike arc dissipated energy. The proposed investigation method in this study could also be used to detect arc decomposition by-products concerning the environmental compatibility of different gas mixtures, as well as for the investigation of switching arc properties under different fault conditions.

5. Conclusion

In summary, pre-strike arc characteristics during the making of short-circuit current in an air MV-LBS model switch is investigated by arc emission spectroscopy. The arc dynamic motion concluded from the temperature profile shows the contact movement cooling impact in arc behavior. Because of the distortion in the direct measurement of arc voltage, the arc voltage and subsequently, the dissipated energy between contacts during making operation are measured using OES. We consider the influence of metallic vapor in the arc voltage. From the pre-strike arc characterization. The proposed method could be a proper diagnostic to understand the physical mechanisms involved in the making operation of MV-LBS, and the performance of the switching device.

Acknowledgment

The work was financially supported by the Norwegian Research Council, grant # 269361. The authors would like to thank Bård Ålmos and Morten Flå from NTNU for technical supports.

References

[1] Niayesh K and Runde M 2017 *Power Switching Components* (Cham, Switzerland: Springer)
[2] Støa-Aanensen N S, Runde M, Jonsson E and Teigset A 2016 *IEEE Transactions on Power Delivery* **31** 278-85
[3] Taxt H, Niayesh K and Runde M 2019 *IEEE Transactions on Power Delivery* **34** 2204-10
[4] Seeger M 2015 *Plasma Chemistry and Plasma Processing* **35** 527-41
[5] Pons F and Cherkaoui M 2008 An electrical arc erosion model valid for high current: Vaporization and Splash Erosion. In: *2008 Proceedings of the 54th IEEE Holm Conference on Electrical Contacts*: IEEE) pp 9-14
[6] Mohammadhosein M, Niayesh K, Shayegani-Akmal A A and Mohseni H 2018 *IEEE Transactions on Power Delivery* **34** 580-7
[7] Kadivar A and Niayesh K 2019 *Journal of Physics D: Applied Physics* **52** 404003
[8] Zhang J L, Yan J D and Fang M T 2004 *IEEE Transactions on Plasma Science* **32** 1352-61
[9] Hartinger K, Pierre L and Cahen C 1998 *Journal of Physics D: Applied Physics* **31** 2566
[10] Valensi F, Pellerin S, Boutaghane A, Dzierzega K, Zielinska S, Pellerin N and Briand F 2010 *Journal of Physics D: Applied Physics* **43** 434002
[11] Khakpour A, Methling R, Franke S, Gortschakow S and Uhrlandt D 2018 *Journal of Applied Physics* **124** 243301
[12] IEC S 2006 62271-101. In: *High-Voltage Switchgear and Controlgear–Part 101: Synthetic Testing,*
[13] Dorraki N and Niayesh K 2020 *IEEE Transactions on Plasma Science* **48** 3698-704
[14] Unnikrishnan V, Alti K, Kartha V, Santhosh C, Gupta G and Suri B 2010 *Pramana* **74** 983-93
[15] NIST Atomic Spectra Database Lines Form. Accessed: Dec. 21, 2020. [Online]. Available: https://physics.nist.gov/PhysRefData/ASD/lines_form.html.
[16] Cressault Y, Hannachi R, Teulet P, Gleizes A, Gonnet J and Battandier J 2008 *Plasma Sources Science and Technology* **17** 035016
[17] Murphy A B and Arundelli C 1994 *Plasma Chemistry and Plasma Processing* **14** 451-90
[18] Capitelli M, Colonna G, Gorse C and d'Angola A 2000 *The European Physical Journal D-Atomic, Molecular, Optical and Plasma Physics* **11** 279-89
[19] Lowke J 1979 *Journal of physics D: Applied physics* **12** 1873
[20] Slade P G 2017 *Electrical contacts: principles and applications* (Boca Raton, FL, USA: CRC press)
[21] Lowke J, Kovitya P and Schmidt H 1992 *Journal of Physics D: Applied Physics* **25** 1600
[22] Baeva M, Uhrlandt D, Benilov M and Cunha M 2013 *Plasma Sources Science and Technology* **22** 065017

Deconvolution based Correction of Pre-strike Arc Voltage Measurement in Medium Voltage.

IEEE Journal of Sensors, Submitted March 2022.

Paper III

This paper is awaiting publication and is not included in NTNU Open

An Experimental Study of Short-Circuit Current Making Operation of Air Medium-Voltage Load Break Switches.

IEEE Transactions on Power Delivery, accepted for publication, February 2022.

Paper IV

An Experimental Study of Short-Circuit Current Making Operation of Air Medium-Voltage Load Break Switches

Naghme Dorraki, and Kaveh Niayesh, *Senior Member, IEEE*

***Abstract*— Replacing SF_6, the most potent greenhouse gas, with an alternative gas is a challenge faced by medium-voltage load break switches (MV-LBS). Air is a possible alternative, but there are some challenges regarding low dielectric strength leading to high arcing time and dissipated energy. Therefore, understanding the switching processes for both interruption and making operations in air MV-LBS is crucial to designing efficient compact switchgear.**

This work focuses on making operations in air MV-LBS. A synthetic test circuit and a model switch are designed based on the standards to simulate making operations under fault conditions similar to a real test. The test condition is set to achieve high pre-strike arcing time and energy. The results show that the most destructive impact of the making short-circuit current occurs in the first half-cycle of the load current when the pre-strike arc is formed. For an average short-circuit current with a peak of 22 kA and a breakdown voltage of 20 kV, the switch failed to re-open due to the arcing contacts welding after four successive making operations without main contacts and seven successive operations with main contacts. It has been shown that the total arcing contact mass loss occurs mainly during the pre-arcing time. Increasing the closing speed could be a possible solution to minimize the impact of arcing.

***Index Terms*—medium voltage (MV), load break switch (LBS), making operations, contacts erosion, arcing contacts, main contacts, arc erosion.**

I. Introduction

System and component development are the prerequisites for evolution in future distribution networks. A high number of successful and reliable operations is required for gas-insulated switchgear (GIS), while the use of SF_6 has been or is going to be banned because of its environmental impact. The California Air Resource Board (CARB) has planned to start SF_6 phase-out in 2025, and European countries have aimed to cut the F-gas emission by two-thirds by 2030 compared to 2014 [1].

So far, SF_6 has been the most efficient insulation gas for arc-based switchgear because of its high dielectric strength and its superior thermal properties leading to an outstanding arc quenching performance. SF_6 alternatives should be chosen to lead the switch design to be compact and efficient at an affordable price. CO_2 is one of the alternatives in a mixture with N_2, F-Ketones, or F-Nitriles, providing reasonable interrupting performance [2-5]. However, this is still not as good as SF_6 based interrupters. Air and air mixtures are considered as other solutions [5, 6]. Air as a cost-efficient alternative to SF_6 has a dielectric strength of approximately one-third of SF_6 at atmospheric pressure, which needs a larger interrupter with a higher gas pressure for a successful interruption performance. Therefore, a total change in the design of SF_6-based switchgears is necessary to make them compatible with air as the insulation gas.

Replacing SF_6 with air as insulation gas in a medium voltage load break switch (MV-LBS) with a compact design based on SF_6 features is challenging. According to IEC 62271-200 [7], medium voltage is generally applied to voltages above 1 kV up to 52 kV. The most common rated operation voltages for MV-LBS are 12 kV, 24 kV and 36 kV. MV-LBS at the rated operation voltages should be designed to successfully interrupt load currents up to 1250 A and withstand short-circuit currents of tens of kiloamperes in the making operation. Evaluating the performance of air-based MV-LBS is essential to reach a practical and cost-efficient design. A number of studies have been performed on interruption performance. Ablation-assisted current interruption and investigation on airflow, contacts, nozzle material and geometries at different switching conditions have been studied to understand the process and find an appropriate design for a successful current interruption for air-based MV-LBS [8-10]. In addition to load current interruption, the switch should be able to withstand different fault conditions.

Short-circuit current levels could be increased by the reinforced network structure. Furthermore, a reduction in network losses leads to larger DC-time constants of the short-circuit current, leading to larger peak values of the fault current. Therefore, the switch should be able to pass short-circuit currents of tens of kiloamperes while closing and be able to re-open for the next operation. While the distance between the contacts is decreasing by closing the switch, a breakdown occurs at a specific distance due to the potential difference across the switch which results in ignition of a pre-strike arc. The short-circuit current flows through the arc column before contacts being fully closed. The dissipated arc energy could be partly absorbed by the contacts' surfaces, resulting in the contact surfaces melting and evaporating. Subsequently, the contacts with melted surfaces could be welded in the closed

This work was supported by the Norwegian Research Council under Grant 269361. *(Corresponding author: Naghme Dorraki.)*
N. Dorraki and K. Niayesh are with the Department of Electric Power Engineering, Norwegian University of Science and Technology, 7491 Trondheim, Norway (e-mail: naghme.dorraki@ntnu.no, kaveh.niayesh@ntnu.no).

position when the majority of fault current passes through them, preventing the switch from re-opening [11]. Since air as an insulation gas alternative to SF_6 has lower dielectric strength, a higher arcing and larger dissipated energy in the pre-strike arc are expected. Therefore, the impact analysis of making operation for air-based MV-LBS is crucial for optimizing the switch design and estimation of its service life. Although there are several studies on electrical contacts erosion as a consequence of arc [12-14], there is still a research gap in understanding the erosion mechanisms of sliding contacts under short-circuit conditions. Pre-strike arcing between the contacts sliding through each other with molten surfaces while passing short-circuit current of kiloamperes represents a complicated case, which has not been investigated thoroughly in the literature. This is not only the case in MV-LBS, but also in earthing switches used in power switchgear. Therefore, understanding the switch behavior during making operation is crucial to avoid switch failure because of contacts welding.

The erosion of electrical contacts exposed to an arc has been shown to be dependent on the contacts material, structure, and geometry. Composite contact materials tend to have higher erosion than pure material due to problems regarding the processing technique, grain size, and impurities [12, 15, 16]. Understanding the mechanism responsible for the increase in erosion requires investigating the switching processes under different test conditions. The purpose of this article is a laboratory assessment of the air-based MV-LBS in making operations for different fault conditions. A synthetic test circuit is established, and a test object similar to the commercial model is designed. The analysis of the switching behavior is presented, including the role of arcing and main contacts in switch failure due to erosion/welding at different short-circuit current levels and closing speeds. The ohmic losses when the contacts with molten surfaces are sliding though each other are also evaluated to extend the results to longer short-circuit making current.

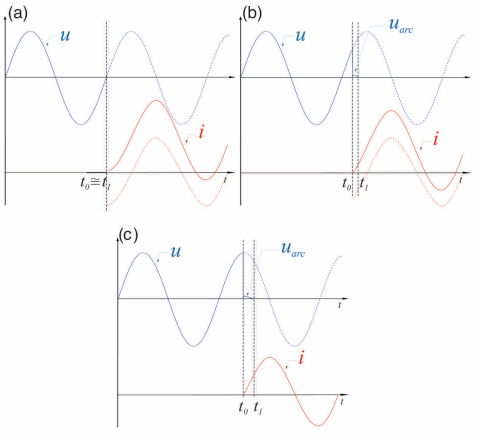

Figure 1. Three typical cases for the moment when the switch is closed; (a) asymmetrical making operation with negligible arc energy, (b) randomly moment of closing, (c) symmetrical making operation with high arc energy

II. Experiment Method

In this section, the method and technique for evaluating the switch behavior under fault conditions are described.

A. Synthetic test circuit

The experiments are designed to achieve the highest level of arc energy to investigate the effect of pre-strike arc on the switch malfunction. The switch could be subjected to different arcing times, depending on the moment of closing. In real-world applications, the switch could be closed at each phase of the power-frequency voltage. Figure 1 shows current and voltage waveforms in a real making operation at three different closing moments. If the switch closes when the applied voltage is zero, an asymmetrical network frequency current passes through the switch, shown in Figure 1 (a). In this case, the arc energy is negligible, but the largest current amplitude flows through the switch, this is called high current case. In contrast, if the breakdown occurs at the peak of the applied voltage, a symmetrical network frequency current passes through the switch. In this case, the largest possible arc energy is dissipated between the contacts, this is called high-energy case (see Figure 1 (c), where u is the network voltage, and i is the making current). The pre-strike arc burns in the time interval between t_0 and t_1; the breakdown occurs at t_0, and the switch is closed at t_1. Figure 1 (b) shows a random moment of closing operation. The current waveshape is between the cases shown in Figure 1 (a) and (c), so that the maximum current is less than case (a), and the maximum energy is less than the case (c).

To simulate the real-world making operation in laboratory, a synthetic test circuit for the making operation according to IEC 62271-101 is established [17]. In this case, the high energy test is performed, which corresponds to the largest energy dissipation in the making switching arc. The schematic of the synthetic test circuit is shown in Figure 2. The circuit consists of two parts, the high current circuit and the high voltage one. The high current part includes a high-power transformer which can supply network frequency short-circuit currents of tents of kiloamperes. The high voltage circuit subjects the test object to the operation voltage by energizing the charged capacitor. The capacitor is charged to the operation voltage by the DC high voltage power supply. Once charged, switch S_1 is disconnected. A pre-strike arc ignites between the contacts due to dielectric breakdown while closing the switch. Immediately after the breakdown, a signal will be sent to the trigger vacuum switch (TVS) and the high current circuit injects one half-cycle of the 50 Hz short circuit current by connecting the transformer output

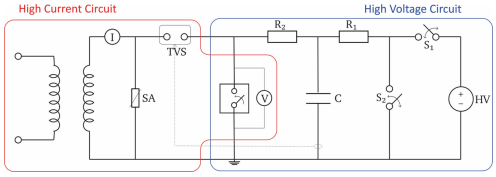

Figure 2. Schematic of the synthetic test circuit for performing the making operation.

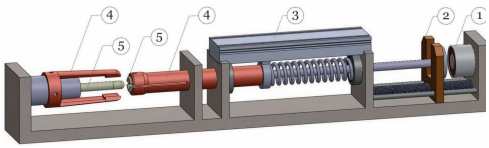

Figure 3. Spring-type test object; (1) Solenoid magnet, (2) Contacts' separator, (3) Position sensor, (4) Main contacts, and (5) Arcing contacts.

to the test object. The time delay between the detection of a current flow caused by breakdown of the switch and connection of the high current circuit is less than 50 µs. Switch S_2 is open during the making test and is closed when the test is over for the sake of safety. A 6015A Tektronix voltage probe together with TDS2014B Tektronix oscilloscope 8-bit measure the arc voltage. The time resolution of the measurements has been 4 µs, and a Rogowski coil measures the arc current. An additional voltage measurement is used to measure the charging voltage of the capacitor. The combination of both measurements is shown in Figure 5b.

The experiments are designed based on the third case (Figure 2 C) at the breakdown voltage of 20 kV, equivalent to the peak of the rated voltage of a 24 kV MV-LBS. It has to be mentioned that there are some uncertainties in having the breakdown precisely on the peak of applied voltage because of the system synchronization accuracy of ±0.001 s, and the random behavior of arc ignition due to the eroded contact surfaces. Therefore, there is a slight difference in di/dt under the same test conditions.

B. Test Object

A spring-type drive mechanism is designed as the test object. A schematic of the test object is shown in Figure 3. The moment of breakdown is adjusted by triggering the solenoid magnet to release the dynamic contact. A position sensor records the movement of the contacts. The arcing contacts include a pin with a diameter of 10 mm and a split tulip with an outer diameter of 20 mm and an inner diameter slightly less than 10 mm to provide full touch in the closed position. The arcing contacts are made of copper/tungsten (20/80), and the clamp-shaped main contacts are made of copper. The main contacts are fixed for all the tests and four pairs of arcing contacts have been examined for different test conditions.

The contacts' material and the closing speed of ~3 m/s are chosen for the model switch not to be too different from the commercial switches. A higher closing speed can shorten the arcing time and reduce the arc energy, while keeping the other design parameters constant. By adjusting the spring length, a higher closing speed of ~ 4 m/s is realized in order to analyze to what extent an increased closing speed would reduce the destructive effects of the making operation on the switch.

A typical travel curve of the dynamic contact is shown in Figure 4. Mechanical closing of the switch without applying any current shows an average speed of ~ 4 m/s (blue dashed line), while passing the short-circuit current reduces the closing speed as indicated by the change in the steepness of the travel curve

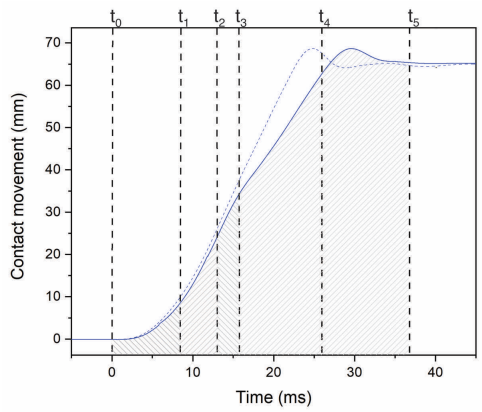

Figure 4. Travel curve of the dynamic contact with a closing speed of ~4 m/s, divided into main operation intervals based on IEC 62271-101; the high-voltage interval (t_0-t_1), pre-arcing interval (t_1-t_2), and latching interval (t_2-t_5).

(blue solid line). The deviation is due to electrodynamics' forces made by the high short-circuit current and the forces caused by the pressure increase due to the pre-strike arc acting against the switch closing.

The making operation under a short-circuit current could be divided into three main intervals based on the contact movement. This helps to better understand the applied stresses on the switch at different stages of the making operation. The time from releasing the contact by the solenoid magnet (t_0) to the arc ignition in between the contact (t_1) is considered as a high-voltage interval. From the breakdown time until the arcing contacts touch (t_2) is called the pre-arcing interval. The latching interval is the time from t_2 when the arc seizes as the contacts touch to the time of full closure of the switch (t_5). t_3 is the moment when the main contacts meet, and t_4 is the zero-crossing of the short-circuit current. The time interval between t_2 and t_3 is considered a part of the latching interval when no arc exists. The short-circuit current passes through the arc column between the arcing contacts in pre-arcing interval. The arc contacts, however, carry a small fraction of the short circuit current in the main part of the latching interval (in the time period from t_3 to t_4) when the arcing and main contacts are both closed.

The experiments are designed to investigate the making performance of the switch at different closing speeds and levels of short-circuit current. The applied voltage of 20 kV is chosen as the breakdown voltage for all the tests, which is equivalent to the peak of the rated voltage for MV-LBS. All the tests have been repeated for four different samples to reduce the measurement error. To distinguish the role of arcing contacts and main contacts, all the tests have been repeated with and without main contacts. The total average weight of arcing contacts (pin+tulip) is ~52 g, which makes it possible to measure the contacts mass loss with a precise scale with accuracy of ±0.00001 g. To avoid the contacts being

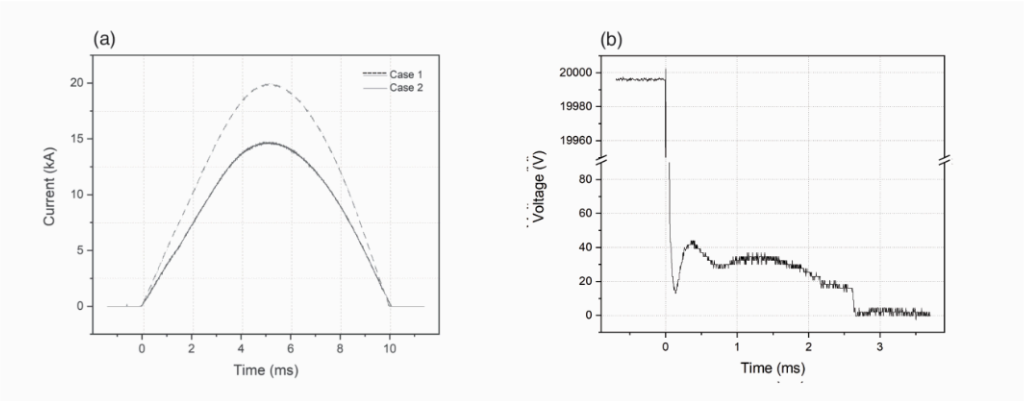

Figure 5. Half-cycle 50 Hz short circuit current with a peak of 14.8 and 20.2 kA (a), arc voltage measurement for the first making test (b).

contaminated during the process, each pair of contacts were kept in a separate enclosure. No specific cleaning procedure was used in order to be close to the real operation. The total arc energy and effective arc energy close to the surface of the contacts are measured for each test to evaluate the switch operation under the specific fault condition.

III. Results

In this section the results regarding pre-strike arcing and contacts erosion are presented to find the interrelation between fault conditions, operational parameters, and the switch wear.

A. Arc energy

The arc voltage and current are directly measured for each test. Because of the 1 ms jitter of the test object, there is a slight difference in di/dt for different tests under the same conditions. In this case, the first half-cycle of the current waveforms differs slightly. It is, however, negligible for the calculation of pre-strike arc energy since the arc current does not vary considerably in the pre-arcing interval. Depending on the series inductance in the primary side of the transformer, the amplitude of the short circuit current can be adjusted. Figure 5 (a) shows half-cycle 50 Hz current waveforms considered as two short-circuit current levels used in the experiments and Figure 5 (b) shows an arc voltage waveform for the first making test. Figure 6 shows a sequence of six making tests following Figure 5 (b) on one pair of arcing contacts under the short circuit current of case 1. All the voltage waveforms show a sharp fall from the dielectric breakdown voltage at 20 kV to the arc voltage, which is in the order of tens of volts. The first 50 µs of the voltage fall is neglected due to interference with electromagnetic noises caused by air breakdown. An increase in the arc voltage is recorded followed by a gradual decay in the waveform. The increase in the arc voltage shows the difference between static and dynamic arcs. As previously mentioned in pre-strike arc characteristics [18], the peak in arc voltage belongs to the stage when the pre-strike arc stabilizes in the center while the contacts are closing. A rapid decrease from 16 – 18 V to zero is observed in all the voltage waveforms at the time of arc contact closure, which refers to the minimum arcing voltage, i.e., the anodic plus cathodic voltage drop for tungsten/copper (80/20) [12, 15, 19, 20]. The pre-strike arc duration is measured based on the voltage waveform from the moment of breakdown to voltage zero, equivalent to the pre-arcing interval. Since it is only possible to measure the arc current and voltage over the electrical contacts, the arc energy is estimated by the following equation:

$$E = \int_{t_1}^{t_2} i_{arc}(t) \,.\, u_{arc}(t)\, dt \qquad (1)$$

A series of operations are performed for two closing speeds of 3 and 4 m/s for four different samples. The making test is repeated on each until the switch fails to re-open due to the arcing contacts welding. The arcing time and energy are measured for each specific test. Figure 7 shows the interrelation between the dissipated arc energy and arcing time for different

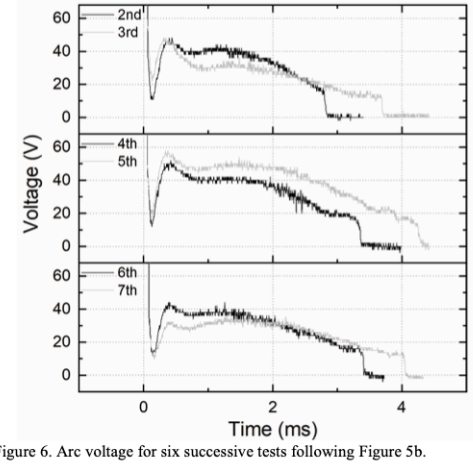

Figure 6. Arc voltage for six successive tests following Figure 5b.

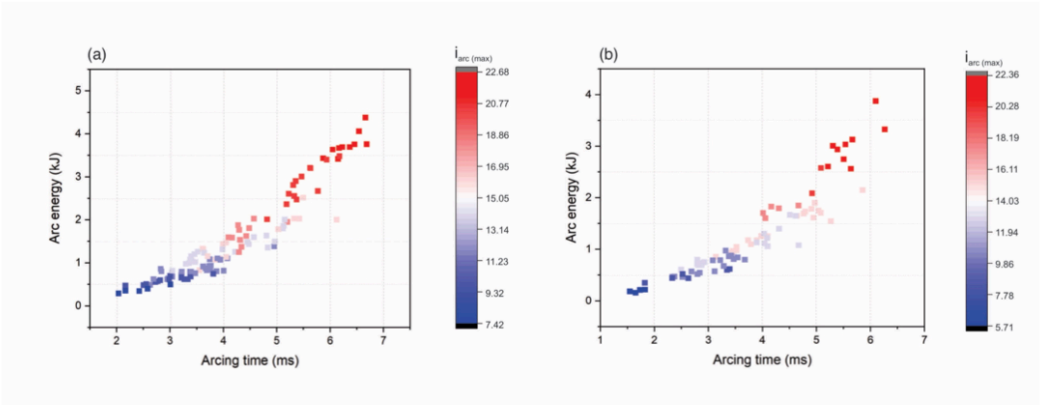

Figure 7. Pre-strike arc energy as a fuction of arcing time for different level of short-circuit current at the touching moment of arcing contacts for two closing speed of (a) 3 m/s and (b) 4 m/s.

short-circuit current values at the touching moment of the arcing contacts (t_2 - Figure 4). It can be seen that the dissipated arc energy is increasing with both the arcing time and the part of short-circuit current that passes through the arc column before the arcing contacts touch (pre-arcing interval).

B. Mass loss

The rate of contacts' mass loss could provide information on the switch service life prediction. The difference in the mass loss at each test and the total mass loss are measured to identify the erosion rate under different fault conditions. After each test, the arcing contacts have been removed to be weighed and reinstalled for the next operation. The reproducibility of the tests has been examined for four different samples. The making test is repeated on same sample until welding of the arcing contacts occurs. Some previous investigations considered the total arc energy involved in the contacts' mass loss including cathode/anode fall energy, radiations, the energy of neutral atoms [15] [21, 22]. However, there are some other studies that presented the mass loss as a function of cathode/anode fall energy [12, 23]. Due to the complexity of distinguishing different energy components, it is still controversial to present each energy component contribution in contact wear. To perform a comparative analysis, both cases are evaluated with/without the main contacts. The arc energy close to the surface of the contacts is estimated by the following equation:

$$E_{C/A} = \int_{t_1}^{t_2} \Delta U_{eff} \cdot i_{arc}(t)\, dt \qquad (2)$$

where ΔU_{eff} is sum of the effective voltages for cathode and anode presented by equations (3) and (4), respectively [12].

$$\Delta U_{eff-} = \Delta U_{cathode} - \left(\frac{5}{2}\frac{kT_e}{e} + \frac{\phi}{e}\right) \qquad (3)$$

$$\Delta U_{eff+} = \Delta U_{anode} - \left(\frac{5}{2}\frac{k(T_p - T_e)}{e} + \frac{\phi}{e}\right) \qquad (4)$$

T_e, T_p, and T_a are the electron, plasma, and anode surface temperatures. ϕ is the work function. Since $T_e \approx (T_p - T_a)$, the effective electrode voltage is defined as:

$$\Delta U_{eff} = \Delta U_{cathode} + \Delta U_{anode} \approx 16.7\ V \qquad (5)$$

The electrodes voltage fall for tungsten/copper(80/20) is assumed to be around 16.7 V [12][15, 19][20], which corresponds to the average voltage drop in the measurements, when the contacts touch. A series of tests were performed with and without main contacts for both closing speeds to show the role of main contacts on reducing the rate of contacts erosion. The difference in mass loss versus the total arc energy (equation. 1) and the electrode fall energy (equation. 2) are evaluated for arcing contacts during making operation with/without main contacts in Figure 8 and Figure 9, respectively. For both cases, an increase in the energy leads to more mass loss, while the total arc energy is significantly higher than electrode fall energy.

To identify the effect of main contacts on the prolongation of the switch service life, a series of tests were repeated on each sample with and without main contacts until switch failure due to contacts welding. Figure 10 and Figure 11 show the total mass loss of the arcing contacts by repeating the making test with and without main contacts, respectively. The mass loss varies a lot in some of the tests, while the average shows a meaningful erosion rate in the series of the experiments. The variation could be due to the difference in the dissipated arc energy because of the random arc ignition on the eroded surfaces. The total mass loss is measured after each test for two cases presented in Figure 5. The average short-circuit current is higher for case 1 compared to case 2. For the model switch, including arcing and main contacts at a closing speed of 3 m/s, the making test was repeated six times on same sample to record the first contacts welding for case 1. Two more samples out of the remaining three were welded after the seventh making test in case 1 with a 3 m/s closing speed. Some erosions on the main contacts have been observed at this step besides the arcing

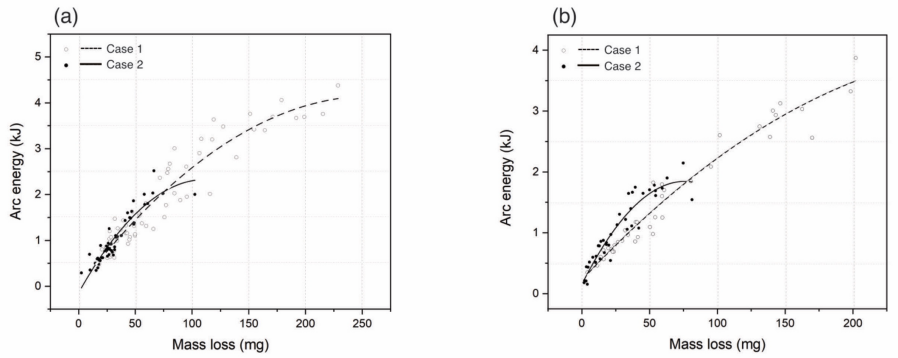

Figure 8. The mass erosion rate as a function of pre-strike arc energy for a series of operations with (a) and without (b) main contacts.

contacts welding. The shaded regions in Figure 10 show the making tests where erosion on the main contacts is observed. At the closing speed of 4 m/s, the increase rate of the total mass loss is slower than 3 m/s for both cases, which means the switch can withstand a higher number of making operations at higher speed of closing. For the model switch including the arcing contacts (without the main contacts), the switch failed to re-open upon three out of four samples after the fourth test in case 1, with a closing speed of 3 m/s. The recorded total mass loss resulting in contacts welding at closing speed of 3 m/s is about three times higher compared to the tests under the same conditions at the closing speed of 4 m/s. The highest mass loss is recorded for case 1, with a higher short-circuit current compared to case 2.

C. *Arcing contacts degradation*

By repeating the making operation on one pair of arcing contacts, more contact wear is observed. Higher pre-strike arcing time and dissipated energy lead to higher contacts erosion. Figure 12 shows the arcing contacts' (cathode) degradation for the tests with and without main contacts. The intermediate states after each test are shown and these ended up welding after four operations without main contacts and after seven operations with main contacts at a short-circuit current in case 1 and a closing speed of 3 m/s. The images illustrate rough and uneven surfaces with fissures and pitting. A gradual decrease in the pin width is observed by repeating the making operation. For these two cases, the total mass loss resulting in contacts welding with and without main contacts is reported 831.3 and 445.1 mg, respectively.

IV. Discussion

For MV-LBS during the making operation under a fault condition, the arcing contacts erosion starts in the pre-arcing interval when the dissipated arc energy is partly absorbed by the contacts' surfaces, resulting in their melting and evaporation. The results show that the probability of switch failure due to contacts welding increases by more erosion in arcing contacts where the contacts' mass loss increases by absorbing dissipated arc energy during the pre-arcing interval (Figure 10 and Figure 11). It can be inferred that the pre-strike arcing causes contact surface melting. However, it is controversial whether the total

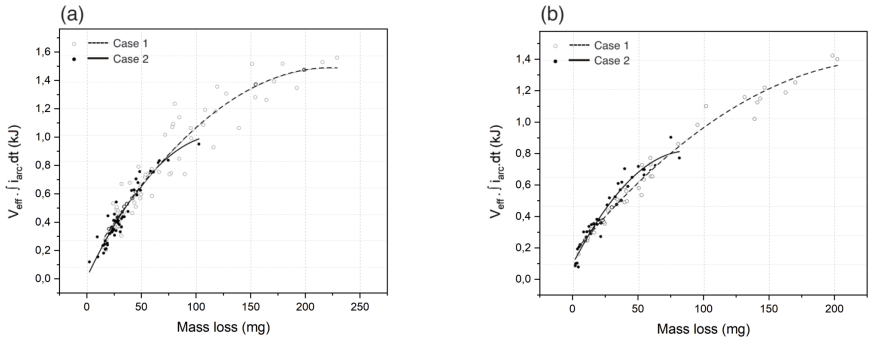

Figure 9. The mass erosion rate as a function of electrodes fall energy for a series of operations with (a) and without (b) main contacts.

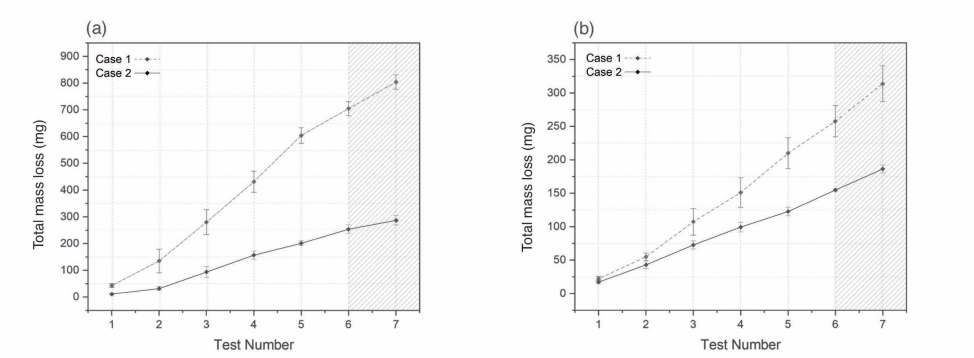

Figure 10. Mass loss from arcing contacts with main contacts in the model switch for two cases of short-circuit current at a closing speed of (a) 3 m/s, and (b) 4 m/s. The shaded parts show the tests where erosion on the main contacts is observed.

dissipated arc energy should be considered as a factor of contacts erosion or the energy close to the surface of contacts regarding the cathodic and anodic voltage fall (electrode fall energy). Figure 8 and Figure 9 show the variation of the total arc energy and electrodes fall energy with the electrodes mass loss. It can be inferred that the variation of total dissipated arc energy is more pronounced than the electrode fall energy with the increase in the electrodes mass loss and there is a significant difference between them in high rate of mass loss. The correlation between mass loss and total arc energy is very good with a non-linear correlation coefficient of 0.97. The calculated non-linear correlation coefficient between electrode fall energy and mass loss was 0.94, which indicates that this parameter can also be used for the mass loss determination almost as good as the total energy. Besides, it can be seen that the same amount of total arc energy at different current levels causes approximately same contacts mass loss (Figure 8). The same results obtained for the electrodes fall energy are shown in Figure 9. However higher level of short-circuit current increases the probability of higher amount of dissipated energy, taking into account that the arcing time could not be longer than the first half-cycle of short-circuit current.

After the arcing contacts touch, the fault current continues to flow through the molten contacts, contributing to more energy dissipation. A part of current flows through the molten bridge between sliding contacts, which can further increase the dissipated energy and possibly contribute to the contact deterioration. While closing the switch, expansion of the molten zone between two sliding contacts [24] changes the contact resistance during latching time.

A closer view of the voltage waveform shows slight changes in the voltage after the abrupt jump associated with the arcing contact touch. Figure 13 shows the typical current and voltage waveforms for a making test where the voltage and current change during arcing (t_1-t_2) and latching (t_2-t_4) intervals. The resistance of moving contacts during latching interval is calculated for operations with just arcing contacts. Typical resistance profiles of sliding arcing contacts for successive tests with the current in case 1 at two closing speeds are shown in Figure 14. In a separate measurement, the contacts' resistance

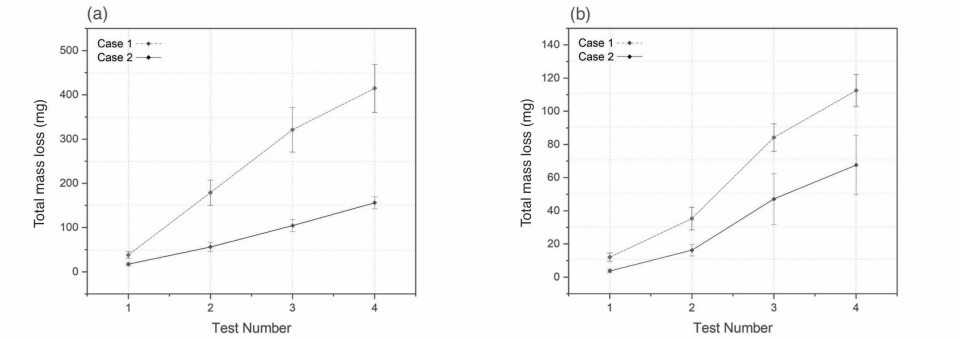

Figure 11. Mass loss from arcing contacts without main contacts in the model switch for two cases of short-circuit current at closing speed of (a) 3 m/s, and (b) 4 m/s.

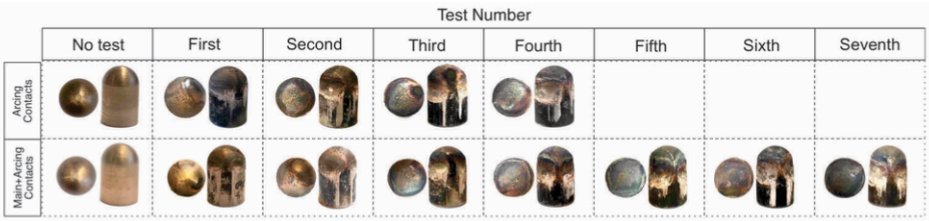

Figure 12. Arcing contacts' degradation after repeating the making test 4 times without main contacts and 7 times with main contacts. Both in case 1 with a closing speed of 3 m/s.

in the closed position of the switch is assessed as being in the range of 300 - 350 μΩ without passing short-circuit current. As shown in Figure 14, the resistances for both closing speeds are less than the steady state cold resistance of the main contacts. This is because of the increased effective contacts area provided by the molten metal on the contacts' surfaces. However, the deterioration of the arcing contact surfaces by repeating the operations makes the contacts' surfaces rougher, and changes the contact diameter, resulting in an increase of the measured resistances.

To evaluate the impact of energy dissipated by ohmic losses on arcing contacts welding, an equivalent circuit at the stage of arcing contacts touching, and the position where the main contacts approach, if this exists, is considered as shown in Figure 15 (a) and (b) respectively. r_c is the resistance of the contacts' touchpoint where the surface temperature is highest (and the surface is most probably molten) due to exposure to the pre-strike arc, and $R(t)$ is the total resistance between the switch contacts. Therefore, the current flowing through the contacts' touchpoint (i_c) is defined as follows:

$$i_c(t) = i(t) \cdot \frac{R(t)}{r_c} \tag{6}$$

where i(t) is the total current flowing through the switch, r_c is the resistance of the touchpoint at t_2 determined from the resistance profile. Consequently, the energy dissipated (Ohmic losses) when the arcing contacts touch is described as follows:

$$E_c = \int_{t_2}^{t_4} r_c \cdot i_c^2(t) \cdot dt = \int_{t_2}^{t_3} \frac{R_1^2(t)}{r_c} \cdot i^2(t) \cdot dt + \int_{t_3}^{t_4} \frac{R_2^2(t)}{r_c} \cdot i^2(t) \cdot dt \tag{7}$$

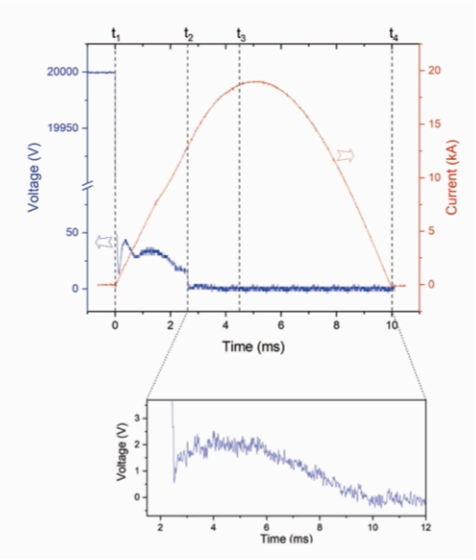

Figure 13. Typical current and voltage waveforms in a full making operation (arcing time: t_1 - t_2; latching time: t_2 - t_3).

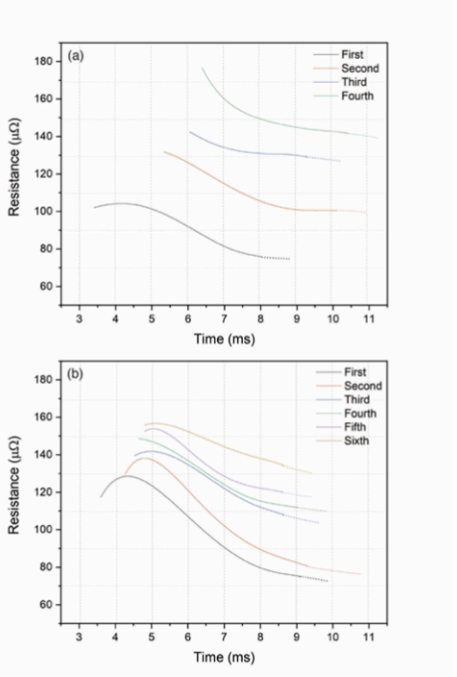

Figure 14. Arcing contacts' resistance in a series of operations under case 1 test conditions during latching time at a closing speed of 3 m/s (a) and 4 m/s (b)

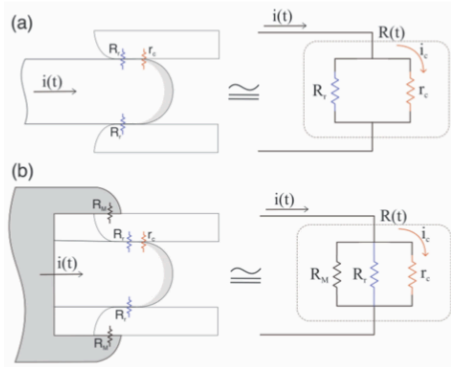

Figure 15. Schematic of the switch in closed position and the equivalent circuit with arcing contacts (a) and arcing and main contacts (b).

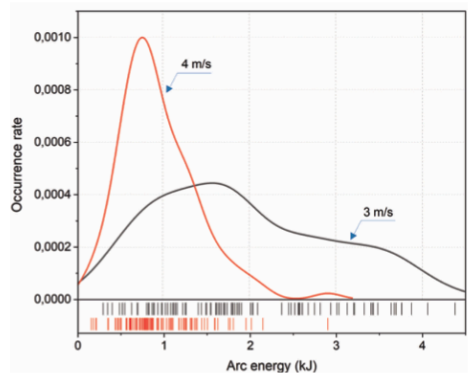

Figure 16. Distribution of the pre-strike arc anergy in case 1 with arcing contacts for closing speed of 3 and 4 m/s

where $R_2(t)$ and $R_1(t)$ are the total resistance between the switch contacts with and without main contacts, respectively. Table 1 shows detailed values of time intervals during arcing and latching stages for one of the measured series. The ohmic loss is calculated for each case. It can be seen by the increase in arcing time after each test, t_2-t_3 is going to be smaller, which indicates the arcing contacts erosion shown in figures 6, 7, and 10. The reduction continues until t_2 becomes equal to t_3, which means the arc still burns between arcing contacts when the main contacts touch (if exist). That is the reason of observed erosion in main contacts mentioned in section III. B. Figure 15 (b) shows the schematic circuit of the switch in closed position if the main contacts are involved. In this case, R_m is the resistance of the main contacts in closed position, which is considerably smaller than r_c. Therefore, if the main contacts exist in the switch, most of the current passes through them, increasing the switch service life from four series of operations to seven times based on the obtained results.

As discussed in section II. A. these series of experiments are designed to reach the highest pre-strike arcing time, which occurs at a symmetrical current waveform. However, in real situations, the switch would be closed randomly, resulting in an asymmetrical current waveform. Equation 8 shows the destructive joule heating energy that causes switch failure in both forms of current waveforms (symmetrical and asymmetrical) includes pre-strike arc energy (E_{arc}) and ohmic loss energy (E_{OL}) which are described in detail in the previous sections

$$E_{destructive} = E_{arc} + E_{OL} = \int_{t_1}^{t_2} i_{arc}.V_{arc}.dt + \int_{t_2}^{t_4} i_c^2(t).r_c\,.dt \quad (8)$$

Table 1. Making operation time intervals and Ohmic losses at two closing speeds (3 and 4 m/s) with arcing contacts at case 1.

Closing speed	Test #	t_{arcing} (ms)	$t_{latching}$ (ms)		E_c (j)		E_T (j)
			t_2-t_3	t_3-t_4	t_2-t_3	t_3-t_4	
3 m/s	1	3.4	1.15	4.35	62.9	38.7	106.8
	2	5.3	0.73	5.17	46.1	126.2	196.03
	3	6.1	-*	4.23	-	90.4	96.4
	4	6.4	-*	5.1	-	182.2	208.8
4 m/s	1	3.6	0.68	5.82	29.07	131.6	171.4
	2	4.2	0.77	5.93	43.98	156.5	225.07
	3	4.5	0.32	4.98	17.15	133.7	157.7
	4	4.6	0.33	4.87	16.5	121.5	153.5
	5	4.8	-*	5.29	-	139.2	153.06
	6	4.8	-*	5.06	-	134.4	140.2

*. at this timing, t_2 would be equal to t_3

Referring to the results shown in Figure 7 and Table 1, E_{arc} is much higher than E_{OL}. Therefore, if no arc burns between the arcing contacts in the first half-cycle of the short-circuit current, the ohmic loss is not sufficiently high to cause switch malfunction. Hence, it can be concluded that the most destructive impact of making operation on switch function occurs in the first half-cycle of short-circuit current, in which the pre-strike arc forms and the short circuit current flows through the sliding arcing contacts before the main contacts touch. Therefore, extending the obtained results in the present study to making tests combined with the rated short-time withstand current of 0.2 s (IEC 62271-103 [25]) is valid.

The presence of main contacts in addition to arcing contacts in MV-LBS could prolong the switch service life, as shown in figures 9 and 10. However, it is not the final solution since the arcing contacts welding occurred after seven successive making operations (Case I). Increasing the closing speed is one of the solutions to reduce the impact of pre-strike arc on switch failure in making operation. The results show a slower rate of mass loss and less dissipated arc energy, with increasing the closing speed shown in the histogram graph in Figure 16. The increase in the closing speed decreases the pre-strike arc dissipated energy and arcing contact wear. Therefore, the rate of increase in the resistance is slower for the higher closing speed. However, there are other methods to decrease the arcing time like using pressurized insulation gas or different types/mixtures of insulation gas with superior insulation properties.

V. Conclusion

The making operation at different fault conditions is investigated for air-based MV-LBS. The factors and parameters involved in operations are evaluated based on synthetic testing,

which is equivalent to direct testing. The following are the main findings of this study:

- The higher the pre-strike arcing time and current, the higher the dissipated arc energy between the contacts while closing.
- Arcing contacts' mass loss is mainly dependent on pre-strike arcing.
- The model switch failed to re-open due to arcing contacts welding after four successive making operations without main contacts and after seven successive operations with main contacts with a short circuit peak current of 22 kA and a breakdown voltage of 20 kV.
- The destructive energy responsible for the degradation of contacts during the pre-strike arc is much higher than the ohmic losses caused by the fault current flow through the sliding contact
- Having the main contacts in the model switch can prolong the switch service life by reducing the ohmic losses between arcing contacts in the closed position.
- The most destructive effects of the making operation occur in the first half-cycle of the short-circuit current (when the pre-strike arc burns). Hence, the results of this study can be extended to longer fault currents.
- Increasing the closing speed reduces the pre-strike arcing time and the rate of increase of sliding contact resistance during the latching interval.

VI. Acknowledgment

This work is financially supported by the Norwegian Research Council, grant # 269361. The authors would like to thank Marius Strand for his contribution in carrying out the experiments, and Bård Ålmos, Morten Flå, and Dominik Häger from NTNU for technical support.

VII. References

[1] N. Hatziargyriou and I. P. de Siqueira, *Electricity supply systems of the future*. Springer Nature, 2020.

[2] M. Seeger, R. Smeets, and J. Yan, "Recent development of alternative gases to SF6 for switching applications," *ELECTRA (cigre),* 2017.

[3] M. Bendig and M. Schaak, "Design Rules for Environmentally Friendly Medium Voltage Load Break Switches," *IEEE Transactions on Power Delivery,* 2020.

[4] M. Taki, D. Maekawa, H. Odaka, H. Mizoguchi, and S. Yanabu, "Interruption capability of CF/sub 3/I Gas as a substitution candidate for SF/sub 6/gas," *IEEE Transactions on Dielectrics and Electrical Insulation,* vol. 14, no. 2, pp. 341-346, 2007.

[5] X. Li, H. Zhao, and A. B. Murphy, "SF6-alternative gases for application in gas-insulated switchgear," *Journal of Physics D: Applied Physics,* vol. 51, no. 15, p. 153001, 2018.

[6] N. S. Støa-Aanensen, M. Runde, E. Jonsson, and A. Teigset, "Empirical relationships between air-load break switch parameters and interrupting performance," *IEEE Transactions on Power Delivery,* vol. 31, no. 1, pp. 278-285, 2016.

[7] *IEC 62271-200: AC metal-enclosed switchgear and controlgear for rated voltages above 1 kV and up to and including 52 kV*, 2021.

[8] H. Taxt, K. Niayesh, and M. Runde, "Self-Blast Current Interruption and Adaption to Medium-Voltage Load Current Switching," *IEEE Transactions on Power Delivery,* vol. 34, no. 6, pp. 2204-2210, 2019.

[9] H. Taxt, K. Niayesh, and M. Runde, "Medium-voltage load current interruption in the presence of ablating polymer material," *IEEE Transactions on Power Delivery,* vol. 33, no. 5, pp. 2535-2540, 2018.

[10] E. Jonsson and M. Runde, "Interruption in air for different medium-voltage switching duties," *IEEE Transactions on Power Delivery,* vol. 30, no. 1, pp. 161-166, 2014.

[11] K. Niayesh and M. Runde, *Power switching components*. Springer, 2017.

[12] J. Tepper, M. Seeger, T. Votteler, V. Behrens, and T. Honig, "Investigation on erosion of Cu/W contacts in high-voltage circuit breakers," *IEEE transactions on components and packaging technologies,* vol. 29, no. 3, pp. 658-665, 2006.

[13] T. Cheng, W. Gao, W. Liu, and R. Li, "Evaluation method of contact erosion for high voltage SF6 circuit breakers using dynamic contact resistance measurement," *Electric Power Systems Research,* vol. 163, pp. 725-732, 2018.

[14] Y. Wu *et al.*, "Visualization and mechanisms of splashing erosion of electrodes in a DC air arc," *Journal of Physics D: Applied Physics,* vol. 50, no. 47, p. 47LT01, 2017.

[15] P. G. Slade, *Electrical contacts: principles and applications*. CRC press, 2017.

[16] J. J. Shea, "Erosion and resistance characteristics of AgW and AgC contacts," *IEEE Transactions on Components and Packaging Technologies,* vol. 22, no. 2, pp. 331-336, 1999.

[17] *IEC 62271-101: Synthetic testing*, 2021.

[18] N. Dorraki and K. Niayesh, "Optical investigation on pre-strike arc characteristics in medium-voltage load break switches," *Journal of Physics D: Applied Physics,* vol. 54, no. 25, p. 255503, 2021.

[19] Y. Yokomizu, T. Matsumura, R. Henmi, and Y. Kito, "Total voltage drops in electrode fall regions of, argon and air arcs in current range from 10 to 20 000 A," *Journal of Physics D: Applied Physics,* vol. 29, no. 5, p. 1260, 1996.

[20] A. Marotta and L. I. Sharakhovsky, "Heat transfer and cold cathode erosion in electric arc heaters," *IEEE Transactions on plasma science,* vol. 25, no. 5, pp. 905-912, 1997.

[21] M. Mohammadhosein, K. Niayesh, A. A. Shayegani-Akmal, and H. Mohseni, "Online assessment of contact erosion in high voltage gas circuit breakers based on different physical quantities," *IEEE Transactions on Power Delivery,* vol. 34, no. 2, pp. 580-587, 2018.

[22] A. Bagherpoor, S. Rahimi-Pordanjani, A. A. Razi-Kazemi, and K. Niayesh, "Online condition assessment of interruption chamber of gas circuit breakers using arc voltage measurement," *IEEE Transactions on Power Delivery,* vol. 32, no. 4, pp. 1776-1783, 2016.

[23] M. Iwata, T. Ohtaka, Y. Kuzuma, and Y. Goda, "Development of a method of calculating the melting characteristics of OPGW strands due to DC arc simulating lightning strike," *IEEE transactions on power delivery,* vol. 28, no. 3, pp. 1314-1321, 2013.

[24] C.-y. Zhu and B.-m. Li, "Analysis of sliding electric contact characteristics in augmented railgun based on the combination of contact resistance and sliding friction coefficient," *Defence Technology,* vol. 16, no. 4, pp. 747-752, 2020.

[25] *IEC 62271-103: Switches for rated voltages above 1 kV up to and including 52 kV*, 2021.

VIII. Biographies

Naghme Dorraki received the B.Sc. degree in optics and laser engineering from the University of Tabriz, Tabriz, Iran, in 2011, and the M.Sc. degree in photonics from the Laser and Plasma Research Institute, Shahid Beheshti University, Tehran, Iran, in 2015. She is currently pursuing the Ph.D. degree with the Department of Electric Power Engineering, Norwegian University of Science and Technology (NTNU), Trondheim, Norway. Her main interests are diagnosis of power switching components and plasma-material interactions.

Kaveh Niayesh (Senior Member, IEEE) received the B.Sc. and M.Sc. degrees in electrical engineering from the University of Tehran, Tehran, Iran, in 1993 and 1996, respectively, and the Ph.D. degree in electrical engineering from the RWTH- Aachen University of Technology, Aachen, Ger- many, in 2001. In the last 19 years, he held different academic and industrial positions including Principal Scientist with the ABB Corporate Research Center, Baden-Dättwil, Switzerland; Associate Professor with the University of Tehran; and Manager, Basic Research, with AREVA T&D, Regensburg, Germany. Currently, he is a Professor with the Department of Electric Power Engineering, Norwegian University of Science and Technology (NTNU), Trondheim, Norway. His research interests are mainly in the broad field of high voltage and switchgear technology; specifically on current interruption in power switching devices in ac and dc power networks, breakdown and aging behavior of insulation materials exposed to HVDC and repetitive fast impulses, as well as diagnostic and condition assessment of power switchgear.

Impact of pre-strike arc on contacts degradation after short circuit current making operation in medium voltage air load break switches.

30th International Conference on Electrical Contacts (ICEC), ISBN 978-3-907255-11-7, June 2021.

Paper V

Impact of pre-strike arc on contacts degradation after short circuit current making operation in medium voltage air load break switches

Naghme Dorraki, Norwegian University of Science and Technology (NTNU), Trondheim, Norway, naghme.dorraki@ntnu.no
Marius Strand, Norwegian University of Science and Technology (NTNU), Trondheim, Norway, mstran@stud.ntnu.no
Kaveh Niayesh, Norwegian University of Science and Technology (NTNU), Trondheim, Norway, kaveh.niayesh@ntnu.no

Abstract

Medium voltage load break switches are required to perform a number of making operation while passing of short circuit current that could be more than tens of kiloamperes. Using air-filled devices as an alternative to SF_6, which is a high impact greenhouse gas, makes the switch more environmentally friendly but leads to more challenging making operation due to higher arcing times and dissipated energies between the contacts. In this case, the pre-strike arc could lead to contacts welding and degradation, which is highly undesirable. This paper reports on an investigation of the pre-strike arc impact on erosion and welding of copper/tungsten (20/80) arcing contacts during short-circuit making operations. For this purpose, a synthetic test circuit consisting of a high current source in combination with a high voltage one is used. Experiments are conducted for different operation voltages, while the short circuit current is kept constant at 22 kA. Mass loss measurement and visual inspection of eroded/welded contacts are examined with regard to pre-strike arc impact on their degradation. The contacts are welded by three times repeating the test at operation voltage of 20 kV and short-circuit current of 22 kA and failed to re-open. Besides, an increase in the contacts' mass loss with arcing time is observed while the making current is constant. This is an indication that the pre-strike arc energy highly impacts the switch reliability and service life.

1 Introduction

Considering the crucial role of Load Break Switches (LBS) in Medium Voltage (MV) distribution networks, high reliable operation of MV-LBS is required [1, 2]. An MV-LBS must be able to interrupt load currents and close under fault conditions. Making of short circuit current results in fault current flow through the contacts while closing. Although MV-LBS are designed to carry fault currents of tens of kiloamperes up to few seconds in the closed position, we should consider that the current flow starts before contacts full touch moment when arc formation makes a bridge between the contacts, which will deteriorate the contacts' surfaces. The local electric field strength between the contacts increases while closing, which causes a breakdown in the insulation gas and arc burning before contacts' touch. The short circuit current flows through the pre-strike arc causes high energy dissipation between the contacts, which are partly absorbed by contact surfaces leading to their melting and evaporation. Closing the contacts with melted surfaces could lead to welding the contacts to each other and failure to re-open, which is one of the main reasons for failure in this type of switches. The stresses applied to the contact are expected to be higher during making operation compared to current interruption because of higher arc energy dissipation between the contacts [3]. The dissipated energy between contacts could be limited by arcing time, which is dependent on the dielectric strength of the insulation gas. Although SF_6 supports the design of compact, low cost, and reliable MV-LBS due to high dielectric strength, it has a high environmental impact, which put an end to using SF_6 in gas-insulated switchgear. Regarding cost-effective and environmentally friendly insulation gas, air or air mixtures could be an alternative to SF_6 [4]. However at the pressure of one bar, air with dielectric strength of 3 kV/mm causes higher arcing time compared to SF_6 with dielectric strength of 8.9 kV/mm at same making test condition which makes the switch operation even more challenging.

From the aspect of arcing contact erosion, several theoretical and experimental investigations have been done [5-7]. Simulation models have been developed based on arc-metal contacts interface to explain arc behavior under the injection of particles and metal vapors [8, 9]. Several parameters have been calculated,

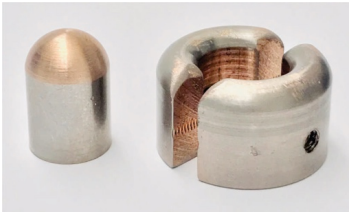

Fig 1. Electrical contacts made of W/Cu (80/20). Pin is the fixed contact (cathode) and split tulip is the dynamic one (anode).

such as contacts surface temperature, material transfer rate, arc temperature, thermal and electrical conductivity [10, 11].

It has been shown that the erosion mechanism at high current is different from the low current. Several factors affect the electrical contacts erosion in switching operation such as arc energy, arcing time, gap distance, closing velocity, contacts shape, and material properties [12]. Besides, there is still a lack of understanding of the impact of pre-strike arc on contacts erosion during making operation in fault conditions.

In this work, we focus on the impact of the pre-strike arc on the contacts degradation during making operation. A spring-type drive test object and a synthetic test circuit are employed. Arc electrical characterizations and mass loss measurement are used to find a meaningful relationship between the pre-strike arc parameters and the contacts degradation.

2 Experimental set-up

For the test type switch, the stationary contact is a pin with a diameter of 10 mm, and the dynamic one is a split tulip with an outer diameter of 20 mm and an inner diameter slightly less than 10 mm. The contacts are shown in Fig 1. The pin is the anode and the split ring is the cathode with an inner diameter slightly smaller than the pin to provide fully touch of the contacts in closed position. The contacts are made of copper-tungsten (20/80), and the closing velocity is 3 m/s. The closing speed and the material type are chosen not to differ too much from the commercial product. The test circuit is a synthetic making circuit based on the IEC 62271 standard [13]. The circuit includes two parts; high current and high voltage sources. The high voltage circuit supplies the test voltage for dielectric breakdown while the switch is closing. Once the breakdown happens, a signal is sent to the high current source to initiate the flow of the transient making current. A schematic of the synthetic circuit is shown in Fig 2 (a). The test object is a spring-type switch with axisymmetric arcing contacts. The synchronization between the time of breakdown by the synthetic circuit and closing the test object is achievable through the time setting for the release of the dynamic contact by a solenoid magnet (Fig 2b)). A sensor records the position of the dynamic contact over time, making it possible to record the arcing time and length while contacts are closing. A Pearson current probe measures the arc current and a 6015A Tektronix voltage probe measures the arc voltage. To avoid the interference of electromagnetic noises, an optical system transmits the measured data to record them.

To make different arcing times to investigate the impact of pre-strike arcing on the contacts erosion and

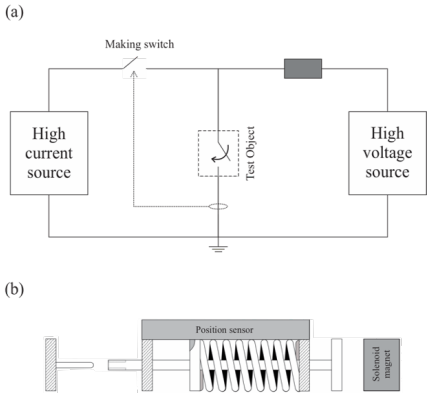

Fig 2. Schematic of the synthetic circuit (a), and the test-object.

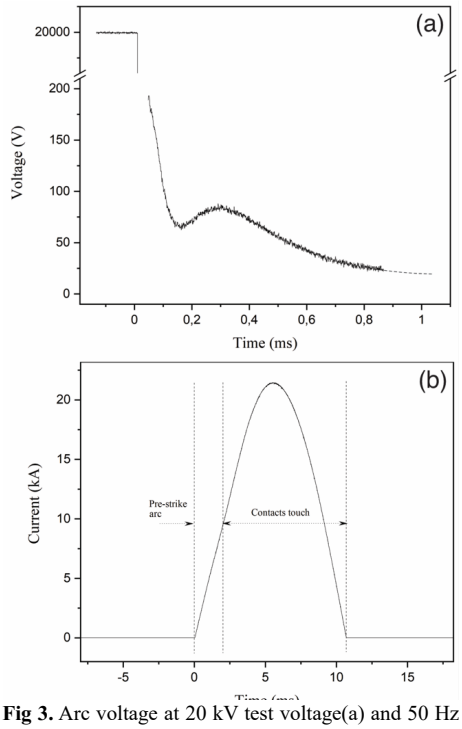

Fig 3. Arc voltage at 20 kV test voltage(a) and 50 Hz half-cycle short circuit current (b).

welding, two test voltages of 10 kV and 20 kV are applied to the test object with a short circuit current of 22kA. The fault currents duration has a tolerance of one to two milliseconds because of inaccuracy in the control system for the synthetic circuit. The difference does not make significant changes in the pre-strike arc current since di/dt is approximately constant in all the tests.

In order to figure out how long the eroded contacts can withstand fault conditions, each test has been repeated on the same set of samples until they weld to each other. The arcing time and mass loss are measured after each test. Fig 3 shows a typical arc voltage and current waveforms. The voltage waveform shows a sharp fall from the dielectric breakdown voltage at 20 kV to arc voltage, which is in the order of tens of volts. The first 50μs of the voltage fall is neglected due to interference with electromagnetic noises caused by air breakdown. Because of limitation on oscilloscope bandwidth, the arc voltage is measured for the first millisecond of arc burning while expecting to decay slightly to 13 V, which is the minimum voltage drop across the plasma sheath in front of the contacts [12, 14]. Fig 3 (b) shows the 50 Hz half-cycle of sinusoidal current with an amplitude of 22 kA. The waveform is divided into two parts. The pre-strike arc burns for 2.2 ms, while the current rises to ∼9 kA. The rest of the current passes through the contacts when they are in touch.

For the sake of accuracy in the obtained results, each test has been repeated for three different samples. The contacts were cleaned after each test, and the mass loss was measured with an accuracy of 0.00001 gr.

3 Results

A summary of results including number of tests at two test voltages of 10 and 20 kV with constant fault current of 22 kA is shown in Table 1. The results show an increase in mass loss with pre-strike arcing time by repeating the test at each specific sample. The highest arcing time is measured for samples 02 and 03 for the third time of repeating the test (3rd-Table 1), which is about four milliseconds and resulted in welding of the contacts. The pre-strike arcing current rises to ∼20 kA before the contacts' touch.

At the test voltage of 10 kV, the results show the mass loss is higher for the second time of repeating the test than the third time. Even for the test voltage of 20 kV, there is a slight difference between the mass loss for the second and third times of repeating the tests. This is an indication of arc ignition at different spot of the contact's surface.

Visual inspection of the pin's eroded area at different test conditions is taken to clarify the difference in mass loss changes. Fig 4 shows the pin's eroded surface for the first and the second samples of each test voltage. The arc ignites at a random spot on the contact's surface by air breakdown. At the test voltage of 10 kV, arc hits the same spot in case of sample one, while for sample two at the second time of repeating the test, two spots close to each other are observed in the side view of the contacts, and eroded surface is larger compared to sample one at the second time of repeating the test. Therefore, hitting at the same spot for arc ignition causes higher mass loss, which could be a reason for electric field enhancement at sharp points or more conductive area due to aggregated molten copper compared to the rest of the contact's surface.

For the test voltage of 20 kV, the contact is eroded for more than 50 % of the first test's surface area. The mass loss at this test condition is more than ten times higher than the test voltage of 10 kA. For the second time of repeating the test, the erosion almost covered the whole contact's surface. After the third time, the contact's surface is totally burnt for sample one, and some deformation on the contact's shape is observed on the side view of the pin. The third time of repeating the test for sample two at test voltage of 20 kV and short-circuit current of 22 kA, causes the contacts to weld and fail to re-open.

Table 1. The arcing time and mass loss for each test and repeated for three times for test voltage of 10 kV and 20 kV with constant fault current of 22 kA.

Breakdown Voltage: 10 kV		Number of tests		
		1st	2nd	3rd
Sample 01	Arcing time (ms)	1.13	1.37	1.37
	Mass loss (mg)	6.62	35.19	32.08
Sample 02	Arcing time (ms)	1.15	1.32	1.37
	Mass loss (mg)	7.32	13.99	24.08
Sample 03	Arcing time (ms)	0.98	1.41	1.47
	Mass loss (mg)	3.96	53.28	28.64

Breakdown Voltage: 20 kV		Number of tests		
		1st	2nd	3rd
Sample 01	Arcing time (ms)	2.5	3.35	2.855
	Mass loss (mg)	67.44	203.68	104.59
Sample 02	Arcing time (ms)	2.18	2.73	4.45
	Mass loss (mg)	69.71	86.8	334.47
Sample 03	Arcing time (ms)	2.62	2.62	3.58
	Mass loss (mg)	65.46	128	336.01

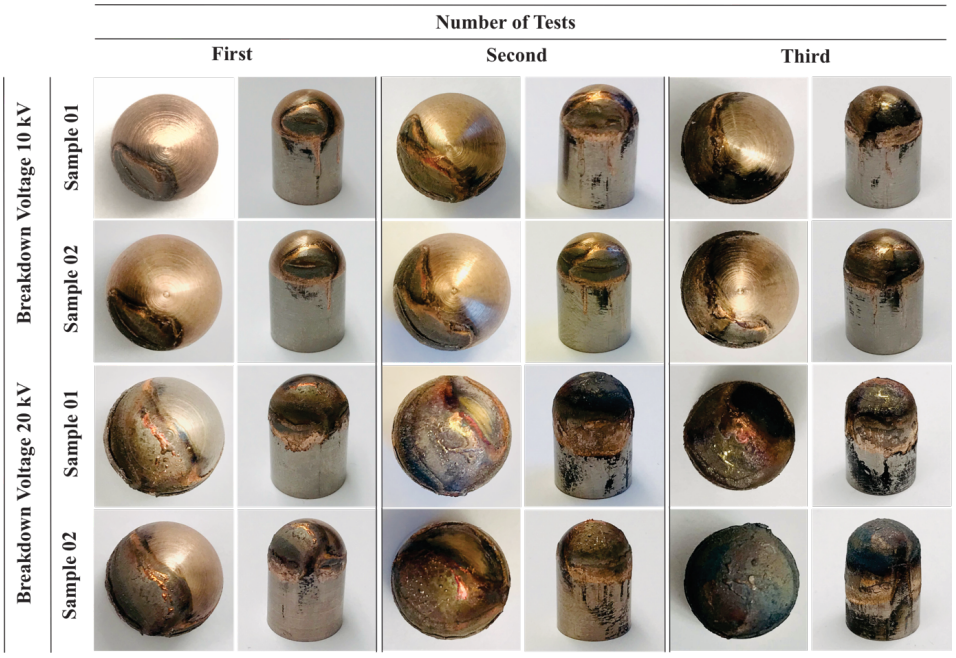

Fig 4. Eroded contacts' surface after each three times repeating the test at test voltage of 10 kV and 20 kV when a short circuit current of 22 kA passed through the contacts.

4 Discussion

Making operation of MV-LBS under fault condition is the main failure reason of the switch. The switching behavior at different pre-strike arcing times with the same short circuit current has shown the interaction between the arc and the contacts could have a deteriorating impact on switch service life by heating up the contacts surfaces to melting and evaporation points and occasionally welding them to each other in the closed position, as has occurred after three times of repeating the test at the voltage of 20 kV and fault current of 22 kA. At test voltage of 10 kV, although the contacts could withstand a couple of times more than the eroded contacts at 20 kV, we should take into account that gradual erosion of the contacts could lead to shortening the length of the contacts that would cause failure in current interruption.

Mass loss measurement is a proper method to get an approach on the contacts' erosion and prediction of the switch failure, though it needs a dedicated assessment of the results. At test voltage of 10 kV, the second time of repeating the test shows higher mass loss compared to the third time. It can be seen in Fig 4 for the contacts surface erosion at 10 kV that the arc did not ignite at same spot by dielectric breakdown. For contacts with smaller front area, the arc could initiate from the same spot each time, enhancing the erosion and shortening the switch service life. Therefore, the size of the contacts plays a crucial role in enduring longer under fault conditions.

Regardless of the eroded area impact on pre-strike arcing time, the mass loss for different arcing time is plotted in Fig 5. The results show an increase in pre-strike arcing time causes higher mass loss and erosion of the electrical contacts. Higher arcing time does not necessarily lead to higher energy dissipation between the contacts since the increase in arc current in the order of kiloampers follows by a slight decrease in arc voltage. However, higher arcing time means more time for heat conduction between the arc and the contacts to melt and evaporate the metal surfaces. In the closed position, the melted metals cool down and could weld the contacts to each other.

The obtained results indicate that the rate of contact erosion caused by making operation is increasing with increasing arcing time which is mainly because of partly absorption of dissipated arc energy by contacts' surfaces. Therefore, if the contacts are in full-touch in the closed position, the erosion only depends on the pre-strike arc time and energy, not the amount of short-circuit current. Therefore, the influential factors and involved parameters in the switch operation should be designed to decrease the impact of pre-strike arc to improve the switch service life.

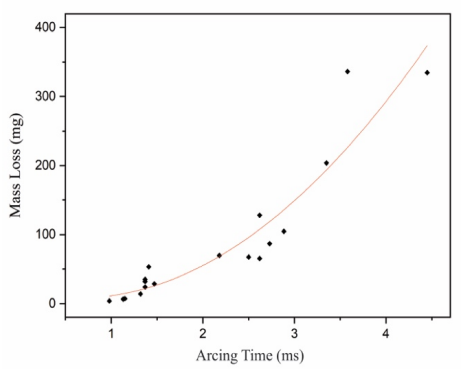

Fig 5. Mass loss as a function of arcing time when the short circuit current is kept constant (22 kA)

5 Conclusion

The electrical arcing contacts erosion/welding in an MV-LBS during making operation was investigated to understand the impact of the pre-strike arc before the contacts touch on switch failure. Experiments were conducted for test voltages of 10 kV and 20 kV, while the 50 Hz half-cycle sinusoidal short circuit current with peak of 22 kA was kept constand.

The results showed switch failure to re-open after three times repeating the test on the same set of contacts at test voltage of 20 kV. Further, an increase in mass loss with arcing time at the same current proved the impact of pre-strike arc on the contacts erosion/welding.

This work should be continued by further studies on optimizing the switch design and finding the interrelation between different parameters involved in switch operation like the speed of closing and the contacts material to minimize the impact of pre-strike arc on the contacts welding.

Acknowledgment

The Norwegian Research Council, grant number 269361, financially supported the work. The authors would like to thank Bård Ålmos and Dominik Häger from NTNU for technical supports.

References

[1] K. Niayesh and M. Runde, *Power Switching Components*. Cham, Switzerland: Springer, 2017.

[2] M. Seeger, "Perspectives on research on high voltage gas circuit breakers," *Plasma Chemistry and Plasma Processing,* vol. 35, no. 3, pp. 527-541, 2015.

[3] M. Mohammadhosein, K. Niayesh, A. A. S. Akmal, and H. Mohseni, "Impact of Surface Morphology on Arcing Induced Erosion of CuW Contacts in Gas Circuit Breakers," in *2018 IEEE Holm Conference on Electrical Contacts*, 2018: IEEE, pp. 99-105.

[4] N. S. Støa-Aanensen, M. Runde, E. Jonsson, and A. Teigset, "Empirical relationships between air-load break switch parameters and interrupting performance," *IEEE Transactions on Power Delivery,* vol. 31, no. 1, pp. 278-285, 2016.

[5] J. Tepper, M. Seeger, T. Votteler, V. Behrens, and T. Honig, "Investigation on erosion of Cu/W contacts in high-voltage circuit breakers," *IEEE transactions on components and packaging technologies,* vol. 29, no. 3, pp. 658-665, 2006.

[6] T. Schoenemann, "Comparing investigations of the erosion phenomena on selected electrode materials in air and sulfurhexafluoride," in *Electrical Contacts-1996. Proceedings of the Forty-Second IEEE Holm Conference on Electrical Contacts. Joint with the 18th International Conference on Electrical Contacts*, 1996: IEEE, pp. 115-120.

[7] E. Hetzmannseder and W. Rieder, "The influence of bounce parameters on the make erosion of silver/metal-oxide contact materials," *IEEE Transactions on Components, Packaging, and Manufacturing Technology: Part A,* vol. 17, no. 1, pp. 8-16, 1994.

[8] A. Kadivar and K. Niayesh, "Two-way interaction between switching arc and solid surfaces: distribution of ablated contact and nozzle materials," *Journal of Physics D: Applied Physics,* vol. 52, no. 40, p. 404003, 2019.

[9] J. L. Zhang, J. D. Yan, and M. T. Fang, "Electrode evaporation and its effects on thermal arc behavior," *IEEE Transactions on Plasma Science,* vol. 32, no. 3, pp. 1352-1361, 2004.

[10] S. Franke, R. Methling, D. Uhrlandt, R. Bianchetti, R. Gati, and M. Schwinne, "Temperature determination in copper-dominated free-burning arcs," *Journal of Physics D: Applied Physics,* vol. 47, no. 1, p. 015202, 2013.

[11] P. Stoller, E. Panousis, J. Carstensen, C. Doiron, and R. Färber, "Speckle measurements of density and temperature profiles in a model gas circuit breaker," *Journal of Physics D: Applied Physics,* vol. 48, no. 1, p. 015501, 2014.

[12] P. G. Slade, *Electrical contacts: principles and applications*. Boca Raton, FL, USA: CRC press, 2017.

[13] IEC *62271-101*, "*High-Voltage Switchgear and Controlgear-Part 101: Synthetic Testing*", S. IEC, 2006.

[14] J. Lowke, "Simple theory of free-burning arcs," *Journal of physics D: Applied physics,* vol. 12, no. 11, p. 1873, 1979.

Spectroscopic Analysis of Pre-strike Arc in Medium Voltage Load Break Switches (MV-LBS) at Different Closing Speeds

Submitted to the 23rd International Conference on Gas Discharge and their Applications (GD), Greifswald, Germany, August 2022.

Paper VI

ISBN 978-82-326-6901-1 (printed ver.)
ISBN 978-82-326-5645-5 (electronic ver.)
ISSN 1503-8181 (printed ver.)
ISSN 2703-8084 (online ver.)

NTNU

Norwegian University of
Science and Technology